Physics – Uspekhi **60** (10) 961 – 993 (2017)

REVIEWS OF TOPICAL PROBLEMS PACS numbers: **95.30.–k**, 95.85.Fm, 95.85.Gn, 97.10.Bt, **98.58.–w**

Interstellar and intergalactic gas in the far IR and submillimeter spectral ranges

Yu A Shchekinov, V N Lukash, E V Mikheeva, S V Pilipenko

DOI: https://doi.org/10.3367/UFNe.2017.02.038059

Contents

Abstract. We discuss key physical problems related to the interstellar and intergalactic medium, which are the subject of far infrared (FIR) and submillimeter (submm) astronomy. We outline the most impressive results of the last 25 years and summarize the characteristics of the most successful space and ground-based FIR and submm observatories: those currently in operation, already inoperative, or under development. A brief discussion is given of those physical problems concerning the evolution of the gaseous medium in galaxies, their vicinity, and the intergalactic medium, whose solution can rely on critically important and sometimes otherwise inaccessible information from the FIR and submm ranges. Among such problems are the origin of the galactic molecular gas, the conversion of gas into stars, the ejection of gas and dust into intergalactic space, the long-term survival of dust in the hostile environment of this space (in particular, in the hot environment of galaxy clusters), and the origin of dust in the Universe. Recent astronomical observations give rise to a variety of surprising findings related to our understanding of the evolution of galaxies, the chemical history of the Universe, etc. A brief discussion of some of these findings is given.

Keywords: far infrared astronomy, submillimeter astronomy, diagnostics of interstellar medium, diagnostics of intergalactic medium, origin of cosmic dust, early galaxies

Yu A Shchekinov Lebedev Physical Institute,
Russian Academy of Sciences, Astro Space Center,
ul. Profsoyuznaya 84/32, 117997 Moscow, Russian Federation;
Raman Research Institute, Sadashiva Nagar, Bangalore 560080, India
E-mail: yus@asc.rssi.ru
V N Lukash, S V Pilipenko Lebedev Physical Institute, Russian Academy of Sciences, Astro Space Center,
ul. Profsoyuznaya 84/32, 117997 Moscow, Russian Federation
E-mail: lukash@asc.rssi.ru, spilipenko@asc.rssi.ru
E V Mikheeva Lebedev Physical Institute,
Russian Academy of Sciences, Astro Space Center,
ul. Profsoyuznaya 84/32, 117997 Moscow, Russian Federation;
Moscow Institute of Physics and Technology (State University),
Institutskii per. 9, 141700 Dolgoprudnyi, Moscow region,
Russian Federation
E-mail: helen@asc.rssi.ru

Received 2 September 2016, revised 2 December 2016
Uspekhi Fizicheskikh Nauk **187** (10) 1033 – 1070 (2017)
DOI: https://doi.org/10.3367/UFNr.2017.02.038059
Translated by K A Postnov; edited by A M Semikhatov

1. Introduction

For natural reasons, astronomy has developed on the basis of optical observations in the 3900–7000 Å spectral range (Fig. 1). In 1930, Karl Jansky, when studying features of high-frequency radio signal propagation over the Atlantic, accidentally discovered background radio emission from our Galaxy and thus reached beyond the optical range [1, 2]. Shklovskii [3] called this event the beginning of the second revolution in astronomy, the first one being related to the invention of optical telescopes.

To say that the new stage in the development of astronomy connected with the start of radio astronomical

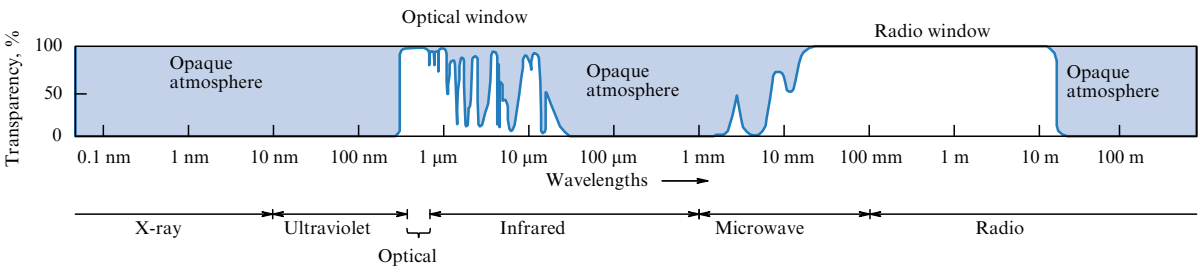

Figure 1. Transparency of Earth's atmosphere at sea level at wavelengths from 1 Å to 100 m. Strong absorption bands from $\lambda > 7000$ Å up to $\lambda \simeq 5.5$ μm are due to molecules of water H_2O, carbon dioxide CO_2, methane CH_4, oxygen O_2, and ozone O_3. At longer wavelengths from $\lambda \gtrsim 30$ μm up to several mm, broad bands of molecules of water and admixtures of CO, CH, NH_3, and HCl make the atmosphere almost opaque at sea level (see [9]). Many minor details of the transparency behavior are not seen on this plot. In particular, in the well-known transparency windows in the submm range near 350, 450, and 850 μm, the transparency at seal level is about 1%.

observations was a revolution is not an exaggeration but reflects the cardinally new understanding of physical processes in the Universe and its evolution as a whole (see [4–9]). Thanks to radio astronomical methods, a radically new fundamental concept of the hot Universe was put forward, and the standard cosmological model was worked out. Relativistic objects (pulsars and radio galaxies) and maser sources were discovered, the superfine-structure atomic hydrogen line at 21 cm was detected, which is now used as one of the most efficient methods to measure the mass of gas in the Universe, complex molecules in the diffuse interstellar medium (ISM) were found, and a new phenomenon — nonthermal synchrotron radiation from relativistic electrons in the galactic ISM — was discovered. This is an incomplete list of the achievements made by radio astronomical methods. Presently, it is hard to imagine an adequate description of the Universe without radio astronomy.

A very important fact related to the development of radio astronomy is also the fundamentally new understanding of the need to develop new observational instruments in those spectral bands where radiation is fully absorbed by Earth's atmosphere. On one hand, this is high-energy ionizing ultraviolet (UV), X-ray, and gamma radiation; on the other hand, this is low-frequency radiation in the far infrared (FIR) and submillimeter (submm) range from 30 μm to 1 mm.[1] This property of Earth's atmosphere is illustrated in Fig. 1, schematically showing the atmosphere transparency. We can see that strong molecular bands almost completely absorb incident radiation in the wavelength interval from several micrometers to several millimeters.[2] From the observational standpoint, the atmospheric opacity makes these spectral bands fundamentally different from the optical and radio ranges. To perform observations, telescopes should be launched beyond the atmosphere or at least should be mounted high above the ground level, where the absorption is significantly weaker.[3]

On the pages of *Physics-Uspekhi*, the features of astronomical research in the submm range, including the need for extra-atmospheric observations, were first discussed in the paper by Salomonovich [10] (see also paper by Kislyakov [11]). However, the specifics of the interactions of both high-energy (UV, X-ray, and gamma) photons and low-energy (terahertz) photons with matter made the detectors very complicated technologically and costly. As regards the submm range, high-sensitivity detectors for astrophysical purposes require superconducting mixers cooled to temperatures below 4 K, which is a challenging problem in and of itself, especially in extra-atmospheric conditions (see [12–14]). For this reason, the wavelength range from 30 μm to 1 mm remains underexplored, a *terra incognita* of some sort. However, simple estimates indicate that the submm range can conceal critically important 'encoded' information about most of the cold matter in the Universe and about many physical processes.

In this review, we discuss some problems with cosmic plasma[4] — the interstellar and intergalactic medium in which observational appearances in the FIR and submm ranges can most sharply characterize some system or phenomenon. In Sections 2 and 3, we present the general characteristics of problems in submm astronomy, describe past, present, and future observatories, and give their comparative characteristics. In Section 4, we address unsolved problems and phenomena related to dust and gas in galaxies from the standpoint of new results obtained in recent years by space observatories and discuss their current understanding. In Sections 5–8, we discuss the physical state of dust and gas in the hot gas of clusters and groups of galaxies, in the intergalactic medium, and in very early galaxies at the beginning of stellar nucleosynthesis in the Universe. In the Conclusion, we briefly formulate the main arguments determining the importance of submm research for cosmic plasma physics and its dust component.

2. Fundamental problems in submillimeter astronomy

The origin and evolution of stars, planets, and life on Earth are among the most fundamental ontological problems and are therefore of general interest. Here, the stellar nucleosynthesis and chemical evolution of the Universe are key questions. In the course of their evolution, stars produce chemical elements that are necessary for living organisms to appear. On the other hand, elemental abundance, i.e., the relative

[1] The submillimeter range is often defined as the terahertz band.

[2] Atmospheric transparency tables in the optical, near, and mid-infrared wavelength ranges are presented by S Lord on the Gemini Observatory website http://www.gemini.edu/sciops/telescopes-and-sites.

[3] For example, at an altitude of 4200 m (Mauna-Kea peak, Hawaii), where the Keck Observatory is located, the absorption at 450 μm is about one order of magnitude lower than at sea level.

[4] Cosmic plasma includes the interstellar, circumgalactic, and intergalactic gas with the ionization degree ranging from $x \sim 10^{-5}$ to $x \simeq 1$, although, strictly speaking, cosmic gas by no means always represents a plasma in the classical sense defined by the condition $N_D = n_e \lambda_D^3 \gg 1$, where n_e is the electron number density and λ_D is the Debye radius.

number densities of different elements that originated in the stellar nucleosynthesis, are closely related to the parent stellar mass, and therefore they represent imprints of physical processes governing the preceding star formation and stellar mass distribution [15–17]. Hence, studying the spatial and temporal chemical abundance can provide key information on evolutionary processes in galaxies and in the Universe as a whole.

In spite of great efforts, the chemical evolution of the Universe remains poorly understood. One of the key factors among the many hampering its study is the effect of dust produced in the thermonuclear evolution of stars.

First, a great amount of information on chemical enrichment of the Universe is unavailable due to the opaqueness of the cosmic medium. Indeed, assuming the mean number density of dust grains in the interstellar plasma to be $n_{\rm d}/n \sim 10^{-11}$ as an estimate, where $n_{\rm d}$ is the dust number density and n is the gas number density, and the mean size of the dust grain to be $a \sim 10^{-5}$ cm, we obtain the mean cross section of optical light extinction per proton in the interstellar medium $\sigma_{\rm d} \sim 10^{-21}$ cm^2 (see [18] for a detailed analysis). This cross section is four orders of magnitude larger than the Thomson one, which for a typical molecular cloud (MC) where stars are formed, with the column density $N_{\rm H} \sim 10^{22}$ cm^{-2}, yields the optical depth $\tau_{\rm v} \sim 10$. The opacity problem can be overcome by IR observations, where the dust optical depth is much lower. Indeed, in the IR range, the wavelength $\lambda \gtrsim 1$ μm exceeds the typical size of interstellar grains, and therefore the extinction cross section decreases as $\sigma_{\rm d} \propto a/\lambda$ (see [18]), which makes molecular clouds almost transparent for quanta with $\lambda > 10$ μm.

Second, the very scenario of chemical enrichment of the Universe, which includes transportation of the enriched stellar matter over large distances greatly exceeding the stellar size, represents another difficulty. Direct observations of absorption lines in quasar spectra at redshifts $z \simeq 2-3$ demonstrate the presence of heavy elements with the mass fraction $Z \sim (10^{-3}-0.3)\,Z_\odot$ in the intergalactic medium (IGM) at distances of the order of 0.5–1 Mpc from the nearest galaxies [19–21].[5] Recently, observations have shown evidence of the presence of cosmic dust[6] in the IGM at $z \lesssim 0.3-2$ and at distances up to 10 Mpc from galaxies [23]. The measured dust mass fraction in the IGM is about $0.1Z_\odot$, which is only a third of the total dust mass fraction produced in galaxies (see Fig. 7 in [23]).

An important feature of these observations based on light extinction from distant sources is the ever present observational bias because only part of gas condensations absorbing or scattering light are on the line of sight to the light source. A certain, probably significant, part does not contribute to the extinction and absorption. Gas and dust emissions, however, are free from such a bias and are more appropriate for more reliable estimates of the mass of heavy elements in the IGM.

The transportation of gas (including heavy elements and dust) is always mediated by powerful dynamical processes: stellar winds and supernova explosions, where gas velocities can be as high as several thousand kilometers per second, and on the galactic scale, by large-scale motions from central regions of galaxies (galactic winds). The dust ejected at large distances from the stellar sources cools down and its emission spectrum shifts toward long wavelengths. As a result, the dust becomes hardly observable in emission in the near ($\lambda = 0.74-2.5$ μm) and middle ($\lambda = 2.5-50$ m) IR range.

Therefore, the most informative spectral range for studying a large variety of problems related to the chemical evolution of galaxies, energy and mass exchange between galaxies and the ambient gas, dust production and transportation, and dust mass budget in galaxies and in the Universe as a whole shifts to the FIR ($\lambda = 50-2000$ μm) and submm ranges.

IR observations carried out by space observatories in the last two decades have led to a revolutionary new understanding of many astrophysical phenomena and qualitatively changed our knowledge about the Universe. A large number of cosmic objects and phenomena have become known thanks to IR observations. An example is provided by the discovery of a new type of object, bright IR galaxies (luminous infrared galaxies, LIRGs) with IR luminosities exceeding $10^{11}L_\odot$ (where $L_\odot \simeq 4 \times 10^{33}$ erg s^{-1} is the Solar luminosity). Other examples include the discovery of details of star formation (SF) processes and formation of protoplanetary disks, the discovery of 'dark' molecular clouds not emitting in the CO molecular lines, and many others. We address some of these phenomena below in Sections 3.2, 3.3, 4.1.1, 4.1.2, and 5–7.

The Herschel Space Observatory (the mirror diameter 3.5 m and the active period 2009–2013) significantly enlarged the class of objects available for FIR and submm studies. However, its results were limited by low sensitivity, which is an Achilles' heel of all modern IR telescopes. The reason for this is insufficient cooling of the mirrors, with the flux sensitivity being determined by the temperature.[7] In particular, the mirror of the Herschel telescope was cooled to $T_{\rm a} = 70$ K, which rather modestly increased the sensitivity compared to previous observations in the 55–670 μm range.

At the same time, an undoubted result of the Herschel telescope is the understanding that important information about many fundamental phenomena in the Universe is hidden in the FIR and submm spectral ranges, beyond he current sensitivity limits. For this reason, several new high-sensitivity IR and submm observatories with mirror cooling below $T < 10$ K are presently under discussion. These projects include SPICA (Space Infrared Telescope for Cosmology and Astrophysics), CALISTO (Cryogenic-Aperture Large Infrared-Submillimeter Telescope Observatory) and Millimetron (MM). The first mission (SPICA) will be equipped with a 2.5 m mirror cooled to $T < 8$ K and is aimed at studies in the mid- and far-IR ranges ($\approx 30-210$ μm). SPICA is scheduled for launch at the end of the 2020s.[8] CALISTO is planned to be equipped with a 5 m mirror cooled to $T < 4.5$ K operating in the wavelength range 30–300 μm. The Russian mission Millimetron is planned to be equipped with a 10 m mirror cooled to $T = 5$ K with the capacity to operate as part of a very-long-base space interferometer.

[5] $Z_\odot \sim 0.01$ is the mass number density of heavy elements in the Sun. This value is typical for relatively young Population I stars in the thin Galaxy disk, where the Sun is located, and also for the interstellar medium.

[6] Cosmic dust represents microscopic solid grains with a size ranging from several Å to 1 μm. The dust grains have various chemical compositions and optical properties (see [22]).

[7] The asymptotic temperature of the receiver — the mirror — is set at the level $T_{\rm b} = T_{\rm s} + P\tau/C$, where $T_{\rm s}$ is its unperturbed temperature set by the thermostat, P is the power of incident radiation, τ is the time relaxation constant, and C is the heat capacity of the mirror (see [24]).

[8] See http://research.uleth.ca/spica/.

Millimetron will cover the wavelength range from 20 to 3000 μm.

The most general class of astrophysical objects for fundamental studies in the FIR and submm ranges includes 1) gas in the Universe; 2) galaxies and galaxy clusters; 3) relativistic objects; 4) radiation in the Universe; 5) life in the Universe.

Among these, the gas component in galaxies and in the Universe as a whole is fundamentally important due to several facts. a) A significant (if not the predominant) fraction of baryons in the Universe is in the form of gas. b) Gas and its important component — dust — re-emit part of high-energy radiation and cosmic rays (permeating the interstellar and intergalactic medium and determining the thermodynamic state of the gas) and can therefore serve as a 'radiometer' of the Universe. c) Under certain conditions, gas is condensed into a cold dense state in which, under the action of gravity, the fundamental SF process occurs. The SF process determines the main properties of the baryonic component of the Universe, namely, the generation of radiation in the course of stellar nucleosynthesis, the observed properties of galaxies, and the chemical composition of the Universe. d) Gas and dust determine the opacity of the Universe in all spectral energy bands and thus the possibility of observational studies of astrophysical objects.

Therefore, studying gas in the Universe is the key problem for most space projects in the IR range.

3. Submillimeter astronomy yesterday, today, and tomorrow

The first observations in the FIR and submm ranges were carried out in the mid-1960s. These experiments included balloon sky surveys in the 300–360 μm range with an angular resolution of 2° [25, 26] and rocket observations of the night sky background in the submm range [27]. These studies were stimulated not only by the 'intriguing' attractiveness of the unknown (see the review by Salomonovich [10] published in 1969) but also by the anticipation of discovering the theoretically predicted cosmic microwave background (CMB) of the Universe [28], which indeed was soon discovered.

The first submm observations were carried out most actively for the brightest sources: the Sun and the Moon [29–31] (submm observations of the Sun carried out in 1969 are reported in [31]), the Galactic center [32], and quasars [33]. The first active studies of the transparency of Earth's atmosphere in the FIR and submm bands started as early as 1957, although their results were reported later [34, 35]. In the second half of the 1960s, the importance of the submm wavelengths for astrophysics was emphasized in the conclusion of the Astronomical Council of Great Britain on the need for submm research.

In general, over a time period of almost half a century, submm astronomy has obtained very interesting results describing the submillimeter Universe. In Sections 3.1–3.3, we briefly present the most significant observational projects carried out over the last 25 years, as well as projects planned for the next decade.

3.1 Breakthrough projects of the 1990s in the infrared and submillimeter spectral ranges

3.1.1 COBE. The COBE (Cosmic Background Explorer) satellite (November 1989–December 1993) had three on-board instruments: a differential microwave radiometer DMR to measure the CMB anisotropy,[9] the multiwavelength detector of IR radiation from dust, DIRBE (Diffuse InfraRed Background Experiment), and the spectrophotometer to measure the CMB spectrum, FIRAS (Far Infra-Red Absolute Spectrophotometer).

In the COBE project, each of these three detectors solved its own fundamental problem. The purpose of DMR was to measure angular variations of the CMB temperature characterizing the level of primordial density fluctuations in the Universe. The constraints on the angular variations $|\Delta T|/T \sim 10^{-4}$ K obtained by that time (see [36, 37]) required higher measurement accuracy. To this aim, two radiometers were used at three frequencies with an accuracy of 1.5×10^{-4} K (at 53 and 90 GHz) and 3×10^{-4} K at 31.5 GHz (the frequencies were chosen near the minimum of the galactic emission) and an angular resolution of 7° in one year of observations [38]. This enabled the quadrupole amplitude $|\Delta T|/T = (4.8 \pm 1.5) \times 10^{-6}$ [39] to be measured and the anisotropy $|\Delta T|/T \sim 10^{-5}$ to be obtained at the mean angular scale of 10° [40]. We note that the same value of anisotropy was obtained somewhat earlier in the Soviet Relikt-1 experiment [41].

The goal of DIRBE was to study the cosmic (background) IR radiation. The cosmic IR background is produced by thermonuclear activity of baryons in the post-reionized Universe with the dominant contribution from localized sources — stars and interstellar galactic dust and infrared and primeval galaxies [42, 43]. The DIRBE instrument operated in almost the entire IR range 1.25–240 μm in several bands centered at wavelengths 1.25, 2.2, 3.5, 4.9, 12, 25, 60, 100, 140, and 240 μm, with the sensitivity $\nu I_\nu = 10^{-9}$ W m^{-2} sr^{-1} in each band (where I_ν is the cosmic IR radiation intensity at a frequency ν). It also included a linear polarimeter operating at wavelengths 1.25, 2.3, and 3.5 μm (Fig. 2). The polarimeter in the near-IR range was used mainly to separate the interplanetary dust emission (the zodiacal light). Its sensitivity threshold was significantly below the sky brightness in this range. In the period from 11.12.1989 until 21.09.1990, the receiver was maintained at a temperature of < 2 K, and later at $\simeq 50$ K, which decreased the sensitivity to a 20% level from the initial one at the temperature $T = 5$ K (see [44]).

The main goals of the FIRAS instrument included the measurement of the CMB spectrum, the establishment of its blackbody nature, and the search for possible deviations from the Planck spectrum in the entire CMB-dominated spectral range 0.1–10 mm [42]. To fulfil these tasks, FIRAS had a wide beam of 7°. The FIRAS detector with the working wavelength range from 100 μm to 1 cm was maintained at a temperature of 1.5 K, the equivalent electromagnetic noise power was 4×10^{-15} W Hz$^{-1/2}$, and the sensitivity in the 500 μm – 3 mm wavelength range averaged over the 10-month observation period was 0.8×10^{-9} W m^{-2} sr^{-1} [45].

The COBE results proved that the CMB spectrum is the black body spectrum with the temperature (2.726 ± 0.01) K. Another important result obtained by COBE was the long-awaited detection of cosmological CMB anisotropy with the quadrupole amplitude of 4.8×10^{-6}.

In addition, the spectrum of the cosmic IR background was measured. Its brightness was found to be (1.5 ± 0.2)

[9] In the Russian literature, the term 'relic radiation' suggested by I S Shklovskii is commonly used.

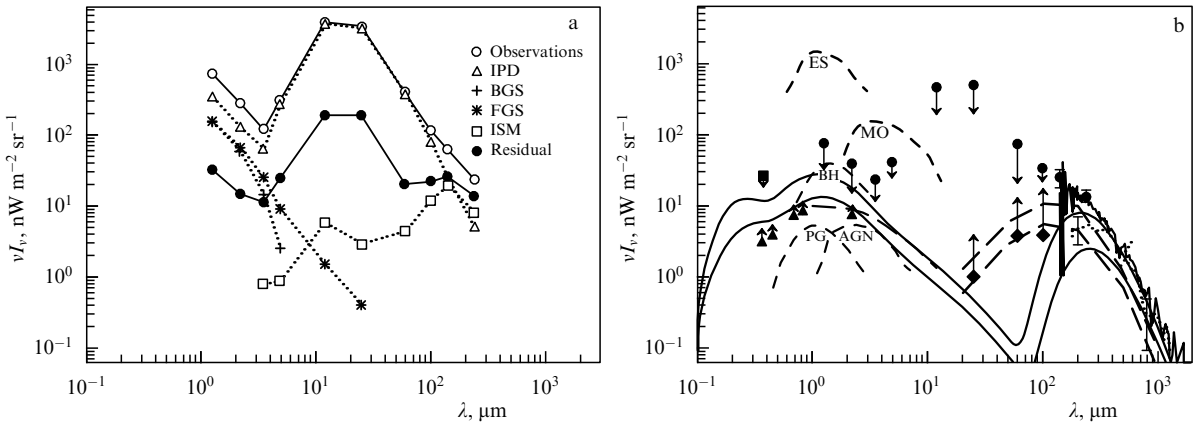

Figure 2. (a) Different source contributions to the background radiation according to the DIRBE data (1.25–240 μm) in the Lockman hole direction [46]. Observed brightness — unfilled circles; contributions from: interplanetary dust (IPD) — triangles, bright Galactic sources (BGS) — crosses, faint galactic sources (FGS) — asterisks, ISM — unfilled squares. Filled circles show the residual brightness after all the above contributions have been subtracted. (b) Comparison of the model extragalactic background calculations [47] with COBE data. ES — exploding stars, MO — massive objects, BH — black holes, AGN — active galactic nuclei, PG — primeval galaxies. Shown are the 2σ DIRBE upper limits (1.25–60 μm) measured at 140 and 240 μm with a 95% confidence interval 5–34 nW m^{-2} sr^{-1} at the 100 μm wavelength [46], the νI_ν FIRAS intensity (125–1000 μm) [48] is shown with a thin broken line. Two solid curves show theoretical predictions of the spectrum of evolving galaxies in the close (bottom curve) and open (upper curve) galactic chemical evolution model [47]. The short-dashed lines show expected IR contributions from different known and assumed sources [46]. The long-dashed lines correspond to predictions of photometrical models of galaxies with two different dust opacities [46].

$\times 10^{-8}$ W m^{-2} sr^{-1}, and the IR background sources were identified in a wide wavelength range (140–1000 μm). As shown in [46], the error in the determination of the contribution to the cosmic IR background from stellar and galactic sources in the FIR and submm ranges due to the need to subtract the significantly brighter CMB radiation in this range can be of the same order of magnitude as the measured signal itself.

3.1.2 Spitzer space observatory. Scientific tasks for an IR telescope in space were first formulated in 1946 by Spitzer [49] in a report presented for the aerospace corporation RAND (Research ANd Development). The technical discussion of the project of the telescope SIRTF (Space InfraRed Telescope Facility) was started by NASA (USA) in 1988, and it was launched into orbit on August 25, 2003. After three months of operation in orbit, the telescope was renamed after Spitzer.

The Spitzer observatory completed its mission in 2009. In the spectroscopic mode, the telescope operated in several overlapping bands with high and low spectral resolutions in the wavelength range 5.3–40 μm (InfraRed Spectrograph, IRS). A three-band photometer operated in the range 21.5–174.5 μm, partially covering the FIR range (Multiband Infrared Photometer for Spitzer, MIPS), and a set of four-band photometers conducted observations at wavelengths of 3.2–9.3 μm (InfraRed Array Camera, IRAC) [50]. The main mirror diameter was only 0.85 m; therefore, the angular resolution of images in the frequency bands of 70, 100, and 160 μm was relatively low, about one arcminute (at 160 μm). The mirror temperature was maintained at 5.5 K; hence, despite the relatively modest mirror size, the Spitzer telescope had quite a high flux sensitivity in the near-IR range, which enabled a 10σ detection of a 'standard' galaxy with a luminosity $L^* = 2 \times 10^{10} L_\odot$ at the redshift $z = 3$, corresponding to 8 μJy in the 8 μm band [51]. The active operation of Spitzer ended when the liquid helium was exhausted, although it should be noted that the originally planned duration of the project was only two and a half years.

Along with other tasks, the observatory conducted a survey of the ISM in our Galaxy and in nearby galaxies, including the Large and Small Magellanic Clouds and M31 (the Andromeda nebula) (see [52]). This, in particular, enabled the first near- and mid-IR imaging of the structure of SF regions, and the determination of dust properties in regions of ionized hydrogen (HII regions) around young massive stars.

As regards the main objectives of the Spitzer observatory, a class of objects unavailable for observations in other spectral ranges was originally identified. It included 1) protoplanetary disks and their fragments, which are practically gas-free and can be observed only by dust emission; 2) brown dwarfs, which are at the threshold of thermonuclear burning; 3) IR galaxies and active galactic nuclei, most of whose emission is screened by dust; and 4) very distant early galaxies, whose optical and ultraviolet spectra are redshifted to the near- and mid-IR ranges [51].[10] The data obtained by the Spitzer space telescope are publically available through NASA's IRSA archive (InfraRed Science Archive) and continue to be used by the astronomical community.[11]

3.1.3 Herschel space observatory. A project for a space telescope in the FIR and submm range (Far InfraRed Space Telescope, FIRST) was presented to the European Space Agency (ESA) in 1988. [12] At the end of the 1990s, the project was re-designed for launch into the Lagrange point L2, and in 2000 it was named after Herschel (Herschel, ESA). The observatory was launched in 2009 and was in operation until 2013, when the liquid helium for cooling scientific instruments was exhausted.

[10] The designers of the observatory said that Spitzer would study "'the old, the cold and the dirty' objects in the universe," meaning old (early) galaxies, cold brown dwarfs, and dust emission and stars screened by the dust (see http://www.spitzer.caltech.edu).

[11] http://irsa.ipac.caltech.edu/about.html.

[12] Several years earlier, at the Space Research Institute of the USSR Academy of Sciences, a similar project was discussed [53, 54]. Unfortunately, its development was abandoned due to lack of financing.

The observatory was equipped with a 3.5 meter main mirror cooled to a temperature of around 70 K and three scientific instruments. A short-wavelength grid array spectrometer, which simultaneously served as a camera (Photodetector Array Camera and Spectrometer, PACS), obtained images at 70 and 160 mcm in the camera mode, and spectra (51–220 μm) with the spectral resolution $R = 1000-4000$. The Fourier spectrometer SPIRE (Spectral and Photometric Imaging Receiver) obtained images in the 250, 350, and 500 μm bands, as well as spectra with the moderate resolution $R = 40-1000$ in the 194–671 μm range. The third instrument, the heterodyne detector HIFI (Heterodyne Instrument for the Far Infrared), operating in the 157–213 and 240–625 μm wavelength ranges, enabled high-resolution spectra.

The general focus of the project was the 'cold' Universe. The following problems were addressed: 1) the origin and evolution of galaxies and objects in the early Universe;[13] 2) the morphology and dynamics of the interstellar gas in SF regions in our Galaxy and other galaxies; 3) observational astrochemistry, i.e., the study of molecules in the Universe; and 4) spectrophotometry and the chemistry of atmospheres of outer planets and small bodies of the Solar System, including trans-Neptunian objects [55].

The analysis of data obtained by the Herschel observatory has not yet been completed. This relates, in particular, to data on extragalactic objects in a 1000-square-degree sky region observed in the HELP project (Herschel Extragalactic Legacy Project).[14] A notable feature of this project is that it produces the multiwavelength sky survey in the Herschel observatory field complemented by data in other spectral ranges [56]. The main results obtained up to now include the recognition that all SF occurs in thin gas–dust filaments; the construction of the distribution of missing hydrogen in the Universe by mapping ionized carbon emission lines; the production of a deep photometric galaxy survey in the submm range; the measurement of the spectra of galaxies in the mid- and far-IR ranges; the measurement of the luminosity function of objects at redshifts up to $z \simeq 4$; the correction of the SF density in the Universe [57] and the discovery of a large number of lensed galaxies; observational evidence of the mechanisms maintaining the joint evolution of active galactic nuclei and their host galaxies [58–60], including the dust emission survey from the central 1 Mpc region in some galaxy clusters [61]; the measurement of the masses of several protoplanetary disks by HD molecule observations; and studies of water in the atmospheres of small Solar System bodies.

3.1.4 Planck space observatory. The scientific objectives and technical realization of the Planck space mission were first discussed in 1994 and 1995, respectively. The original name of the project COBRAS/SAMBA stemmed from the merging of two ESA projects in 1993: Cosmic Background Radiation Anisotropy Satellite (COBRAS) and SAtellite for Measurement of Background Anisotropy (SAMBA). In 1997, the observatory was named after Max Planck (Planck, ESA). The mission is equipped with a Gregory telescope with elliptical mirrors cooled to 40 K (the primary mirror is 1.9×1.5 m and the secondary mirror is 1.1×1.0 m) and two receivers: a high-frequency (submillimeter) detector at frequencies from 100 to 897 GHz (from 350 μm to 0.3 μm) and a low-frequency (microwave) detector at frequencies of 30–70 GHz (0.3–3 mm). Only two of nine frequency bands did not allow polarimetric measurements.

The main objectives of the Planck mission included 1) high-sensitivity ($\Delta T/T \sim 10^{-6}$) and high-resolution ($< 1'$) measurements of the CMB intensity and polarization; 2) tests of cosmological models and models of the origin of the Universe, measurements of the spectral slope of the primordial density perturbations, studies of hypothetical topological defects, and determination of cosmological parameters; 3) measurement of the Sunyaev–Zeldovich effect, determination of peculiar velocities of galaxy clusters, and production of a catalog of galaxy clusters; 4) studies of radio galaxies and active galactic nuclei; 5) studies of the interstellar dust; 6) studies of the interstellar magnetic field and properties of relativistic electrons; and 7) studies of the Solar System and zodiacal light.

The goals of the Planck mission have generally been completed: in 2015, the 'Planck Legacy'[15] archive was completed, and the results are now being interpreted. Apparently, a full analysis will require a long time; however, many of the scientific goals have already been achieved. For example, the cosmological model parameters [62] (see also a review of the main cosmological results in [63]), a catalog of the Sunyaev–Zeldovich sources [64], and the results of studies of the relative orientation of the interstellar magnetic field and dust structures [65] have been published.

3.1.5 SCUBA/SCUBA-2. The SCUBA project (Submillimeter Common-Use Bolometer Array) started in the late 1990s. It included bolometric receivers installed at the ground-based submm James Clerk Maxwell Telescope (JCMT)[16] (Mauna-Kea, Hawaii). The SCUBA bolometer operates in the atmospheric transparency windows at 450 and 850 μm; the respective transparency at these wavelengths at the altitude of Mauna Kea (4084 m) is about 40 and 80% [66, 67].[17]

Using SCUBA, the first large ($\sim 10^4$ objects) systematic submm observations of galaxies in the local Universe ($z < 0.1$) were carried out and the first galaxy luminosity functions at 850 μm were constructed [68, 69]. It is significant that the galactic luminosity function constructed based on the IRAS (InfraRed Astronomical Satellite) observations at 12, 25, 60, and 100 μm demonstrates a clear deficit at high luminosities compared to the SCUBA data. This deficit is naturally explained by the fact that the IRAS observations do not cover a significant part of the cold ($T < 30$ K) dust, whose emission peak is shifted to the submm range. It is most clearly seen for $L \gtrsim 3 \times 10^{11} L_\odot$ [70].

The SCUBA and VLA (Very Large Array) local galaxy survey observed galaxies in the local Universe at respective wavelengths of 850 nm and 21 cm. An important result, in particular, is the conclusion that the brightness profile of galaxies at the 21 cm line frequently shows a minimum (which is sometimes significant) in the central regions, in contrast to a maximum at 850 μm. In the radial direction, HI emission

[13] The early Universe is here assumed to be at redshifts $1 < z \leqslant z_r$, with an upper bound $z_r \lesssim 20$ corresponding to the beginning of reionization.

[14] See http://herschel.sussex.ac.uk.

[15] http://sci.esa.int/planck/56288-planck-legacy-archive-is-complete.

[16] JCMT is one of the largest ground-based telescopes for observations in the FIR and submm ranges, with a mirror diameter of 15 m. It started operating in 1987.

[17] This corresponds to the H_2O column density $2 \times (10^{21} - 10^{22})$ cm^{-2} [66], which is two orders of magnitude lower than at sea level.

extends to longer distances than does the dust emission at 850 μm, with the scale difference of 50–100% [71], which, apparently, corresponds to the radial gradient in number density of heavy elements.

The 850 μm emission polarization measurements in the molecular cluster cores (for example, in L183) were very important for establishing the role of the magnetic field and turbulence in the SF process. Namely, it turned out that inside the dense protostellar cores, turbulent motions do not significantly affect the magnetic field structure, and it is therefore sufficiently homogeneous within the 21″ angular resolution of the SCUBAPOL polarimeter, which is significantly smaller than the angular size $\sim 10'$ of the dense core [72–74]. This conclusion was soon confirmed by polarization measurements in several other SF regions (for example, in the OMC-2 region in the Orion nebula [75]).

In the period from 1997 to 2005, polarization measurements for more than 100 SF regions were performed in total; one third of them are described in detail in [76]. Later observations by the Herschel and Planck space observatories generally confirmed the conclusions on the magnetic field structure in the molecular cloud cores obtained by the SCUBAPOL project [77, 78].

In 2012, the SCUBA array was substituted by a more sensitive bolometer SCUBA-2 operating at the same 450 and 850 μm [79], but enabling mapping equal sky areas two times faster than its predecessor.

The SCUBA-2 instrument continues conducting unique sky surveys of the JCMT telescope: [18]

1) the sky survey in two 10°-wide strips, one of which is directed along the galactic plane (GP) (the GP-wide survey) and the other perpendicular to the GP centered at the north galactic pole (the P2P, Pole to Pole, survey);

2) the cosmological survey (SCUBA-2 Cosmology Legacy Survey, S2CLS), aimed at creating the first large sample of extragalactic sources at 450 and 850 nm, including luminous IR galaxies at large redshifts;

3) the survey of 155 galaxies in the local Universe (within 25 Mpc) at 450 and 850 μm and in the CO lines ($J = 3-2$) using the HARP (Heterodyne Array Receiver Program) instrument;

4) the galactic plane survey (JPS, James Clerk Maxwell Telescope Galactic Plane Survey) aimed at distinguishing evolutionary sequences of massive SF regions and of stimulated SF regions in molecular clouds, as well as at discovering cold dark molecular clouds and establishing their distribution in the Galaxy;

5) the Gould Belt survey (GBS) of the SF regions nearest to the Sun ($D < 500$ pc), including molecular clouds of the Gould Belt: Orion, Taurus, Perseus, Serpens, and Ophiuchus, based on the joint use of SCUBA-2, HARP, and POL-2 polarimeter. This survey should address many fundamental issues of SF physics;

6) the survey of the protoplanetary disk remnants aimed at creating their database, determining the masses of these disks, and estimating the possibility of their detection by other IR observatories, measuring the dust emission spectral index, etc.

Presently, SCUBA-2 continues the survey programs. These surveys largely complement the Herschel surveys, encompassing larger sky fields but with a smaller depth.

[18] http://www.eaobservatory.org/jcmt/science/legacy-survey/.

3.2 Operating submillimeter observatories

3.2.1 ALMA. The ALMA observatory (Atacama Large Millimeter Array), located on the Chajnantor Plateau at 5050 m above sea level,[19] includes 50 individual 12-meter dishes operating in the wavelength range from 315 μm to 9.7 mm. The emission is detected by heterodyne receivers with a bandpass width reaching 16 GHz and operating in up to 10 bands. The angular resolution of the array reaches 0.01″. The submm observations are primarily limited by the atmospheric opaqueness (Fig. 3). To decrease the noise temperature, the receivers are kept at low temperatures ranging from $T = 17$ K (in the 31–45 GHz band) to $T = 230$ K (in the 787–950 GHz band), depending on the channel frequency [81].

Scientific observations at ALMA started in the second half of 2011. The first object was the Antenna galaxy representing two tight colliding galaxies NGC 4038/4039 (Antenna galaxies), in the merging region of which molecular clouds where observed in the CO molecule rotation lines CO(3-2) with an angular resolution of 1″ [82].

Since the start in 2011, ALMA has obtained detailed images and spectra of protoplanetary disks and detected planet formation in very young protoplanetary systems (100 thousand – 1 mln years). In addition, the observatory imaged distant galaxies and SF regions in nearby galaxies and in the Galaxy and made the first studies of HCN and H_2CO molecules and dust distribution in cometary nuclei. Reports have appeared on the possibility of exotic chains of chemical reactions in the densest parts of molecular clouds, which might require the further development of high-resolution laboratory molecular spectroscopy [83].

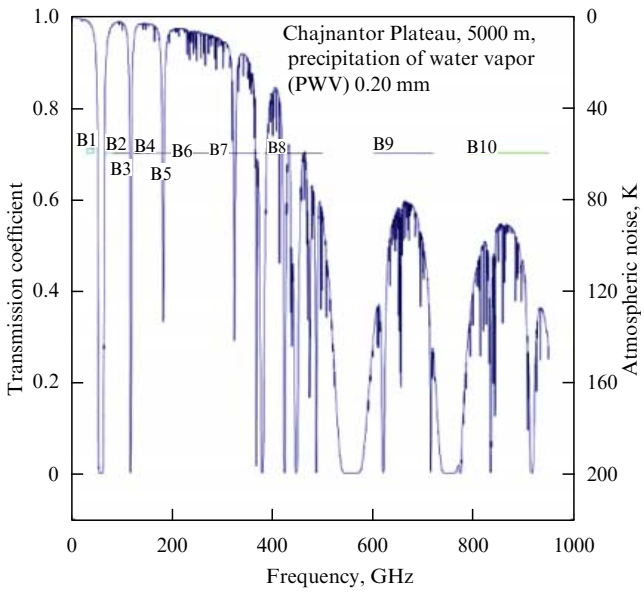

Figure 3. Transmission coefficient of Earth's atmosphere for the ALMA observatory site in the best conditions. The horizontal segments B1–B10 show working bands of the observatory (source: www.almaobservatory.org/component/content/article/166-newsletter-no-2).

[19] The average yearly amount of water in the atmospheric column at the Chajnantor plateau is only 1.1 mm; therefore, it is sometimes called a paradise for infrared, submillimeter, and millimeter astronomy. The Comisión Nacional de Investigatión Cientifica y Tecnológica (CONICYT) of the Chilean Government was the initiator of creating the Atacama Astronomical Park there, with more than ten telescopes for millimeter and submillimeter observations [80].

Table. Designed parameters of the Millimetron (MM) observatory in comparison with parameters of other observatories.

Parameter	Herschel, 2009–2013	ALMA, 2011	SPICA, 2029	MM, 2015
Range, μm	50 – 670	315 – 9680	5 – 210	20 – 3000
Resolution, arc sec.	3.5 – 40	0.01 – 5	0.4 – 20	3 – 60
Field of view	up to $4' \times 8'$	up to $25''$	$5' \times 5'$	$6' \times 6'$
Photometry	1 mJy	> 10μJy	30 μJy	20 nJy
Spectroscopy, resolution $R \sim 10^3$	20 mJy	60 μJy	200 μJy	4 μJy
Spectroscopy, resolution $R \geqslant 10^6$	2 Jy	50 mJy	—	200 nJy

The ALMA results are very impressive in studies of submm galaxies (SMGs) with high luminosity, among which there are a significant number of double and multiple galaxies with ultra-luminous infrared galaxies (ULIRGs) as secondary components [84, 85]. When spectroscopic redshift measurements are possible, the measured redshifts are close to $z \simeq 2.5$ [85]. Observations of the continuum and molecular line (HCN/HCO^+) emission from nearby ULIRGs with active galactic nuclei (AGNs) [86] enable studies of the molecular gas properties in AGNs and SF bursts in the central parts of galaxies.

In this connection, it is worth noting the ALMA observations of highly dust-abundant bright galaxies with high SF rate (Dusty StarForming Galaxies, DSFGs) at high redshifts $z \sim 4$ [87]. The high SF rate (SFR) in these galaxies follows from the high dust temperature $T_{\rm d} \simeq 40$ K obtained by averaging over the sampling. Their total luminosity in the FIR band, by rough estimates, can reach $L_{\rm FIR} \sim 10^{11} - 10^{13} L_{\odot}$; therefore, by assuming the presence of LIRGs/ULIRGs among them,[20] their further studies in HCN/HCO^+ lines can provide clues about the relation between the central SF burst and AGNs in the early Universe and about early stages of galactic evolution.

Equally impressive are the results of the recent deep sky survey in the Hubble Ultra Deep Field covering a 4.5 square arcminute area [89], which were used to preliminarily conclude that SF at redshifts $z \simeq 2$ mostly occurs in massive galaxies with the stellar mass $M_* > 2 \times 10^{10} M_{\odot}$, with most SF regions being obscured by dust. This fact can suggest that DSFGs, which started evolution at $z \sim 4$ or earlier, continue evolving to at least an age of 2 Gyr. This conclusion can have critical consequences for our understanding of the entire SF history in the Universe.

3.2.2 SOFIA. The SOFIA observatory (Stratospheric Observatory For Infrared Astronomy)[21] was designed for stratospheric observations aboard an airplane. It is equipped with a 2.5 m primary mirror and a range of scientific instruments, including EXES (Echelon Cross Echelle Spectrograph), a high-, medium-, and low-resolution spectrometer in the 4.5–28.3 μm range; FIFI-LS (Field Imaging Far Infrared Line Spectrometer), a low-resolution spectrometer in the 51–203-μm range; FLITECAM (First Light Infrared Test Experiment CAMera), a 1024×1024-pixel camera in the 1.0–5.5 μm range; FORCAST (Faint Object infraRed Camera for the Sofia Telescope), a camera and low-resolution spectrograph in the 5–40 μm range; GREAT (German REceiver for Astronomy at Terahertz frequencies), a two-channel heterodyne instrument with a high resolution (up to $R = 10^8$) in the 60–200 μm spectral range; and HAWC+ (High resolution Airborne Wideband Camera), a camera and polarimeter for the 40–300 μm range.

[20] Presently, whether DSFGs are genetically connected with LIRGs/ULIRGs or are overlapping classes of objects remains an open issue.

[21] http://www.sofia.usra.edu.

3.3 Future cosmic observatories

3.3.1 SPICA. The space observatory SPICA (SPace Infrared telescope for Cosmology and Astrophysics), which is being developed by the Japanese Aerospace Agency (JAXA), is designed to operate in the 5–210 μm range. SPICA will have a primary 2.5 m mirror cooled to 6–8 K. The planned instruments include matrix cameras and medium-resolution spectrometers [90] to carry out detailed spectral surveys with the aim of studying galactic evolution, as well as observing lines of water, ice, and HD molecules in protoplanetary disks.

3.3.2 James Webb space telescope. NASA's James Webb Space Telescope (JWST)[22] will operate in the near and mid-IR range from 0.6 to 28 mcm; its 6 m primary mirror will be cooled to a temperature below 50 K.

3.3.3 Millimetron space observatory (Spectr-M). The Table lists the main parameters of the Millimetron space observatory [91–93] in the single-dish observation mode in comparison with other observatories.[23] The photometric and spectroscopic data are estimated for the 1σ sensitivity level ($\lambda \sim 200 - 300$ μm) and an exposure time of 3600 s.

The flux sensitivities of future space telescopes in the infrared and submm range are plotted in Fig. 4.

Generally, as can be easily seen from the Table and Fig. 4, the operation of new IR and submm observatories can bring breakthrough results in astrophysics and cosmology in the fairly near future. Among the future instruments, Millimetron can lead in the 20–3000 μm range because

1) the Millimetron observatory will fill the important broad 28–55 μm band, which was not covered by the Herschel and JWST telescopes, with a sensitivity higher than that of SPICA;

2) in the 50–500 μm range, the angular resolution of Millimetron will be four times as high as SPICA's;

3) thanks to the exceptionally high sensitivity, Millimetron will enable making high-resolution photometric images much faster than other instruments operating at the same wavelengths (for example, SPICA);

[22] www.jwst.nasa.gov.

[23] The Table presents the characteristics of observatories comparable to Millimetron. In particular, it does not include the Planck telescope — a dedicated mission aimed at performing an all-sky survey with a relatively low angular resolution not exceeding $45''$ at the shortest wavelengths. In addition, the Planck mission carried out sky observations solely in the scanning mode and was not able to point at the individual sources. Information about other projects, for example CALISTO, is still insufficient for inclusion in this Table.

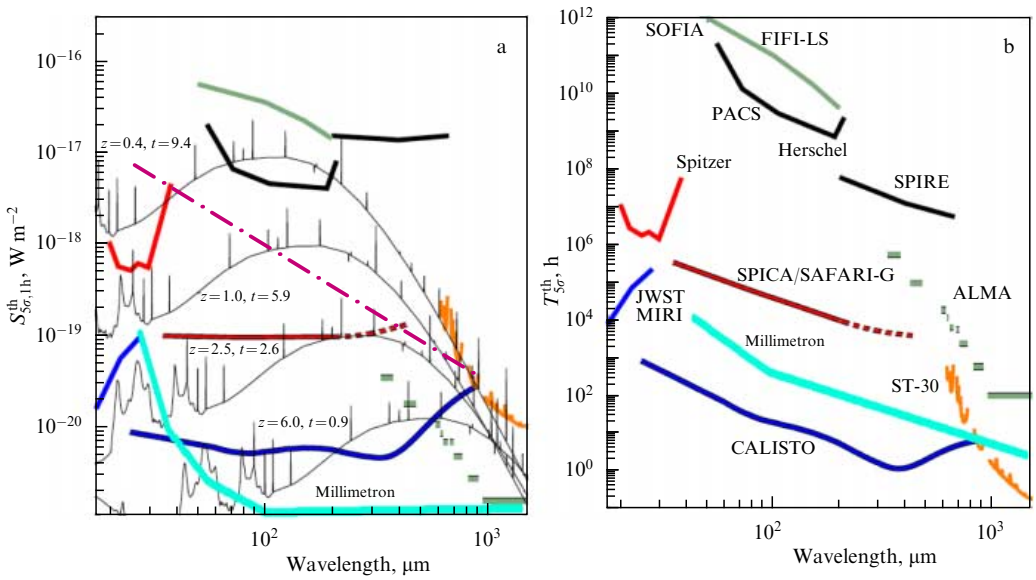

Figure 4. (Color online.) Comparison of the Millimetron flux sensitivity to other IR and submm telescopes. (a) The sensitivity threshold $S^{\rm th}_{5\sigma,1\rm h}$ for the exposure time 1 h and spectral resolution $R = 500$. The thin curves show the characteristic spectra of galaxies with the luminosity $10^{12} L_\odot$ at different redshifts z and the corresponding ages t of the Universe (in bln years). Different colored curves relate to different spacecraft shown in panel (b) near curves of the same color. The violet dashed-dotted curve shows the sensitivity of an ideal heterodyne spectrometer with the quantum limit ($T_{\rm sys} = h\nu/k$) and a bandwidth of 10 km s^{-1}. (b) The exposure time $T^{\rm th}_{5\sigma}$ needed to perform a 'blind' spectral survey with a sensitivity of 10^{-19} W m^{-2} and the spectral resolution $R = 500$ with the number of spatial rays of the spectrometer and the instantaneously observed bandwidth taken into account. The closest rivals of Millimetron are: SPICA, the US 5 m telescope project CALISTO, and the hypothetical ground-based high-altitude 30 m submm telescope ST-30 [94]. SFARI-G (SPICA Far Infrared Instrument) is an FIR device on SPICA, MIRI (Mid-InfraRed Instrument) is a mid-IR device on JWST. (Other acronyms are specified in the text.)

4) a similar conclusion can be made with regard to spectral measurements, including in the high-resolution spectroscopy mode, which enables observations of high-redshift galaxies up to $z = 1-2$ with a relatively short exposure time;

5) the 10-meter aperture of Millimetron will allow obtaining breakthrough results in such fields as the evolution of galaxies and their SFRs, including the evolution of galaxies with active nuclei and central SF bursts, and the solution to the problem of the possible relation between them and LIRGs and ULIRGs.

4. Dust and gas in galaxies

In recent years, our knowledge of the gas distribution in galaxies has changed significantly. Evidence appeared that interstellar (gaseous) galactic disks extend much further both radially and perpendicularly to the stellar disk. Recently, data were obtained that intermediate halos beyond the 30 kpc distance from the galactic centers transform into extended circumgalactic gaseous coronae, which apparently represent a mixture of the gas ejected from the interstellar disks and the gas accreted from the inter-galactic space. Such coronae can extend to 150–300 kpc, i.e., about the virial galactic radius determined as $M_{200} = (4\pi/3)\, 200\rho_{\rm cr}(z)\, R^3_{200}$, where $\rho_{\rm cr}(z) = 3H^2(z)/(8\pi G)$ is the critical density of the Universe, $H(z)$ is the Hubble constant, R_{200} is the virial radius, and G is the Newton gravity constant. Inside a volume with the radius R_{200}, the mean total density (including baryonic and nonbaryonic (dark) matter density) is about 200 times the critical density of the Universe [95].

Galactic evolution is governed by a complex system of feedback between the stellar and gas components. Dust is a necessary link because it provides energy exchange in the gas, determines its ability to transform into the molecular form, and determines its opacity. Observations of the proper IR dust emission provide information on dust heating sources, i.e., on *how galaxies work*. On the other hand, sources whose optical and UV emission is obscured by dust can be visible in the IR band (especially in the FIR and submm ranges), where the dust opacity is much lower. This enables detailed studies of *what the galaxies are made of*. Good illustrations of the potential of the submm observations for understanding how galaxies work can be found in [96, 97].

Dust is the main agent determining the interstellar gas thermodynamics. It ensures the transformation of the radiation energy into thermal gas energy and stimulates the molecularization of atomic gas and ultimately SF from gas. The very existence of molecular gas in the ISM is due to the presence of dust: molecular kinetics in the ISM starts from H_2 molecules, which, because of their zero dipole momentum, can form only in $H + H$ collisions in the presence of a third body, like a dust grain in the ISM ($2H +$ dust grain $\rightarrow H_2 +$ dust grain), and H_2 molecules further stimulate all chemical reactions.

Generally, the analysis of nearly every phenomenon in the ISM requires the knowledge of dust properties in some form. Therefore, explaining dust transformations in the Galaxy is one of the key problems in ISM physics and astrophysics in general. It can be fully addressed only using IR and submm observations, because extinction and reddening observations in the optical range do not provide information about its thermal state. Moreover, observations of extinction and reddening of external radiation sources suffer from observational bias to some extent because some dusty structures may not be crossed by the line of sight.

4.1 Cold dust in interstellar galactic disks

4.1.1 Molecular clouds and star-forming regions. Star formation is one of the key problems in the physics of galaxies that

requires FIR and millimeter observations. The SF process is interesting and important in and of itself because it largely determines the properties of stars in the Universe, stellar light and chemical production, and the powerful energy release in stellar explosions. Essentially, the very possibility of observing the Universe is due to SF processes. Therefore, understanding the phenomena leading to SF is of key significance.

The contraction of rarefied (diffuse) atomic interstellar hydrogen into molecular clouds immediately precedes SF. In the last few years, it became clear that SF is determined by a cascade of complex nonlinear processes spanning the scales from several tens of kiloparsecs to 0.1–1 pc at the end of the cascade, where protostellar condensations start forming.

The hierarchical process begins with accretion of the circumgalactic gas and satellites onto the galactic disk and its radiative cooling and recombination. On scales of a few kiloparsecs, the accreted gas is mixed with the interstellar HI gas, stimulating instabilities leading to molecular cloud formation (on scales of a few tens to hundreds of parsecs), fragmentation in molecular clouds, and the formation of protostellar nuclei (on scales of 0.1–1 pc) [98].

To some extent, only the initial and final stages of this process can be explained, and the entire sequence of phenomena (the characteristic times, scales, instability features, etc.) remains largely undetermined. It is quite natural to assume that each of these phenomena generates a characteristic emission: for example, molecular cloud formation is accompanied by the compression of the diffuse atomic gas and the HI $\rightarrow$ H_2 transition, with the cooling mainly due to excitation and subsequent radiation in the CII (158 μm) and CI (370 and 609 μm) fine structure lines.

Further contraction and fragmentation of molecular clouds is controlled by gravity and heat removal in rotational molecular lines, including the $\lambda = 2.6$ mm CO(1–0) line. For this reason, one of the key objectives of submm astronomy is SF diagnostics. Even the initial elements of this cascade are visible in the FIR and submm ranges. Indeed, the cooling of accretion flow during its interaction with the interstellar gas disk is determined by emission in the oxygen [OIII] 88 μm and nitrogen [NII] 122 and 205 μm fine-structure lines. Their ratio can be used to probe the transitional processes in gas with a temperature $T = 10^4 - 10^5$ K [99].

The further evolution of molecular gas includes the following stages: gravitational contraction of early protostellar objects (class 0);[24] the initial stages of protoplanetary disk formation; the dynamics of angular momentum redistribution and other details of cloud transformation into a protoplanetary system that should lead to spectral deformations; and the appearance of the short-wavelength part in the mid-IR range due to the young protoplanetary disk heating, with the subsequent 'heating' of the spectra at later evolutionary stages (i.e., the appearance of near-IR emission from young protostellar objects [101]). Therefore, the most intriguing part of star and circumstellar disk formation, including the transformation of the collapsing molecular cloud into a protostar, is likely to be 'scanned' in detail by the submm observations.

In addition to the submm continuum, the spectroscopy of molecular lines (CH, OH, H_2O, etc.), also emitted in the FIR and millimeter range [102], can be important (see also [91]). This is confirmed by 'synthetic' observations[25] of class 0 Keplerian protostellar objects by ALMA in the ^{13}CO, $C^{18}O$, and HCO^+ spectral lines [103]. The main conclusion is that under optimal conditions, the ALMA observations enable detections of protoplanetary disks at very early formation stages. Unfortunately, the standard ALMA resolution of $\sim 0.1''$ allows disk scanning only beyond 50 astronomical units (a.u.)[26] from the central protostar, while it is inside this central region where the main emission can be produced at the initial disk formation stage. However, cold dust emission with a temperature $T_d \leqslant 20$ K can also be informative.

The first results in this field have been rather modest so far: even for one of the SF regions closest to the Sun in the molecular cloud Cam I (containing young protostellar objects at initial stages), within the ALMA angular resolution $r \simeq 300$ a.u., the dust emission at 3 mm turns out to be below the 5σ flux sensitivity threshold [104]. In other nearby SF regions, the preliminary data suggest evolutionary growth of the protoplanetary disk near low-mass protostellar objects [105].

At scales larger than the dense cores of molecular clouds, where protostellar objects and disks have already started forming and conditions for dense core formation are likely to emerge, the first results obtained in the FIR by the Herschel observatory were surprising. It turned out that the 'preparation' of the molecular gas for SF begins with the formation of giant filamentary structures — strips, which in some cases demonstrate signatures of longitudinal fragmentation into the subsequent protostellar seeds [106].

The mass distribution function of such seeds $\Delta N/\Delta(\log M)$ is qualitatively similar to the initial stellar mass function, although it is shifted by almost one order of magnitude toward higher masses in some cases (in the Aquila molecular cloud) and toward smaller masses in other cases (in the Polaris molecular cloud) (see Fig. 2 in [107] and also [108]).

Observations of filaments in the $C^{18}O$(1–0), $C^{18}O$(2–1), and N_2H^+(1–0) molecular lines demonstrated the existence of two regimes characterizing the dynamical state of the filaments: gravitationally unbound and gravitationally bound (Fig. 5c) [109]. The tilted straight line in Fig. 5e corresponds to the relation $D_J = 2\sigma_t^2/(G\Sigma_0)$, where $\sigma_t = (\sigma_{nT}^2 + \sigma_T^2)^{1/2}$ is the full velocity dispersion including the nonthermal ('turbulent') and thermal components, $\Sigma_0 = \mu m_H N_{H_2}^0$ is the surface density across the filament, μ is the molecular weight, and $N_{H_2}^0$ is the column density across the diameter [110–112].

The filaments are embedded very deeply into molecular cloud interiors. Figure 6a shows the multicolor gas distribution in the Vela molecular cloud, in the very central part of which a young protostellar object can be seen illuminating the entire nebula. Fig. 6b shows structures in this nebula with filaments corresponding to specific extinction values $A_v = 25$, 50, and 100, which are respectively colored in light blue, blue, and violet. In the regions with maximal extinction with the column number density clearly exceeding the critical Jeans value, protostellar sources that correspond to higher dust emission temperatures are localized. Figure 6c presents the

[24] In 1987, Lada proposed the classification of protostellar sources by their IR spectral slope $\alpha \equiv d \log \lambda F_\lambda / d \log \lambda$ ($\lambda = 1-20$ μm): Class I with $0 < \alpha < +3$, Class II with $-2 \lesssim \alpha \lesssim 0$, and Class III with $-3 < \alpha \lesssim -2$. Class 0 includes cold objects without the $\lambda = 1-20$ μm continuum [100].

[25] That is, numerical simulation of observations compatible with the technical characteristics of the observatory.

[26] One a.e. is the mean distance between the Sun and Earth.

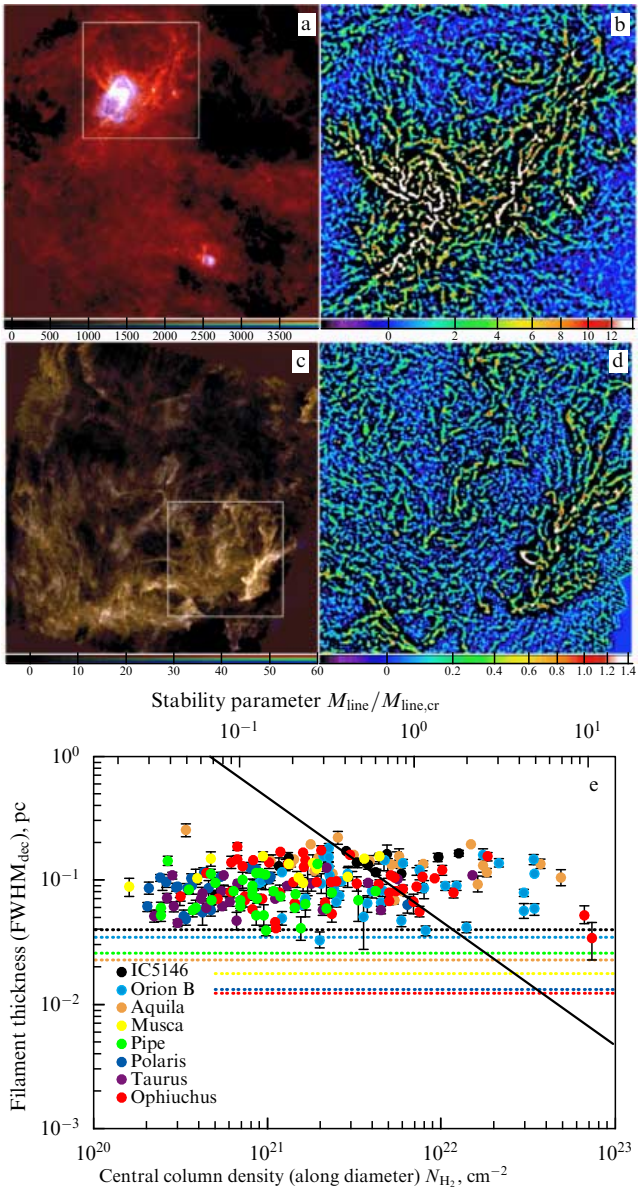

Figure 5. (Color online.) (a) Composite three-color image of the Aquila cloud, field size 3° × 3° (physical size 15 pc for the cloud distance 260 pc); 350 μm emission is shown in red, hotter regions emitting at 160 and 70 μm are respectively shown in green and blue (see the color scale under panel b). (b) High-contrast decomposition of the gas distribution [106] emitting in the 350 μm band from the cloud region shown in panel a by the white square. The color scale at the bottom shows the intensity in units MJy sr^{-1}. (c, d) The same as in panels a and b for the Polaris cloud (physical size 9 pc for the cloud distance 150 pc). (e) Relation between the column density along a filament and its Jeans length corresponding to the transition to gravitational instability, $\lambda_J = c_s^2/(G\Sigma_0)$, where c_s is the sound velocity in the filament and Σ_0 is the central surface (column) density. Symbols in different colors show observational values of the relation between the cross size of a filament and the column density along its diameter for different clouds specified in the legend. The tilted straight line shows the gravitational instability boundary of thin cylinders: observed points to the right are in the gravitational instability region (from [109]).

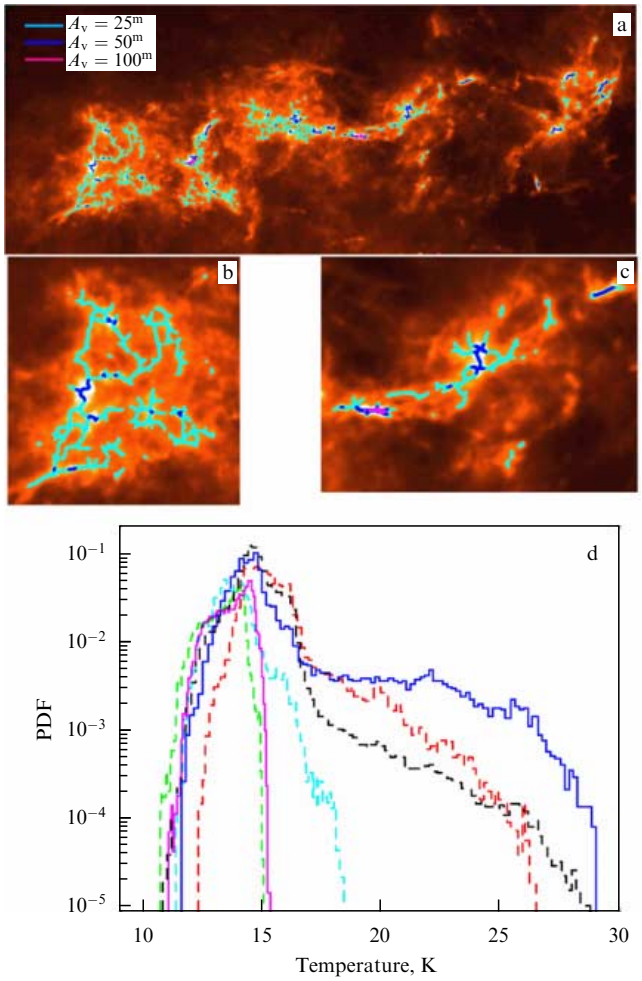

Figure 6. (Color online.) (a) Three-color image of the density distribution in the SF region in the Vela nebula, including the filamentary structure shown in light blue, blue, and light-violet in accordance with increasing density for the respective stellar magnitudes $A_v > 25$, 50, and 100. Five regions are clearly distinguished (from right to left): northern (N), central ridge (CR) with the bright protostellar source, central nest to the right of the protostellar source (CN), southern ridge (SR), and southern nest (SN). Separately shown are the brightest (b) southern and (c) central regions of the nebula. (d) Normalized temperature distribution (probability density function, PDF). The red curve corresponds to region N, blue to region CR, light blue to region CN, green to region SR, violet to region SN, and black to the entire SF region shown in panel a. The central part of the cloud shown in blue generally exhibits a flat bimodal distribution (the bimodality is due to dust heating in the ionized gas zone). The southern part of the cloud (red dashed line) shows a narrower (more homogeneous) distribution [113].

dust temperature distributions in different regions of the cloud, starting from the north part (the right-hand part of Fig. 6a). Clearly, the temperature distributions are broad or two-peak exactly in the protostellar source localization regions. Farther away from the sources, the dust is cold.

Thus, even active SF regions contain a large amount of cold dust with the mean temperature $\langle T_d \rangle \leqslant 20$ K. The Vela cloud example suggests that the coldest dust ($T_d \simeq 10$ K) is present everywhere in SF regions, both in extended filaments and inside prestellar condensations [113]. From this standpoint, SF regions in our Galaxy and other galaxies are of great interest for submm astronomy. Moreover, the cold ($T_d \simeq 10$ K) dust with the number density $n \geqslant 10^5$ cm^{-3} and the temperature $T \leqslant 10$ K is undoubtedly also present in dense cores of molecular clouds, where protostellar condensations and the protoplanetary disks surrounding them form. A significant advantage of the FIR and submm observations of such regions over those in the near- and mid-IR ranges is the possibility of more reliable measurements of the density and temperature profiles and the opacity coefficient in the deepest protostellar core interiors [114].

Of great interest from this standpoint, and for understanding the subsequent stages of the formation of protoplanetary disks and their chemistry in particular, is the molecular spectroscopy of the molecular cloud cores and SF regions, because the 850 μm — 3 mm range is highly populated with molecular lines and is therefore very informative. However, the molecular spectroscopy of SF regions is a separate topic beyond the scope of this review.

The new SF concept, suggested by Herschel observatory results, at first glance appears to be an alternative to the widely known trigger SF scenario and clearly requires further detailed observational studies of the filamentary structure formation and dynamics up to the emergence of protostars and protoplanetary disks. However, it is pertinent to note another fact discovered by the Herschel telescope, which allows us to look at the trigger SF in a different way. Namely, studies of warm and cold dust near the ionized HII regions M16, RCW 120, and in the Rosetta and Vela C clouds revealed wide non-Gaussian hydrogen column density distributions $f(N_{H_2})$ of dust structures, sometimes with two peaks, typically demonstrating a pronounced decrease at low column number densities $N_{H_2} < (0.3-3)\times 10^{21}$ cm^{-2} and a broad, flatter behavior at large $N_{H_2} > (1-10)\times 10^{21}$ cm^{-2} [115]. This can be explained by the effect of a type-D ionization front: on the one hand, low-density gas regions are easily ionized by the Lyman continuum of central stars; on the other hand, the mean free path of Ly_α quanta is shorter in denser regions, and the shock preceding the D-front induces the subsequent compression of denser regions. Therefore, the classical trigger SF scenario is supported here [116–122]. An additional element to the trigger SF, which appears here in the form of filamentary structures, is supersonic turbulence and related quasi-one-dimensional caustics [123, 124]. The shocks acting on the filaments stimulate gravitational instability.

Therefore, the dust distribution suggests that the highly efficient SF process stimulates the appearance of positive feedback, namely, leads to the dynamical regime (kinematics, spatial gas distribution, and physical gas properties) favoring new SF regions to emerge. Generally, submm and millimeter observations of emission from the coldest interstellar gas regions enable studying new features of SF and understanding the SF phenomenon from a novel standpoint.

4.1.2 Origin of molecular clouds. *The time scale of molecular gas.* The determination of the lifetime of molecular clouds and the related question of their formation is a fundamental problem in SF physics.

Despite intensive research, the issue remains open: there are observations indicating both short (10–30 Myr) and long (> 100 Myr) time scales.

Details of the physical mechanism forcing interstellar atomic hydrogen to transform into molecular gas are still under discussion, although it is generally clear that because the gas density is higher in spiral galactic arms than between them,[27] the contraction of gas in the arms is more efficient than in the interarm space.

Modern hypotheses are based on two classic concepts. The first assumes that the spiral density wave stimulates radiative gas cooling, the fast HI $\rightarrow$ H_2 transition, and the appearance of giant molecular clouds and initiates the SF process in them with the subsequent cloud destruction by the energy release from massive stars [126–128]. The alternative hypothesis assumes that the HI $\rightarrow$ H_2 transition occurs permanently, and hence molecular clouds are present both in the arms and between them, the only difference being that the clouds grow up to giant sizes in the arms and SF mainly occurs in such clouds [129–131]. A clear observational distinction between these scenarios is that in the first case the molecular gas is observed only in spiral arms and in the second case, both in the arms and between them.

Early observations of the spatial distribution of galactic molecular gas were rather supportive of the first scenario more (see, e.g., [132–134], and a historical review in [131]). On the other hand, interferometric OVRO (Owens Valley Radio Observatory) observations of CO molecules between the arms of the M51 galaxy favored the second scenario [135] (Fig. 7).

However, the observational identification of signatures of one scenario or another is hampered by instrumental effects that complicate reliable interpretation, in particular due to the loss of spatial distribution details on small scales during radiointerferometric observations with fewer than 10 dishes (see the discussion in [136]). A careful analysis of high-quality images of M51 obtained by the CARMA (Combined Array for Research in Millimeter Astronomy) observatory and single-dish observations with the NRO45 telescope (45 m Nobeyama Radio Astronomy telescope) discovered a large amount of molecular gas between the arms [136]. This result is confirmed by interferometric observations by PdBI (Plateau de Bure Interferometer) and by the 30 m dish of the IRAM-30 telescope (IRAM from the French Institut de radioastronomie millimétrique) [137]. From this standpoint, the improvement in the image quality is critically important for the correct choice of the atomic-to-molecular gas transformation model.

Similar observations of the HI $\rightarrow$ H_2 transition in our Galaxy were recently reported in [131]. One of the principal difficulties of observations of the physical state of gas in the Galaxy is related to the duality in the kinematic distance to a gas cloud as derived from the Doppler shift of spectral lines (the 21 cm HI line for the atomic gas, the rotational CO(1–0) 2.6 mm line typical for the molecular gas). The problem is that the line of sight along the galactic interstellar disk crosses the circle (or the cylindrical surface, if the line of sight is tilted to the galactic plane) of a given radius with the corresponding rotational velocity twice (see, e.g., Fig. 1 in [138]). Two equal gas volumes located at different distances from the Sun have the same radial velocity component. This sometimes leads to errors in determining the spatial gas distribution and, consequently, to an error in estimating the molecular hydrogen fraction in some parts of the Galaxy. This, in particular, explains the difference in the molecular fraction radial density profiles in the 4–8 kpc region reported in [139, 140].

In recent paper [131], this duality is overcome using the following simple approach: the analysis of the molecular hydrogen fraction $f_{mol} = \Sigma_{H_2}/(\Sigma_{H_2} + \Sigma_{HI})$ was performed in coordinates "galactic longitude (l) — radial velocity (v)" without recalculating this distribution to heliocentric distances; here, Σ_{HI} and Σ_{H_2} are the respective surface mass densities of the atomic and molecular hydrogen.[28] This allows

[27] This is not a large difference, about two times [125]; nevertheless, it can be significant, for example, because radiative processes determining the thermal state of the gas are proportional to the density squared.

[28] The mass surface densities are defined by integration over the galactic latitudes b in the range $b < |30°|$.

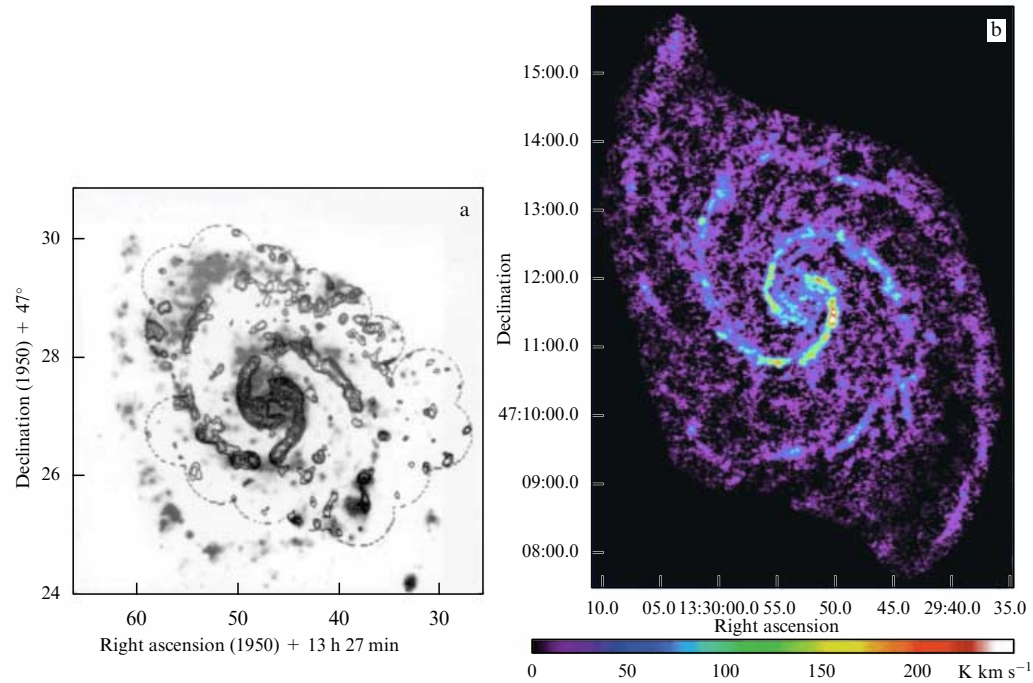

Figure 7. (Color online.) (a) CO map (contours) superimposed on the H_α map (in gray) of the M51 galaxy obtained in [135] by the ORVO observatory. (b) For comparison, shown is the CO map of the same galaxy obtained in [136] by combining CARMA and NRO45 observations.

determining both the radial galactic distribution f_{H_2} and variations of f_{H_2} in the gas in and between the arms. Because the arm tangents are clearly distinguished in $l-v$ diagrams and, as in evident from Fig. 8, the dispersion in f_{H_2} in the tangents is little different from the dispersion in other directions, it is natural to assume that this dispersion reflects differences between the fractions of f_{H_2} in the arms and between them [131]. As a result, it is concluded that the azimuthal variations of f_{H_2} (and hence variations in passing from the arms to the interarm medium) are less than 20% in the molecular-gas-dominated region within $R \leqslant 6$ kpc. Beyond the molecular disk, for $R \geqslant 6$ kpc, these variations increase to $\sim 40-50\%$, which is apparently related to the mean gas density decrease in the outer parts of the disk. Therefore, molecular clouds are more easily destroyed by active stars. This conclusion is in agreement with the fact that in galaxies dominated by atomic gas, molecular hydrogen is typically not observed in the interarm space, which suggests a short timescale of molecular clouds, $\sim 20-30$ mln years [141].

At the same time, there have been recent attempts to map the molecular fraction distribution based on the HI and H_2 density determination in the Galaxy, $\bar{f}_{H_2} = \rho_{H_2}/(\rho_{HI} + \rho_{H_2})$ [142], using data [140] taken from the same atomic [143–145] and molecular [132] gas surveys that were used in [131]. The conclusion on the difference between spatial variations of the molecular gas fraction in spiral arms and the interarm space differs from that made from estimates inferred from the HI and H_2 *surface* density measurements. For example, it was shown that at galactocentric distances $R = 6-10$kpc, the $\bar{f}_{H_2}$ maps clearly demonstrate a spiral structure. Beyond this region, the tendency of molecular gas to concentrate primarily in spirals is not seen: in the inner regions because the difference in concentrations is smoothened by the molecular gas dominance, and in the outer regions because the atomic gas dominates the disk as a whole. The crossing time of the interarm space ranges from several

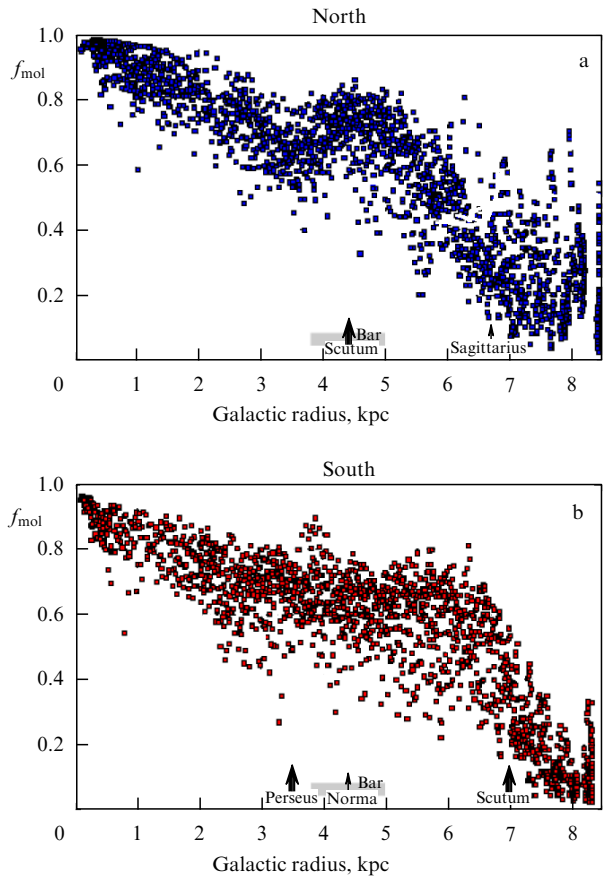

Figure 8. Molecular hydrogen fraction f_{mol} in (a) the northern and (b) the southern parts of the galactic interstellar disk [131]. Arrows show the location of tangents to the known spiral arms; other parts of the arms are distributed over all radii. Thick arrows point to the enhanced stellar content and related gravitational potential enhancement. The dispersion of f_{H_2} at each fixed radius apparently reflects variations in the molecular gas fraction in the arms and interarm space [131].

hundred Myr to 1 Gyr in the $R = 6-10$ kpc region, and it therefore follows that the upper bound on the lifetime of molecular clouds is several hundred Myr. We emphasize that the approach in [146] suffers from the aforementioned velocity degeneracy effect.

One more uncertainty factor in molecular hydrogen observations in galactic spiral arms is the observational bias due to the molecular gas being detected by emission lines of dipole molecules, such as CO. Such molecules are destroyed by the external UV radiation more easily than molecular hydrogen H_2. This is because during the hydrogen molecularization, a self-shielding effect arises in hydrogen-dominated gas: the inner parts of molecular clouds are protected from dissociating UV emission by H_2 molecules in the outer parts of the cloud [147]. As a result, part of the H_2 in the ISM can remain undetected in the CO lines [148, 149]. This effect, referred to as the 'CO-dark gas' (see the discussion below), can lead to clouds with certain sizes (optical depths) being essentially molecular (i.e., consisting of mostly H_2), but unseen because dipole molecules, such as CO, are still absent there. With the last fact taken into account, it is possible to assume that even when the molecular gas is observed only in spiral arms (as, e.g., in [142]), it can also be present in the interarm medium, but in the form of sufficiently rarefied and transparent small-size clouds where CO molecules are dissociated by the external UV radiation. From this standpoint, the absence of the interarm molecular gas can only be a necessary but not sufficient condition for the first scenario with the short MC time scale.

IR observations can be helpful in this case because dark molecular clouds can be observed by dust emission. Indeed, observations of the M51 galaxy by the JCMT and Spitzer telescopes revealed the presence of interarm emission both in the CO(3–2) lines (although with a low angular resolution of $\sim 10'' \simeq 600$ pc, which is much larger than the cloud size) and in the IR range from tiny dust grains (polycyclic aromatic hydrocarbons, PAHs) at 8 μm, as well as from warm dust at 24 μm [150] (Fig. 9). However, due to a low spatial resolution, these observations can be consistent with both long and short time scales.

A counter-example is the M33 galaxy with a very weak and amorphous spiral structure [151] (Fig. 10). The molecular (CO) gas is represented there by weak fragmentary emissions from the spiral arms, which most likely suggests their short time scale, although, because of the low density of the clouds, the inhomogeneous CO emission conversion into the H_2 mass can be significant. It is also impossible to rule out that a certain fraction of H_2 molecular clouds can be transparent to CO-destroying radiation.

The FIR and submm ranges can be even more favorable for studies of the transformations HI $\leftrightarrow$ H_2 in the ISM of galaxies. First of all, this can be seen as excess emission from dust compared to the standard value for the hydrogen column density $N = N_{\rm HI} + 2N_{\rm H_2}$, because molecular clouds with a CO deficit do not contribute to H_2. Such an excess was generally discovered in the Planck HFI (350 μm–2 mm) all-sky survey jointly with the IRAS data at 100 μm [152] and was related to dark molecular gas. The uncertainty here can be due to the dust temperature variations, which, according to [153], can be significant, ranging from 14 to 25 K.

In the FIR and submillimeter bands, there are also good prospects for identifying and probing the unseen molecular gas in spectral lines of various atoms and ions.

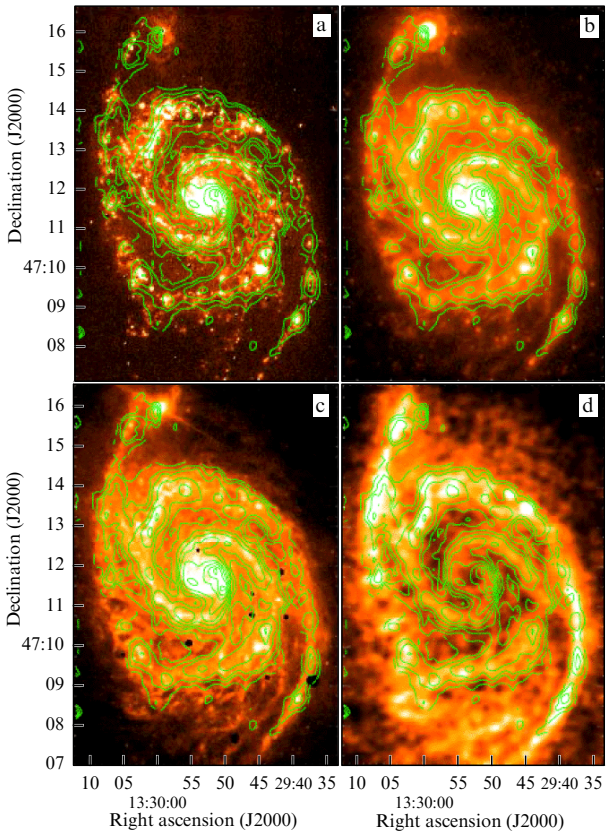

Figure 9. (Color online.) CO maps (contours) superimposed on emission maps of (a) H_α, (b) 24 μm, (c) 8 μm from polycyclic aromatic hydrocarbons, and (d) 21 cm HI in the M51 galaxy [150].

For example, the fine-structure lines of atomic and single-ionized carbon are known to fall in the FIR spectrum: [CI] ($\lambda = 370$ and 609 μm) and [CII] ($\lambda = 158$ μm). Clearly, in the region of HI $\leftrightarrow$ H_2 transitions, the ionization state of carbon depends on the thermal and ionization states of the gas and, generally, on its evolutionary state. Under these conditions, it is natural to expect that the CII-to-CI ratio can characterize the gas state in the HI $\leftrightarrow$ H_2 regions, including the molecular gas fraction (see the discussion in [154]). This is confirmed observationally [155] by searches for dark molecular gas by the Mopra Radio Telescope (Australia) as part of the CO survey in the south galactic plane, and by the HEAT (High Elevation Antarctic TeraHertz) telescope in the Antarctic in the galactic ISM atomic carbon survey: near the molecular clouds, the [CI]/^{13}CO ratio increases by about 50%, and the [CI]/HI ratio decreases by $\simeq 10\%$. The dark molecular gas can be found in the Herschel telescope survey in the $\lambda = 158$ μm [CII] line [156]. The radial distribution of regions emitting at 158 μm and not emitting in the CO lines (diffuse molecular clouds) is very broad: it has a maximum at $R \simeq 7$ kpc and extends to $R \gtrsim 8.5$ kpc, where a deficit of CO was found in the interarm space [131].

CO-dark molecular gas. In molecular clouds ($n > 10$ cm^{-3}, $T < 100$ K), H_2 molecules are in the ground electron state $X^1\Sigma_g^+$, in the vibrational state $v = 0$, and mainly in the rotational ground state $J = 0$ (parahydrogen) and $J = 1$ (orthohydrogen). The excitation energy of the $J = 0-2$ transitions (parahydrogen) and $J = 1-3$ transitions (orthohydrogen) are $E_{0.2}/k_{\rm B} = 540$ K and $E_{1.3}/k_{\rm B} = 720$ K. Therefore, the population of these and higher levels is low and,

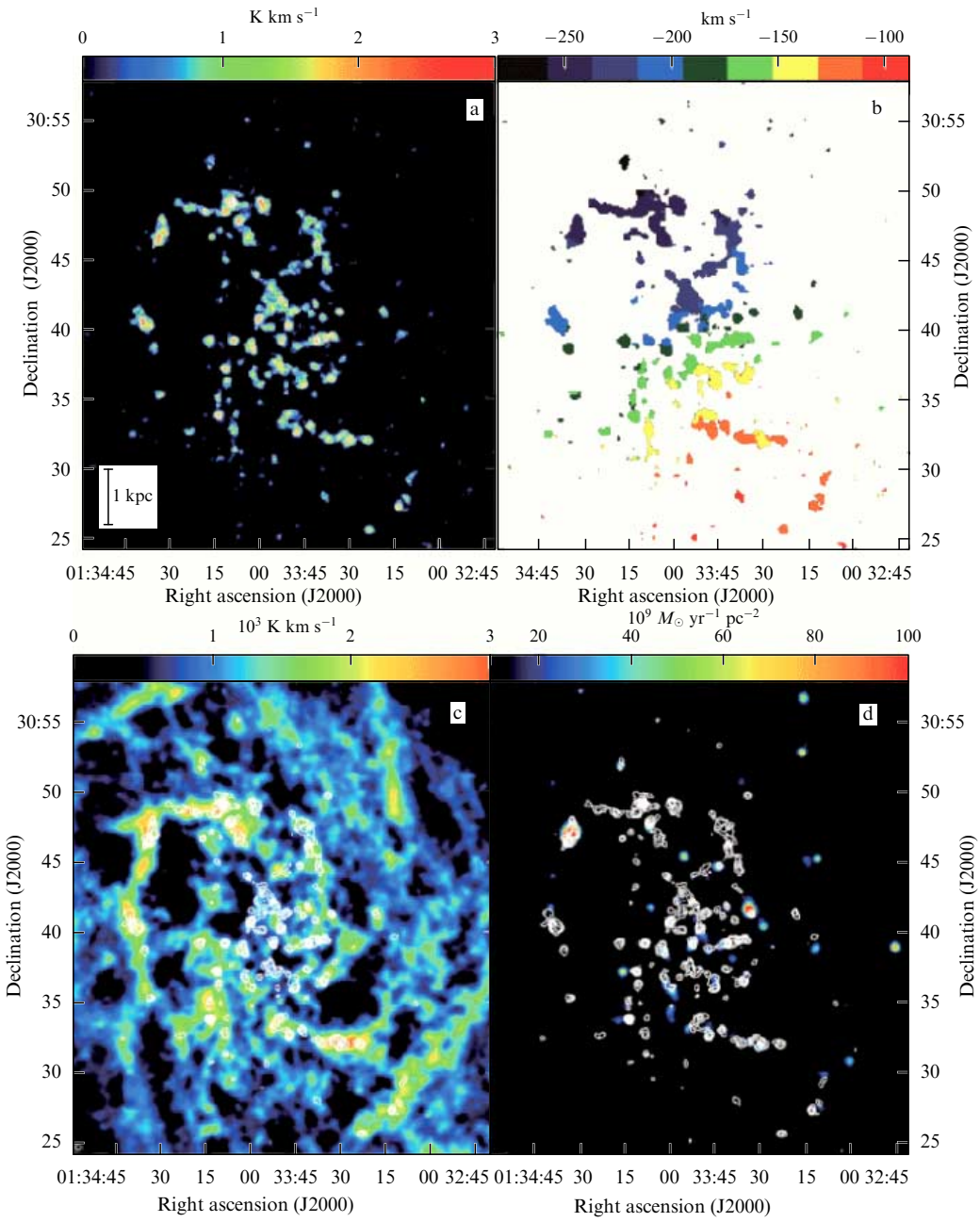

Figure 10. (Color online.) Maps of (a) the intensity and (b) the velocity field in the ^{12}CO ($J = 1-0$) line in the M33 galaxy. The field size is $30' \times 30'$, the resolution is $19''$, corresponding to the linear scale 7×7 kpc and 81 pc for the M33 distance $D = 840$ kpc. ^{12}CO ($J = 1 - 0$) intensity contours (in white) superimposed on (c) 21 cm and (d) H_α emission maps [151].

moreover, probabilities of spontaneous quadrupole transitions are as low as 2×10^{-9} and 4×10^{-9} s^{-1}. This makes the emission from H_2 molecules in molecular clouds unobservable. For the same reason, unseen is the H_2 emission for a gas with intermediate temperatures $T \sim 10^3$ K corresponding to HI transformation to the molecular H_2 gas. [29]

Therefore, low-excitation CO molecules with fast spontaneous transitions are the main tool to search for the molecular gas in the ISM and to study its dynamics. On average in the Galaxy, the following relation between the emission in the CO lines and the H_2 column density is adopted: $N_{H_2} = X_{CO} W(^{12}C^{16}O\colon J{=}1 \to 0)$, with the conversion factor $X_{CO} = 2 \times 10^{20}$ cm^{-2} (K km s^{-1})$^{-1}$. Here, $W(^{12}C^{16}O\colon J = 1 \to 0)$ is the intensity integrated over the line width [K km s^{-1}]. For the ISM in other galaxies, the X_{CO} factor is assumed to be the same as in our Galaxy, which in principle is supported by observations, albeit with significant deviations and uncertainties (see the discussion in [158]).

Thus, intensity measurements usually yield a unique estimate of the H_2 column density. The first assumptions regarding the existence of the CO-dark gas (unseen in the emission rotational CO lines) were put forward in [159], where the IRAS discovery of excessive IR emission compared to the column density of atomic HI (measured from the 21 cm line observations) and molecular H_2 hydrogen (inferred from the CO emission lines) was reported.

[29] The molecular gas in the molecular gas photodissociation zones in the immediate vicinity of young massive stars in SF regions is an exception.

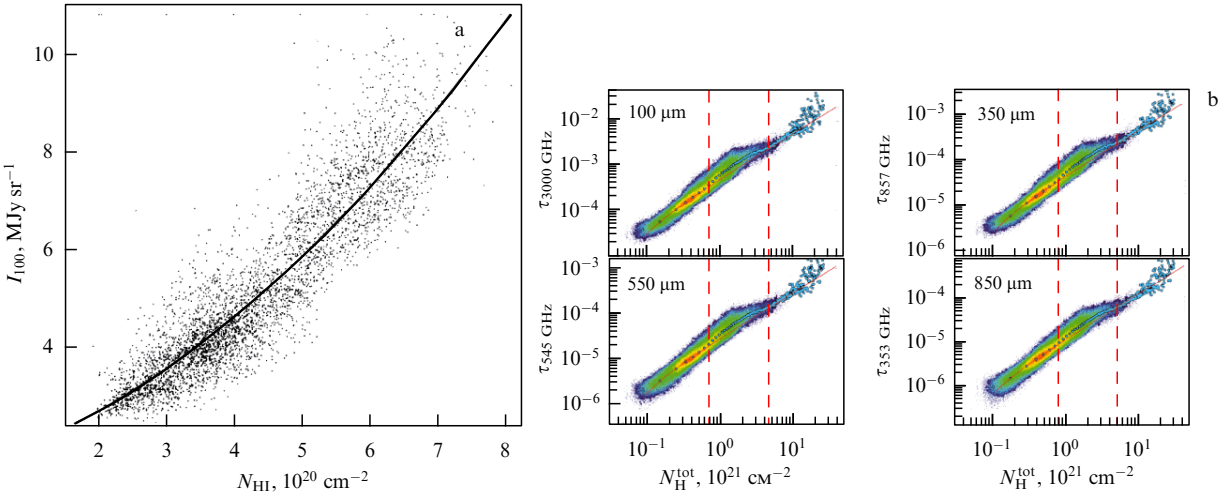

Figure 11. (Color online.) IR surface brightness I_{100} at 100 μm as a function of the $N_{\rm HI}$ column density in the 21 cm line for the molecular cloud G236 + 39 for 4400 positions in the cloud (points). An IR excess (deviation from the linear law for column densities $N_{\rm HI} > 3 \times 10^{20}$ cm^{-2}) is clearly seen, which is presumably due to a molecular hydrogen H_2 excess. The solid curve shows a quadratic dependence corresponding to the stationary equilibrium H_2 kinetics in the cloud [160]. (b) The dust extinction optical depth τ at different wavelengths shown as a function of the total hydrogen column density. The thin red line shows the standard linear relation for optical extinction. It is seen that there is a high extinction excess in the column density interval $N({\rm H}) = 7 \times 10^{20} - 5 \times 10^{21}$ cm^{-2}, which corresponds to a transitional region where some of the hydrogen is already in the molecular form, but the UV opacity is still insufficient to prevent CO molecules from destruction [161].

Later, the assumptions that H_2 molecules are more abundant than CO emission were confirmed in [160] by the analysis of IR emission and HI and CO spectra of several molecular clouds discovered by IRAS 100 μm observations. The observations revealed two remarkable features compellingly suggesting possible deviations of the $X_{\rm CO}$ conversion factor from the 'standard' mean value. A sample of 26 isolated IR clouds with angular sizes of about 1° were scanned in the 21 cm line with an angular resolution of 3′ and in the CO lines with a resolution of 1′–2′, which allowed a much more detailed picture to be obtained.

As a result, it was discovered that, first, the CO emission typically encompasses the central region with a size ranging from 2′ to 10′, whereas the IR and 21 cm emission is observed from the entire cloud. Second, for high HI column densities ($N_{\rm HI} > 3 \times 10^{20}$ cm^{-2}), a clear IR excess is observed, which, as suggested by its quadratic dependence on $N_{\rm HI}$ (Fig. 11a), can most likely be explained by the presence of molecular hydrogen in these regions.[30]

The IR emission excess at 100 μm is essentially only a reflection of the fact that the $X_{\rm CO}$ conversion factor can be significantly different from the mean value usually assumed. The physical reason for large variations of the H_2-to-CO ratio is that unlike H_2 molecules, which can provide self-shielding from the destructive radiation, CO molecules, being less abundant in the ISM, cannot maintain a significant optical depth that would withstand the destructive radiation, and cannot therefore present their destruction [162, 163].

Based on these considerations, the authors of [148] showed that the conversion factor for the galactic ISM is $X_{\rm CO} \simeq X_{\rm CO,\infty}[1 - \tau_{\rm v}(n/10^3\ {\rm cm}^{-3})^{1/2}]^{-1}$, where $\tau_{\rm v}$ is the optical depth of the cloud in the optical band, n is the gas number density, and $X_{\rm CO,\infty}$ is the conversion factor at $\tau_{\rm v} = \infty$. When integrated with the observed mass spectrum of molecular clouds [164] for the entire Galaxy, this equation yields an estimate of the total mass of the molecular gas, which is a half-order of magnitude higher than the one obtained from the CO emission. A more conservative estimate based on the direct measurements of the absorption of extragalactic X-ray emission ($E = 0.1-2.4$ keV) at high galactic latitudes ($|b| > 25°$) [165] yielded a comparable number of atomic hydrogen and H_2 molecules unseen in the CO emission.

An analysis of the thermal dust emission and γ radiation from π^0 decays arising in cosmic ray hadron collisions with protons in the ISM showed that the mass of the unseen molecular gas is comparable by an order of magnitude with the H_2 mass as inferred from the CO lines [166]. The galactic disk survey in the fine structure [CI] 370 μm line, as well as in the 21 cm atomic hydrogen line and rotational CO lines, suggested that about one third of the 'dark' molecular gas is concentrated in the transitional surface layers of the clouds [155]. Later, a detailed theory describing the CO-line-dark molecular gas was developed in [167].

The recognition that the widely used conversion coefficient $X_{\rm CO}$ from the observed CO emission to the molecular hydrogen mass is not a constant but is sensitive to many parameters of the clouds, their geometric characteristics, and UV radiation stimulated detailed studies of the relations between the CO and H_2 number densities and the development of alternative methods of molecular gas detection in the cases where the CO emission is insufficient. Naturally, such methods were associated with IR observations, and here not only the dust emission but also emissions in the fine-structure lines of atoms and ions of some elements are important.

As noted above, the transformation of atomic gas into molecular gas in the ISM should be accompanied by radiation cooling of the gas. In the temperature range of interest here, the cooling is dominated by the fine-structure lines of single-ionized and atomic carbon: [CII] ($\lambda = 158$ μm) and [CI] ($\lambda = 340$ and 609 μm). On the other hand, because atomic carbon, like CO, cannot shield itself from ionizing radiation

[30] In the stationary kinetics of the H_2 molecules on dust grains, their number density is determined by the equation $\gamma(T)\,n({\rm HI})\,n = R_0 \beta N_{\rm H_2}^{-1/2} n({\rm H_2})$, where R_0 is the photodissociation rate of molecules by the Lyman UV emission and the factor $\beta N_{\rm H_2}^{-1/2}$ describes self-shielding of the H_2 molecules in the large optical depth limit.

due to its low abundance, enhanced [CII] emission must be produced in the molecular gas regions with a CO deficit (see the discussion in Section 4.1.2). Based on this, in [168], molecular gas was discovered in SF regions in dwarf galaxies by a 10-fold excess of the C[II] 158/CO (1–0) ratio compared to the galactic value. Moreover, a 3–4-fold excess of the [CII] 158 μm/FIR 100 μm ratio in these galaxies compared to normal galaxies was demonstrated in [169].[31] Generally, it turned out that the amount of molecular H_2 gas in dwarf galaxies obtained using the 'standard' $CO-H_2$ conversion coefficient adopted for our Galaxy [170] is underestimated more than 10-fold.

Meanwhile, the issue with CO-dark molecular gas remains open. Recent Planck observations revealed the presence in the Galaxy of a significant amount (28% of the HI mass) of CO-dark molecular gas, as inferred from the IR excess in regions with $7\times10^{20} < N(\mathrm{H}) < 5\times10^{21}$ cm^{-2} (see Fig. 11) [161]. These estimates are based, however, on the simplest assumptions on the small optical depth in the 21 cm line and on the constant HI spin temperature $T_s = 80$ K, assumptions that can be too stringent considering the complex dynamical state of the ISM gas. There are quite compelling arguments that the CO-dark molecular gas can be a mere consequence of the HI mass underestimation due to the optical depth effects ignored [171, 172]. Apparently, hopes to explain the CO-dark molecular gas phenomenon can be related to FIR and submm observations of the fine-structure lines of atoms and ions, as well as of thermal dust emission.

4.2 Diagnostic of cosmic plasma thermodynamics

4.2.1 Features of the interstellar and intergalactic gas thermodynamics. Thermal properties of the ISM are determined by the energy inflow from 'external' sources: cosmic rays, X-ray emission, and the dissipation of magnetohydrodynamic motions, as well as by the photoemission of electrons from the dust grain surface caused by interstellar UV radiation and thermal energy losses in nonelastic collisions between atoms and ions, and excitation of the internal degrees of freedom with subsequent reemission of energy, which freely escapes the emission region.

As a result, in slow processes with characteristic dynamical times exceeding the heating and cooling times, an equilibrium state sets in, in which the gas temperature is a function of its density: the temperature decreases as the density increases. In a more general case of dynamical processes with a broad time scale, in the ISM of galaxies, three preferential temperatures appear: the cold gas temperature $T \lesssim 100$ K, the warm gas temperature $T \sim 10^4$ K, and the hot gas temperature $T \sim 10^6$ K. In the IGM, the hot gas can have a temperature one to two orders of magnitude higher than in the ISM. Therefore, observations of emissions responsible for the energy removal from the system can serve as an indicator of the physical state of the emitting gas.

4.2.2 Excitation temperature and line intensities. The very possibility of probing the thermodynamic state of cosmic plasma is based on the relation between the excitation temperature of an energy level in an atom, ion, or molecule and the gas number density. The excitation temperature is defined as the temperature T_x at which populations of the upper (u) and lower (l) levels correspond to the Boltzmann formula:

$$\frac{n_\mathrm{u}}{n_\mathrm{l}} = \frac{g_\mathrm{u}}{g_\mathrm{l}} \exp\left(-\frac{E_{\mathrm{u,l}}}{k_\mathrm{B} T_x}\right), \tag{1}$$

where $n_{\mathrm{u,l}}$ are populations of the upper and lower levels, $g_{\mathrm{u,l}}$ are their statistical weights, and $E_{\mathrm{u,l}}$ is the energy difference between the u and l levels. In general, cosmic plasma is not in thermodynamic equilibrium; therefore, in the simplest two-level system, in which the detailed balance between levels is maintained by collisional excitations and deactivations and spontaneous radiative transitions, the populations are related as [173]

$$\frac{n_\mathrm{u}}{n_\mathrm{l}} = \frac{g_\mathrm{u}}{g_\mathrm{l}} \exp\left(-\frac{E_{\mathrm{u,l}}}{k_\mathrm{B} T}\right)\left(1+\frac{n_\mathrm{cr}}{n}\right)^{-1}, \tag{2}$$

where $n_\mathrm{cr}(n,T) = A_\mathrm{ul}/\beta_\mathrm{ul}$ is the critical density, A_ul is the probability of radiative transitions, and $\beta_\mathrm{ul} = \beta_\mathrm{ul}(n,T)$ is the probability of collisional transitions between the levels u and l. At densities above the critical one, the level populations approach the collisional Boltzmann equilibrium. The solution of the balance equation for the two-level system results in the following relation between the excitation and kinetic gas temperature:

$$\frac{T_x}{T} = \left[1+\frac{k_\mathrm{B} T}{E_{\mathrm{u,l}}} \ln\left(1+\frac{n_\mathrm{cr}}{n}\right)\right]^{-1}. \tag{3}$$

In the simplest case of an optically thin medium, the intensity of a line with a frequency $\nu_{\mathrm{u,l}}$ is determined by the rate of spontaneous decays u → l: $A_\mathrm{ul} n_\mathrm{u}$. Therefore, it is easy to see that the line intensity ratio corresponding to transitions between levels is determined by the excitation temperature and hence by n_cr. On the other hand, $n_\mathrm{cr} = f_{\mathrm{u,l}}(n,T)$, which then offers the possibility of measuring the density and temperature of the emitting gas from the intensity ratio of different lines [174]. The most effective cosmic plasma diagnostics can be done with the lines of atoms or molecules that dominate in maintaining the energy balance from external sources and radiative losses in nonelastic collisions between plasma particles.

The radiative gas cooling is dominated, in particular, by the following species: 1) at high temperatures, by OIII ($10^4 < T < 3\times10^5$ K), Ne ions ($3\times10^5 < T < 10^6$ K), and Fe ions ($10^6 < T < 10^7$ K); 2) at intermediate temperatures, by HI, CII, and OI, with some contribution from NII ($100 < T < 10^4$ K); and 3) at low temperatures, by CI and CO molecules ($T < 10^2$ K), [OIII] (88 μm), [CII] (157.7 μm), [OI] (63.2 μm), [NII] (122 and 205 μm), [CI] (370 and 610 μm), and CO ($J = 12 \to 11, \ldots, J = 1 \to 0$) in the 300–3000 μm range. This enables the characteristic emissions from cooling agents to be used not only to probe the current state of the gas (see, e.g., [175], where the method of pressure measurements in the interstellar gas using the [CI] 370 and 610 μm line intensity ratio is described) but also to study its thermal history [176]. That all these lines fall into the mid-IR, FIR, and submm ranges makes the Millimetron mission (see review [91]) a unique tool to study these galactic and extragalactic gas problems both in the nearby and distant Universe and thus opens new possibilities of explaining phenomena in the interstellar and intergalactic medium at the 'atomic level'.

[31] Emission from photodissociation zones of molecular gas in SF regions was studied in [168, 169]; the vibration–rotational H_2 lines 1–0 S(1) (2.1 μm) were also detected, which enabled the [CII] emission to be more reliably related to a deficit or absence of CO molecules.

Because the [CII] 158 μm and [CI] 370 and 610 μm lines ensure most of the heat removal from the respective warm and cold phases [177], the galactic luminosity in these lines can be as significant as, for example, in rotational CO lines; therefore, distant galaxies at cosmological distances can be observed in these lines. Indeed, the characteristic radiative cooling rate for the interstellar gas in the temperature range $T = 10^2 - 10^4$ K, in which most of the atomic hydrogen falls, is $\Lambda_{\rm m} \sim (0.1-1)\, n\, [{\rm erg\ s^{-1}\ g^{-1}}]$ [178, 179]. For a galaxy at the redshift $z = 5$ with the gas mass $M_{\rm g} \sim 10^{10} M_\odot$, this yields $L_{\rm [CII]} \sim 10^9 - 10^{10} L_\odot$, which gives about 1–10 mJy.

Thus, lines from carbon ions can be used to probe early phases of galactic evolution. Recently, this diagnostic tool enabled very interesting and sometimes unexpected results. We consider only the most prominent examples here.

4.2.3 Dwarf galaxies in the [CII] 158 μm line. Most (by mass) of the interstellar galactic gas has the temperature $T = 10^2 - 10^4$ K; therefore, the main fraction of the energy emitted by stars is reradiated in the [CII] 158 μm line, which is why observations of this line have been widely used to estimate SFR in galaxies.

This method has recently been applied to low-metallicity blue compact galaxies (blue compact dwarf, BCD), which are interesting because by the thermal properties of their gas they can mimic early galaxies.

A feature of the [CII] 158 μm line that distinguishes it from other lines such as [OIII] 88 μm and [OI] 63.2 μm or, for example, CO(1–0), which are also used to probe physical conditions of the gas in dwarf galaxies [180], is the lower value of the critical density. This makes the [CII] 158 μm line more sensitive to the gas temperature and density variations in the ranges where it substantially contributes to the cooling. For this reason, all correlations with the participation of the flux (or intensity ratio) in the [CII] 158 μm line can demonstrate a larger dispersion than similar relations with [OIII] 88 μm and [OI] 63.2 μm lines. In any case, the bright [CII] 158 μm line together with the [OIII] and [OI] fine-structure lines are very sensitive SF indicators in local galaxies, enabling SF detection at a rate of $\sim 10^{-3} M_\odot$ per year [181].

At the same time, observations of the IR fine-structure lines in dwarf galaxies revealed an unusually high [OIII] 88 μm to [CII] 158 μm emission ratio [180–182], almost one order of magnitude higher than in normal galaxies. This fact can suggest unusual ISM properties in dwarf galaxies [183], for example, a lower metallicity of the gas or elemental abundance peculiarities, (namely, a deficit of carbon relative to oxygen). Such a deficit can be due to either evolutionary features of BCD galaxies with an excess of activity of stars with $M \gtrsim 10\, M_\odot$, or features of the ionizing radiation in the ISM. For example, this can reflect the fact that the detected IR emission in fine-structure lines is produced in compact SF regions with an [OIII] excess, as suggested by the ratio of the [CII] 158 μm emission to the total FIR emission [183]. In any case, poorly understood physical processes are behind these observations.

4.2.4 Fine-structure lines from young galaxies. The high luminosity of gas in the [CII] 158 μm line can be used to probe physical conditions in the interstellar gas of young galaxies. In the first submm observations of young galaxies ($z > 4$) with an extremely high SFR ($\sim 10^3 M_\odot$ per year), only [CI] 370 μm and [CII] 158 μm lines were detected [184–187].

ALMA observations with higher sensitivity and angular resolution gave new results. It was found, in particular, that the emission excess in the [OIII] 880 μm and [CII] 158 μm lines detected from nearby low-metallicity dwarf galaxies is also typical for the young Universe, especially at $z > 6$ [188, 189].

Of special interest here is the galaxy SXDF-NB 1006-2 ($z = 7.2$). Observations in the near-IR band carried out by the Subaru telescope [190] revealed that the emission corresponds to the $\rm Ly_\alpha$ line, and therefore SXDF-NB 1006-2 belongs to LAE (Lyman Alpha Emitter) galaxies — early galaxies with a high SF rate, in which most of the ionized photons are reradiated in the $\rm Ly_\alpha$ line. The ALMA observations of this galaxy detected the [OIII] 88 μm line at a significance level of 5.3σ, corresponding to the luminosity $L([{\rm OIII}]\, 88\ \mu{\rm m}) = 3.8 \times 10^{42}$ erg s^{-1}, while only an upper estimate was obtained for the [CII] 158 μm luminosity $L([{\rm CII}]\, 158\ \mu{\rm m}) < 3.2 \times 10^{41}$ erg s^{-1} at the 3σ level. We note that at the 3.5σ significance level, a weak [CII] 158 μm signal was detected from a distance of 2 kpc (corresponding to an angular distance of 0.4″ at $z = 7.2$) from the [OIII] 88 μm emission region. The [OIII] 88 μm emission region is overlapped by the $\rm Ly_\alpha$ emission, although resonance multiple scatterings make the $\rm Ly_\alpha$ emission region larger than the [OIII] 88 μm one.

A weak [CII] 158 μm emission or even its absence in the spatial localization of the main emission suggests a small amount of atomic gas in the galaxy SXDF-NB 1006-2. This is consistent with the fact that, due to resonance scatterings, the $\rm Ly_\alpha$ line is shifted with respect to [OII] 88 μm by $\Delta v_{\rm Ly_\alpha} = 1.1(\pm 0.3) \times 10^2$ km s^{-1}, which is smaller than in similar galaxies at lower z, which in turn can correspond to an upper bound on the atomic gas column density $N_{\rm HI} < 10^{20}$ cm^{-2} [191, 192]. This suggests that most of the gas in the galaxy is ionized; therefore, the fraction of the Lyman continuum photons ($E \geqslant 13.6$ eV) that are able to leave the galaxy and contribute to reionization, can be extremely large: in [189], this fraction is estimated to be $\sim 50\%$.

A remarkable feature of the submm spectrum of SXDF-NB 1006-2 is the absence of noticeable dust emission, especially if we recall that its interstellar gas metallicity at the upper limit can be as high as 5 to 100% of the solar one. Possible reasons underlying this finding can be discussed, but it certainly makes SXDF-NB 1006-2 different from the population of extremely luminous galaxies in the young Universe.[32]

The recent ASPECS (ALMA Spectroscopic Survey) survey of galaxies inside the Hubble Ultra-Deep Field (HUDF) confirms the significance of the submm spectroscopy of the distant Universe in fine-structure lines. The survey encompasses 212–272 GHz frequencies and thus includes [CII] 158 μm galactic emission in the redshift interval $z = 6-8$ with a sensitivity $L([{\rm CII}]\, 158) < (1.6-2.5) \times 10^8 L_\odot$ ($L([{\rm CII}]\, 158) < (0.6-1) \times 10^{42}$ erg s^{-1}) with an angular resolution of $\sim 1''$. In total, 14 candidate galaxies were found with the signal-to-noise ratio S/N > 4.5. As in the case of SXDF-NB 1006-2, none of the candidates demonstrated continuum dust emission, although the SFR in them is much lower than in SXDF-NB 1006-2, of the order of $3\, M_\odot$ per year. One of the important preliminary results of the ASPECS survey suggests a significantly larger volume number density of galaxies with [CII] 158 μm emission at $z = 6-8$ than predicted by modern models.

[32] We note that in the local Universe, there is a good spatial correlation between dust emission and Hα [193]; however, the SFR in them is rather modest: $\sim (10^{-2} - 10^{-3})\, M_\odot$ per year.

4.2.5 Distant radio galaxies. Radio galaxies at cosmological distances are interesting because their physical state is key to understanding their origin. Among these galaxies, the distant radio galaxy MRC 1138-262 ($z = 2.161$) is also interesting because its nearest surroundings are overcrowded with galaxies: they contain an excessive number of galaxies within a 1 Mpc volume [195–198]. The radio galaxy MRC 1138-262 can be the center of a cluster, as suggested by its physical and morphological features, including the enhanced galaxy concentration in its surroundings, a hot X-ray halo, and a high galactic mass [199]. The SFR in MRC 11380262 is extremely high: multicolor photometry yields $\simeq 1400\, M_\odot$ per year, one order of magnitude higher than follows from UV emissions [200]. Here, despite the high SF rate, a strong galactic wind that brings away more than $400\, M_\odot$ per year is apparently caused by acceleration from a radio jet [201].

Generally, the radio galaxy MRC 1138-262 is an extremely interesting object, and the logic of the ALMA observations is as follows: a high SFR, on the one hand, implies a high molecular gas mass and the corresponding line emissions, and on the other hand, also implies a high rate of strong shocks from supernova explosions and possible synchrotron continuum emission. Using this model, it was possible not only to detect the expected synchrotron radiation at frequencies 238.28 and 253.48 GHz and emission in lines [CI] 370 μm and CO (7–6) (with the CO(7–6)/[CI] 370 μm intensity ratio smaller than the standard value) from a relatively low-density gas ($\sim 10^2 - 10^3$ cm^{-3}) and H_2O $2_{11} - 2_{02}$ emission (pointing to the high gas density $10^3 - 10^5$ cm^{-3}) but also to unexpectedly discover (from the width and profile of the [CI] 370 μm line) a second radio-quiet component at a distance of 4 kpc from the known radio bright active galactic nucleus of MRC 1138-262. It is not ruled out that the last fact suggests the merging of two active galactic nuclei. In and of itself, this fact requires further detailed studies of emissions from the central regions of MRC 1138-262.

The properties of SF in MRC 1138-262 and its stimulating mechanisms are fraught with some uncertainties: the arbitrarily assumed solar metallicity of the gas and the presumed constant temperature $T_d = 40$ K of the emitting dust. Neither assumption seems to be fully justified. For example, one of the [CI] 370 μm emission components has a Lorentzian profile, suggesting a high optical depth in the line, which in turn allows inhomogeneous dust heating. On the other hand, with the high mean emission gas densities and short cooling times (from 10^3 to 10^4 years), it is difficult to expect effective metallicity mixing for all the gas mass $M_g \gtrsim 10^{10}\, M_\odot$.

4.2.6 'Memory' effect in the ISM and the possibility of probing its evolution. We emphasize that until recently the probing of the thermodynamic state of interstellar and intergalactic gas by IR emission from cooling atoms and ions was based on the thermal 'equilibrium' assumption,[33] i.e., on the stationary ionization state of the medium. In reality, this assumption cannot always be valid because in some cases the characteristic times of ionization processes can be comparable to the dynamical and thermal times and even exceed them. This can be easily verified by comparing the characteristic time of hydrogen recombination, $t_r \sim 3 \times 10^{13} T_6^{1/2}/n$ [s], where $T_6 \equiv T/(10^6\ \mathrm{K})$ and n is the gas number density, with the radiative cooling time in the temperature range $\sim 10^5 - 10^6$ K, $t_c \sim 10^{12}/n$ [s] [202]. A consequence of this, for example, is the possible 'mimicry' of an already cooled gas of supernova remnants with a hot gas, if its temperature is inferred from absorption lines of highly charged ions such as NV and OVI [203, 204].

The appearance of the characteristic times of thermal and ionization processes in the ISM and IGM means a transition from the thermal 'equilibrium' to an evolutionary state, i.e., to a dependence of the current state of the medium on the initial conditions. This especially relates to number densities of different ions and hence to ratios between different emission lines. Thus, they can provide direct information on the evolutionary state of the gas. In other words, thermal and ionization processes in the ISM can be regarded as 'memory devices'. This offers the possibility of studying evolution by making a single observation of the object.

For many problems of ISM physics, in particular, for dust physics, this possibility allows obtaining critical information on the processes determining the dust budget in our Galaxy and other galaxies and on features of chemical element mixing injected into the ISM by supernova explosions or by stellar winds. In particular, when probing the hot gas behind a supernova shock front, during the radiation stages of the supernova remnant expansion, the gas energy losses occur in the fine-structure lines [OIII] 88 μm, [CII] 157.7 μm, [OI] 63.2 μm, [NII] 122 and 205 μm, and [CI] 370 and 610 μm. The intensity ratios of these lines provide the fundamental possibility to determine both the evolutionary state and the elemental abundance of supernova ejecta, as shown in Fig. 12.

In the last few years, the evolutionary effects in cosmic plasma have been actively studied in the UV spectrum (see the discussion in [205, 206]). In the infrared and submm ranges, this research has not been so active, although as noted above it can be very promising.

4.3 Dust circulation in galaxies: creation and destruction of dust

4.3.1 Dust sources in galaxies. The problem of the origin of cosmic dust has recently been actively investigated. This is largely due to the discovery of dust at high redshifts, although to the same extent this research is motivated by the old unsolved problem of dust budget in the ISM (see the discussion in [207, 208]). Until recently, it was recognized that the dust grains are condensed in extended cold atmospheres of AGB (asymptotic giant branch) stars [209], which produce about $0.003\, M_\odot$ of dust per year in the galactic ISM [210]. A significant portion of the dust is deposited into the ISM by planetary nebulae. Estimates in [207] show that the corresponding dust production rate can be $\sim 0.004\, M_\odot$ per year. This is comparable to what is injected into the ISM by stellar winds from giant and supergiant stars.

The situation radically changed after the discovery of dust traces in the Ly_α-forest lines and especially after the direct detection of dust in the FIR in SCUBA observations at high redshifts ($z \sim 5-6$) [211]. This discovery initiated a number of studies exploring the possibility of dust production by type-II supernovae on a short evolutionary timescale corresponding to redshifts $z > 5$ [212, 213]. Further studies showed that the AGB stars and massive core-collapse supernovae (CCSNs) in Milky Way-type galaxies could make a

[33] Thermal equilibrium in the interstellar and intergalactic plasma is not a thermal equilibrium in the full sense: it only means a balance between sources and sinks. In the thermodynamic sense, these media are strongly nonequilibrium: they include nonthermal components, volume heating, and volume radiative energy losses.

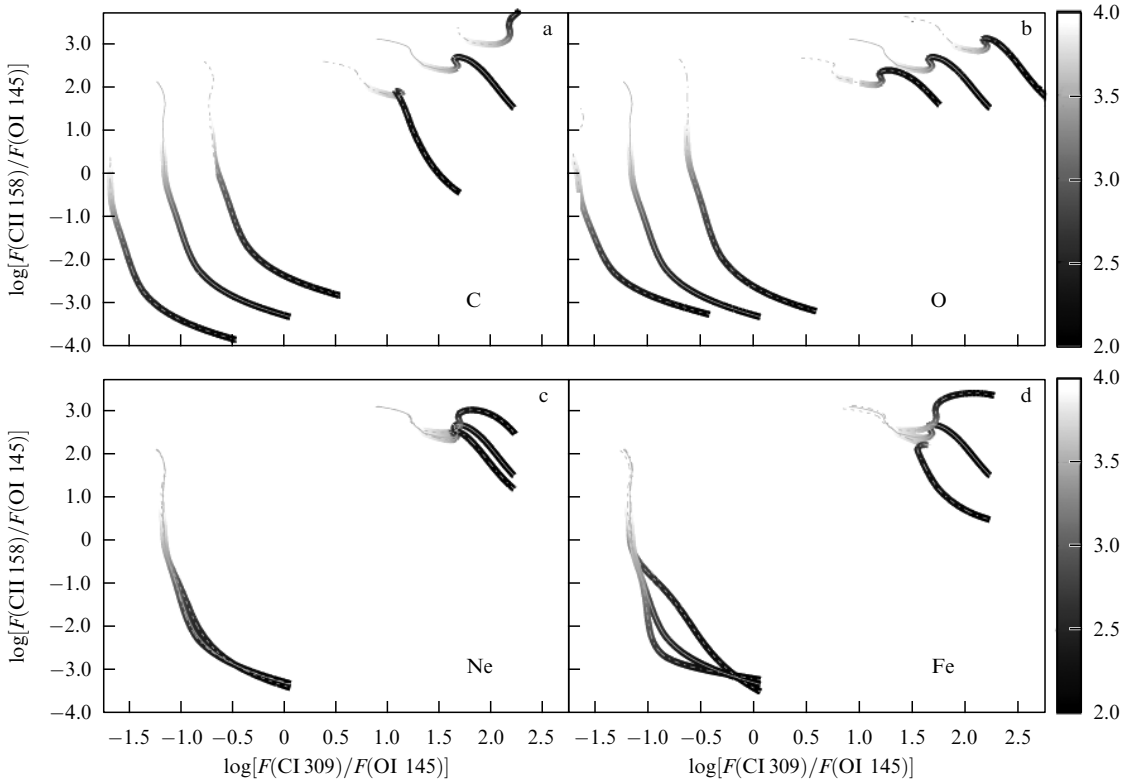

Figure 12. (a–d) Relative intensities of the fine-structure lines of atoms and ions CII 158 μm, CI 309 μm, and OI 145 μm in cooling plasma as a function of the relative abundance of carbon, oxygen, neon, and iron, respectively. The group of tracks in panels c and b corresponds to respective isobaric and isochoric processes. The middle line in each group of tracks is for the solar metallicity; the two other lines correspond to variations of the element C (panel a), O (panel b), Ne (panel c), and Fe (panel d) by −0.5 dex and +0.5 dex.

comparable contribution if each supernova produces 0.1–1 $M_\odot$ of dust [213].

However, measurements of dust in more than 20 type-II supernovae by the Spitzer telescope, the Kuiper Airborne Observatory, and the Herschel Space Telescope [214] suggested the dust mass in the range $(10^{-4}-10^{-5})\,M_\odot$, which is far from sufficient to explain the presence of dust in the young Universe, assuming that the dust production by type-II supernovae in the young Universe is as effective as in Galaxy's surroundings. The only exception to date is SN 1987A, for which the Herschel data revealed the presence of a relatively large amount of cold dust ($T_{\rm d} = 20-25$ K) with the mass $0.4-0.7\,M_\odot$ [215]. Such a large dust mass, which is several orders of magnitude higher than the mean value found in more than 20 supernova remnants, requires a detailed analysis. One possible reason could be a large amount of the circumstellar dust around the SN 1987A progenitor. This seems very plausible considering that the Herschel angular resolution $\Delta\theta > 3.5''$ is clearly insufficient to distinguish the dust produced by an explosion from the circumstellar and interstellar dust compressed by the pre-supernova wind. Observations of SN 1987A with high angular resolution in the near and far IR range by the Gemini South telescope revealed the presence of only $\sim 10^{-4}\,M_\odot$ of warm dust [216, 217]. However, recent ALMA observations at 2.8 mm, 1.4 mm, 870 μm, and 450 μm with a much better angular resolution, which enabled the separation of emission from the supernova ejecta, gave a much more optimistic estimate, according to which more than $0.2\,M_\odot$ of the dust can be produced by the supernova itself [218] (Fig. 13). This is probably one of the most exciting recent ALMA results in the field of cosmic plasma physics.

4.3.2 Anomalously large dust grains in the ISM. In recent years, the question of the limit size of dust grains has become very topical. Observations of light extinction in the optical and ultraviolet ranges constrain the dust grain size to the interval $a \in [30\ \text{Å}-0.3\ \mu\text{m}]$ (see, e.g., [207]). At the same time, over the last 20 years, observational evidence has appeared suggesting the presence of larger dust grains in the ISM. Direct measurements by the Ulysses [219] and Galileo [220, 221] spacecraft revealed the presence in the interplanetary medium of interstellar dust grains 0.3–1.5 μm in size (Fig. 14). The drastic decrease in the distribution at small masses seen in Fig. 14 is due to the limited sensitivity of mass spectrometers.

On the other hand, the rapid fall-off of the distribution function at large masses, although expected according to interstellar dust concepts [222], seems to be exaggerated. Apparently, it is due to the observational bias caused by the fact that the charge-to-mass ratios decrease as the mass increases and the Larmor radius of dust in the interstellar magnetic field increases; therefore, large dust grains are captured into orbits in the inner part of the Solar System, where Galileo and Ulysses operated [221].

Radar observations of micrometeorites at NAIC Arecibo (National Astronomical and Ionosphere Center at Arecibo) (USA) discovered about 3000 micro particles with a radius of about 1 μm decelerating in Earth's atmosphere and measured their velocities [223]. The loop-back trajectory integration enabled recovering particle trajectories and their kinematical

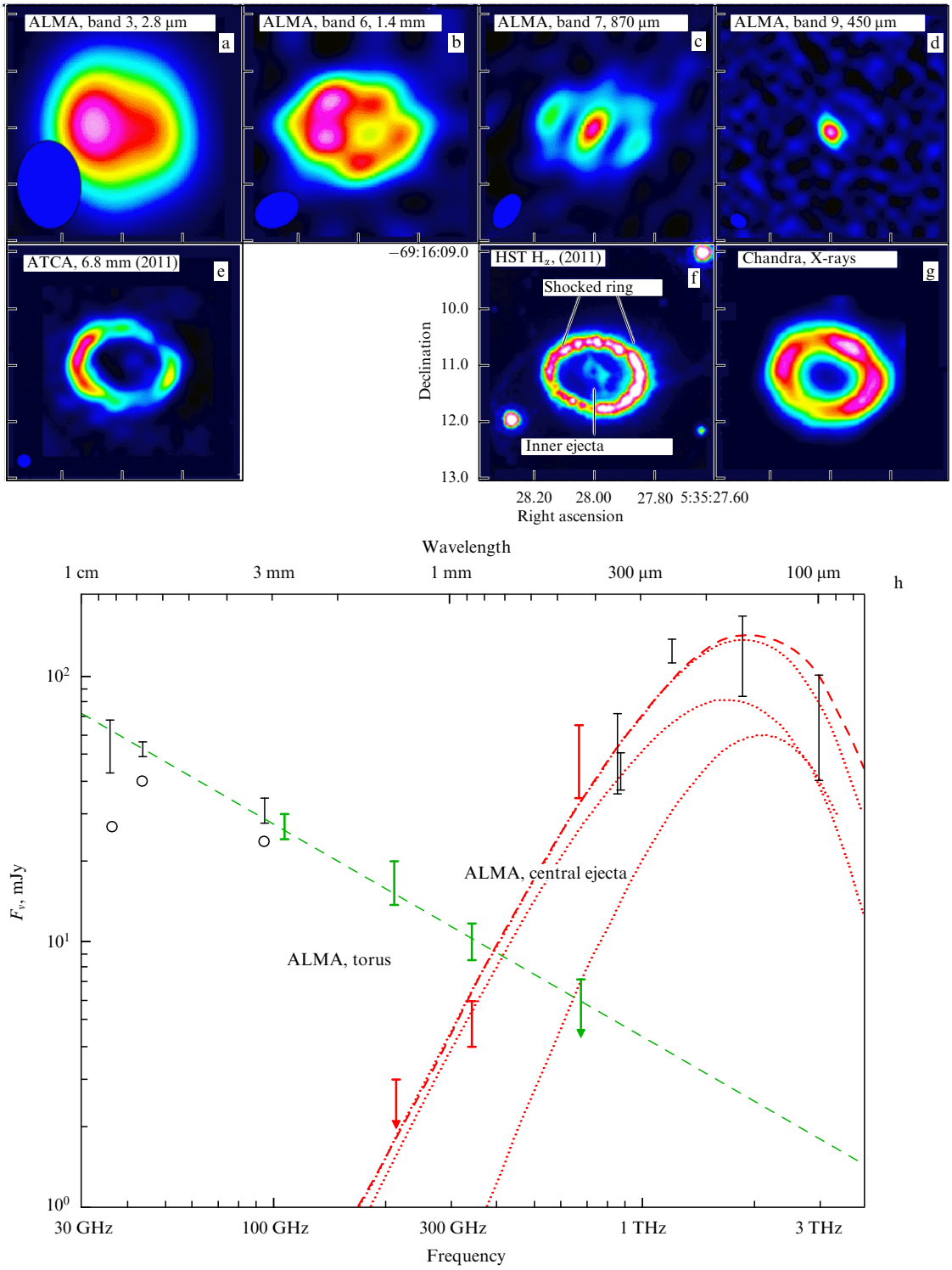

Figure 13. (Color online.) Images of SN 1987A at different wavelengths: (a) ALMA 2.8 mm, (b) ALMA 1.4 mm, (c) ALMA 870 μm, and (d) ALMA 450 μm. The same supernova images obtained by (e) the ATCA (Australia Telescope Compact Array) at 6.8 mm, (f) the Hubble space telescope HST H_α, and (g) the Chandra X-ray telescope. (h) Low-frequency (dust + synchrotron) spectrum with individual contributions from the torus (i.e., the supernova shell) and the central ejecta [218].

and physical parameters 10 years before their entering the atmosphere. The reconstructed parameters (in particular, the particle velocity relative to the Sun $v_{\rm ISP} \simeq 40$ km s^{-1}) suggested the interstellar origin of the particles (ISP). Their masses were in the range $m_{\rm g} \simeq 10^{-14} - 3 \times 10^{-9}$ g, which at the upper bound is three orders of magnitude higher than detected by Ulysses. With the measured mass flux $\rho_{\rm ISP} v_{\rm ISP} \sim 10^{-21}$ g cm^{-2} s^{-1}, this yields the ISM dust density $\rho_{\rm ISP} \simeq 5.3 \times 10^{-27}$ g cm^{-3} [224].

With the mean interstellar gas number density assumed to be $\langle n \rangle \sim 0.3$ cm^{-3}, the NAIC Arecibo radar observations suggest the interstellar dust density $\rho_{\rm ISP} \simeq 0.015 \langle n \rangle m_{\rm p}$ (where $m_{\rm p}$ is the proton mass), which is comparable to the density of heavy elements in the ISM and is 2–3 times as high

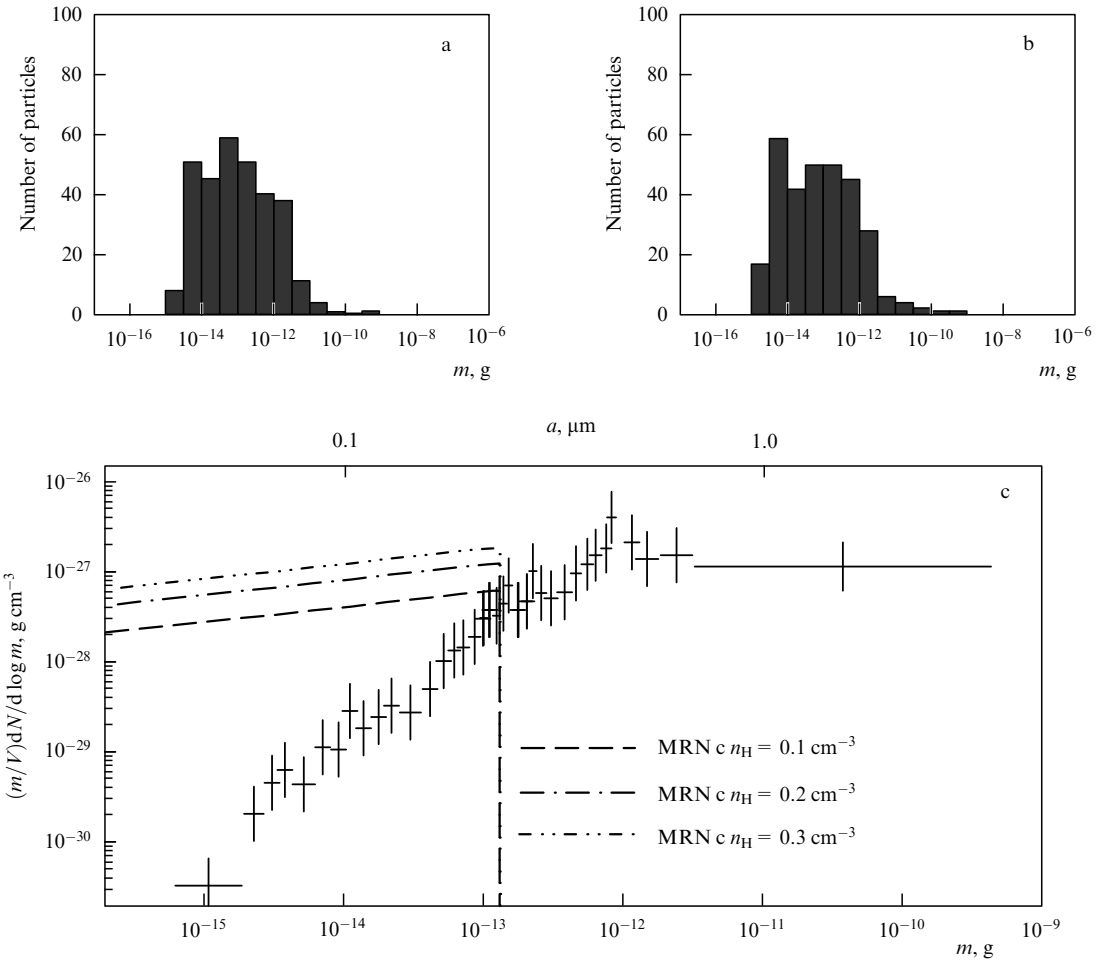

Figure 14. Dust grain mass distributions from measurements by (a) Galileo and (b) Ulysses. The sharp decrease at small masses is due to the insufficient sensitivity of mass spectrometers and at large masses can be due to observational bias. (c) Differential mass distribution of interstellar dust (the so-called MRN distribution, after Mathis, Rumpl, and Nordsieck, the authors of [222]) derived from the cumulative Galileo and Ulysses data [221]. The dashed, dashed-dotted, and dashed-dotted-dotted lines show the expected dust grain distribution corresponding to the 'standard' interstellar dust spectrum [222] for various local ISM densities; V is the unitary interstellar volume and m is the dust grain mass.

as the interstellar dust density estimated from light extinction. This fact by itself suggests the incompleteness of our hypotheses on the origin of dust and even on its total mass in the Galaxy.

The last conclusion can be formulated more reliably if radar observations by the AMOR (Advanced Meteor Orbit Radar Facility) instrument are taken into account [225, 226] (see also [227]). The AMOR complex detects only large particles ($a > 15$ μm, $m > 3 \times 10^{-7}$ g), and therefore, for the mean particle flux $\sim 2 \times 10^{-13}$ cm^{-2} s^{-1} (see the discussion in [227]) and velocity $v_{\rm ISP} \simeq 40$ km s^{-1}, this yields $\rho_{\rm ISP} > 10^{-26}$ g cm^{-3}, which is two times as high as the density of heavy elements in the ISM.

Recently, archival FIR and submm observations by the COBE/DIRBE, COBE/FIRAS, and Planck missions jointly with observations of extinction in the near and mid-IR by the IRAS, Spitzer, and Herschel space telescopes were processed. The data suggest that about 15% of the interstellar dust mass can be concentrated in large 1.4 μm grains, which can account for about 3% of the total thermal emission in the ISM [228]. Although the mass fraction of such grains and their contribution to the total thermal emission are insignificant, these data are very important to clarify the role of dust particles in planet formation and should be analyzed further. In this connection, it is very important to understand the following complications related to large dust grains in the ISM.

First, with the temperature of interstellar grains decreasing with their size as $T_{\rm d} \sim a^{-1/6}$, and the thermal flux from a grain at maximum changing as $\propto T_{\rm d}^5$, estimating the contribution of cold grains to the total thermal spectrum is a very difficult task.

Second, the contribution of such grains to extinction is very small due to their small number. Moreover, for optical extinction measurements, large dust grains become gray, i.e., their contribution to extinction becomes independent of the wavelength. To some extent, this difficulty can be bypassed by measurements of extinction at long wavelengths in directions with a very high surface density, but they are extremely difficult and can hardly significantly improve the contribution from large grains to extinction. Apparently, it can be possible to detect traces of large grains in the ISM by measuring the submm emission from hot plasma behind shock fronts of historical supernovae.

It seems quite likely that the mass fraction estimate of $\sim 15\%$ for large (1.4 μm in diameter) dust grains in the ISM, as inferred from extinction measurements in the near- and mid-IR toward the galactic center carried out by the IRAS, Spitzer, and Herschel telescopes [228], is underestimated.

One of the reasons is that the model of dust grains used in [228] implicitly assumes the total mixing of grains of any size, which is a very strong assumption (important from the standpoint of numerical estimates), because the charge-to-mass ratio $q/m_{\rm d}$ decreases with mass in any model of dust charging. As a result, large grains are distributed in much larger volumes and are scarce in regions where the extinction is measured. Another important fact is that under equal conditions, larger grains are destroyed more slowly than smaller ones: the destruction time of a grain increases with its size as $\tau_{\rm dest} \propto a$. Therefore, it can be expected that large grains accumulate in the ISM. However, due to the decrease in the $q/m_{\rm d}$ ratio for large grains poorly coupled with plasma and their more diffusive distribution in the ISM, their contribution to extinction can be small. Indeed, if we assume that large dust grains with a size a have the total mass equal to the dust mass in the Galaxy $M_{\rm d} \sim 2 \times 10^7\, M_\odot$, then their contribution to extinction is $A_{\rm v}/L \sim [0.3/(a/1\ \mu{\rm m})]^{\rm mag}$ per kpc, which is one fifth the observed value.

In the last decade, new data on the existence of large intergalactic grains has emerged. Compelling evidence of large dust grains in the Galaxy and possibly in the intergalactic space was published in [229]. In July 2006, the 6-meter telescope of the Special Astrophysical Observatory (SAO) RAS detected a weak emission in FeI, MgI, OI, and NI lines and in the N_2 bands typical for meteor glowing. The entry velocity of the meteor into the atmosphere was estimated to be 300 km s^{-1} and its size from a few tenths of a millimeter to 1 mm, with atmospheric uncertainties taken into account. These properties suggest the chondrule nature of the meteor. The meteor was also detected by the CCD-TV (charge-coupled device television) camera of the binary telescope FAVOR (FAst Variability Optical Registration) at a more than 96% confidence level. This is a unique event, because all previously detected microscopic or dust particles coming into the Solar System from the ISM had limited sizes (about 1 μm) and velocities (as a rule, about 10–15 km s^{-1}), as suggested by data from many space missions (see, e.g., the Ulysses data [230, 231] and recent StarDust data [232]). Because the velocity of the meteor glow was unusually high for the Galaxy and its direction toward the Local group centroid, the origin of this meteor was naturally associated with the IGM [229].

Assuming the commonly accepted view that dust is formed in stellar sources, the presence of large dust grains in the IGM should indicate its high abundance in the ISM of our Galaxy and other galaxies. Optical polarimetric observations of the star VY CMa suggested the presence of large dust grains (up to 0.5 μm in size) in its envelope [233]. Recently. ALMA observed [234] the variable AGM star Mira A with the aim to search for dust production signs in the upper stellar atmosphere and the circumstellar shell. Unfortunately, no clear signatures of dust were found, although dust production is suggested by the rapid decrease (by more than an order of magnitude) in the SiO molecule number density at the stellar photosphere boundary (around five radii of the star). The dust in this region should be too hot ($T > 100$ K) to glow in the FIR. However, the submm ALMA observations [235] of emission from SiO molecules [234], which are direct precursors of dust grains, as well as emission from AlO molecules (preceding the formation of Al_2O_3 clusters), suggest an optimistic outlook as regards the detection of submm emission from the highest aluminum oxides (such as Al_2O_3) and from cold large dust grains in the circumstellar gas around red giants.

It cannot be ruled out, however, that the dust observed in [229] was produced at very early stages of the stellar nucleosynthesis, as suggested by its velocity atypical for the ISM. In this case, measurements of the amount of large-grain dust in our ISM becomes more intriguing. IR and submm observations of emission from large dust grains have not been carried out yet.

5. Cold dust near galaxies

5.1 Dust and gas in the hot galactic halo

In the last decade, the problem of missing baryons has been actively discussed. In essence, the mass of baryons in galaxies, clusters, and the IGS at the present time ($z \simeq 0$) is found to be at least two times as small as suggested by cosmological data on the light element abundance and CMB anisotropy. It is assumed that the missing baryons can be hidden in extended (100–200 kpc) galactic gas halos. However, despite extensive efforts, no missing baryons have so far been discovered in the halo of our Galaxy.

The first observations suggesting a large number of high-charged oxygen ions OVII in the Galactic halo were reported in [236]. However, the baryon mass estimate in the halo $M \sim 10^{11}\, M_\odot$ is very sensitive to the relative number density of absorbing ions, f^{-5}(OVII), and the metallicity, Z^{-3}. Recently, the discovery of X-ray absorption lines from atomic and single-ionized oxygen from condensations of warm ($T \sim 10^4$ K) ionized gas localized apparently within a 15 kpc distance from the galactic center with the total mass $M_{\rm WIM} \sim 10^9\, M_\odot$ was reported in [237]. This is much smaller than the usual estimate of the missing baryon mass in our Galaxy. An important point, however, is that the warm ionized gas discovered in [237] must be confined in relatively compact ($\leqslant 25$ pc) regions, and therefore the probability of its location on the line of sight is too low. In addition, such condensations must be kept in equilibrium by the surrounding hot gas pressure, and therefore the estimate in [237] provides only a lower bound.

Thus, the X-ray data allows concluding that the extended Galactic halo contains a much larger baryon mass (up to $M \sim 10^{11}\, M_\odot$). However, this conclusion is valid if the dark matter profile is not a 'cusp', as predicted by the Navarro–Frenk–White (NFW) model, but has a smoother form with a nonsingular core corresponding to hydrostatic equilibrium [238].

A baryon mass estimate lower by half an order of magnitude is obtained from the requirement of gas mass conservation in the Large Magellanic Cloud, which is moving in the extended gas halo of the Galaxy: $M \simeq 2.6 \times 10^{10}\, M_\odot$ [239]. Recently, 20 absorption lines of high-charged OVI ions from the Galactic halo were detected in X-ray spectra of active galactic nuclei [240]. It is difficult to estimate the mass of the absorbing gas halo from these observations. There can be hope of observing the periphery of galaxies in the FIR and especially in the submm range. These hopes are based on the standard assumption that the dust mass in the interstellar gas is proportional to the mass of heavy elements with the proportionality coefficient equal to 0.3–0.4 [241], which can somewhat change apparently only in very low-metallicity galaxies [242, 243]. Therefore, if heavy elements are observed in the circumgalactic gas, a comparable amount of dust can be assumed, and the dust emission can be used to estimate the total mass of the gas in the circumgalactic (or intergalactic)

medium. Clearly, under such conditions, the dust should have a low temperature $T_d \lesssim 15$ K, unless it is embedded in a hot gas in galaxy clusters (see the discussion in [244]).

5.2 Observations of cold dust in intermediate galactic halos

A significant part of the galactic gas is found far beyond the optical radii of galaxies $r > R_{25}$, where R_{25} is the radius of the galaxy where the optical surface brightness is 25 stellar magnitudes per square arcsecond. The radial size of the atomic hydrogen distribution in galaxies is frequently found to be 3–5 times as large as R_{25}. Under such conditions, the ionized gas with low emission (which is therefore difficult to observe in the optical and radio spectra) can naturally be expected to occupy an even larger volume [245]. On the other hand, the dust in such extended circumgalactic regions can be observed by emission in the IR spectrum; here, at a distance from the stars, the dust remains cold and should therefore mostly emit in the FIR and submm ranges.

Observations of edge-on galaxies by the Herschel telescope revealed the presence of dust beyond stellar disks in the direction perpendicular to the disk plane. For example, in the spiral galaxy NGC 891, not only the presence of a rather thick dust layer (2–3 kpc) over the stellar disk was confirmed [246, 247] (which was earlier discovered in the optical range) but also a more extended dust halo (up to 10–12 kpc over the disk plane) with the dust temperature decreasing along the normal to the disk was found. The dust mass fraction in this galaxy is two times as high as in the Milky Way [248, 249].

A significant (fourfold) increase in the dust mass fraction with decreasing the temperature (from $\Sigma_d/\Sigma_{H_2} = 0.012$ at $T = 245$ K to 0.05 at $T = 20$ K) is interesting and promising as regards further studies of the cold dust in galactic halos. Because this suggests that most of the cold dust is located at a distance of 10 kpc over the galactic plane, there must be a selective mechanism of dust transportation from the galaxy, which is more efficient than the transport of gas from the galaxy. Radiation pressure could be such a mechanism, and although there are still no detailed calculations of this transportation, the connection between charged dust particles and magnetic fields apparently limits such transportation. Moreover, because of the complicated magnetic field topology, both in the galactic disk and beyond, such calculations can be very laborious [250]. An important feature of such a two-temperature dust distribution is that in observations of edge-on galaxies at short wavelengths ($\sim 0.5-3$ μm), only (or predominantly) hot dust with scale heights of 150–250 pc and 1–2.5 kpc can be probed [249]. Unfortunately, the comparatively weak flux sensitivity of the Herschel telescope has not so far enabled making any reliable conclusions on radially extended dust disks.

A very interesting result related to the cold dust in the intermediate halos of edge-on galaxies NGC 3044 and NGC 4157 was reported in [251], where a correlation between the thermal emission from cold dust at 850 μm and the synchrotron continuum at 617 MHz, $S_{617} \propto S_{850}^{2.2}$ was discovered. The result is unexpected, and although the authors of [251] propose an interpretation based on the likely assumption that synchrotron radiation is related to the magnetic field and relativistic electrons and thermal dust emission is related to the dust density, qualitative estimates do not seem to be compelling and require further analysis. Indeed, relativistic electrons are more diffusive and in any case should have a different spatial distribution than the dust particles; therefore, arguments ignoring these points have to be supported by further evidence. In any case, the possible close relation between thermal dust emission and nonthermal radiation from relativistic electrons requires careful observational studies using a larger sampling of galaxies observed edge-on with better sensitivity and better spatial resolution than those of the GMRT (Giant Meterwave Radio Telescope) and JCMT in the respective radio and submm ranges.

In addition, measurements of dust emission on galactic scales, in particular at the peripheries of galactic disks, are also of interest from the standpoint of dust transportation into the interstellar and intergalactic medium, as well as in the more general context of matter exchange between galaxies and the IGM. In this connection, studies of the spatial variations of the dust and metal abundance in the ISM of galaxies should be noted.

Presently, there are indications of two types of radial dependence of the dust-to-metal mass ratio in galaxies: in one case, this ratio increases on average with the metallicity decreasing from the galactic center to the periphery [252, 253]; in the other case, the dust density decreases along the radial distance from the galactic center proportionally to the density of metals [254, 255].

If this dichotomy is real, it suggests important consequences for the physics of dust in the ISM. The first distribution type — an increase in the dust-to-metal mass ratio at the galactic periphery — can suggest either less effective dust destruction behind supernova shock fronts or selective dust transportation in the radial direction. The second distribution type can suggest that the radial transport of dust and heavy elements is controlled by similar mechanisms with a constant fraction of metals bound in dust grains, or that the dust is directly produced in stellar wind ejecta into the ISM in the same proportion.

Spatial variations of the dust-to-metal mass ratio can be greatly affected by the degeneracy related to the uncertainty in the emissivity index β, the CO-to-H_2 conversion factor $X(\mathrm{CO})$, and other physical parameters of the dust and interstellar gas [256]. The broadband Millimetron 20 μm–3 mm observations can significantly contribute to resolving this issue, in particular, to removing the degeneracy in the emissivity index β and improving the conversion factor $X(\mathrm{CO})$ from simultaneous observations of CO and thermal dust emission.

Meanwhile, direct observations of dust at galactic interstellar disk peripheries are very rare. The first compelling observational evidence of the presence of a dusty interstellar disk with a radius exceeding the stellar disk at least twofold is presented in [257]. In the optical range, a spiral galaxy was discovered (inclined by $\simeq 45°$ to the line of sight), which was projected onto a larger background galaxy observed almost face-on. The dust disk orientation prevents estimating the low optical depth of the dust; therefore, the minimal extinction estimate is $A_v \lesssim 0.1$. Taking the exponential character of the radial optical depth profile into account, it is possible to expect that the entire extension of the dust disk with the optical depth $\tau \sim 0.01$, which still enables its IR visibility, can be as high as three optical radii of the galaxy. The dusty interstellar disk demonstrates optical properties similar to those of the dust in our Galaxy.

Recently, compelling observational evidence has appeared of the existence of extended interstellar gas disks seen in the 21 cm line with radii several times as large as optical stellar disks [258, 259]. Taking the surrounding

ionized HII gas coronae into account [245], such disks are likely to constitute most of the gas mass. Clearly, such disks should also have a dust component, as observed in the case of 'shadowed' galaxies [257]. Presently, however, there are no data revealing dust in galaxies in the catalogs [258, 259], although quite detectable extinction values $A_v \gtrsim 1$ and high FIR and submm emissions can be expected in view of sufficiently high hydrogen $N(\mathrm{HI} + \mathrm{HII})$ column densities ($\sim 10^{21} - 10^{22}$ cm^{-2}).

It is currently unclear how ubiquitous such extended interstellar disks around galaxies could be, and whether their size depends on the morphological type, the mass of the galaxy, etc. In any case, it is clear that the presence of an extended interstellar disk around a galaxy should correlate with an extended hot gas corona, as well as with the mass and density profile of the dark matter halo. Therefore, the detection of extended interstellar disks by submm emission observations would be invaluable for the physics of galaxies and cosmology.

Studies of dust at galactic peripheries both in extended interstellar disks and in intermediate halos in the direction perpendicular to the disk plane have another important aspect for observational cosmology. In the early 1990s, several papers (see especially [47, 260]) proposed that the dust filling the interstellar galactic disk peripheries can significantly contribute to the extinction of distant background objects, including distant supernovae. At large redshifts, protogalaxies or young galaxies (such as extended disks of Damped Lyman-Alpha (DLA) systems) can also contribute.

Besides being able to absorb optical and UV emission from distant sources, the extended dust interstellar disks heated by the proper stellar population can contribute to the intergalactic mid-IR and FIR cosmic background. This contribution, thoroughly analyzed in [261], turned out to be in very good agreement with the observed COBE/DIRBE spectrum at 140 and 240 μm with an uncertainty factor of 1.5–2 [262] and the COBE/FIRAS 150–2000 μm spectrum with an uncertainty factor of 3–5 [263]. The larger error in the second case is apparently due to the enhanced CMB contribution in this range. Clearly, dusty interstellar disks can lead to a significant underestimation of the amount of optical and UV photons in the Universe, and hence to the underestimation of the SF rate, heavy element production, cosmic ray contribution, and other factors relevant to thermonuclear evolution in the Universe after the recombination stage. Moreover, intermediate dusty galactic gas halos, such as that around NGC 891, can shield or absorb more than 37% of light from a proper stellar disk and up to 71% of light from the bulge of these galaxies. This fact can be one reason for the recently discovered UV deficit in the Universe [265].

5.3 Cold dust in distant galactic surroundings: circumgalactic gas

Extinction measurements in distant galaxies ($z \sim 0.3$) from the Sloan Digital Sky Survey (SDSS) suggest that the dust extends far beyond galactic limits in accordance with the power law $\Sigma_d \propto r_p^{-0.8}$ (where Σ_d is the dust surface density along the line of sight and r_p is the impact parameter from the line of sight to the galaxy), which yields the cosmological dust density in the local Universe $\Omega_d \simeq 5 \times 10^{-6}$. This value is consistent with the average metallicity estimate $Z_d \sim 0.1 Z_\odot$, which, with the standard dust-to-gas mass ratio $Z_d/Z = 0.2$, gives a comparable amount of cosmological dust $\Omega_d = 1.6 \times 10^{-5}$, even if larger by half an order of magnitude. This discrepancy in Ω_d reflects the uncertainty in the metallicity estimates, which are mainly derived from measurements of absorption lines in quasars and gamma-ray burst afterglows.

X-ray and radio data suggest that our Galaxy can have a substantial number of baryons in the extended halo. The dark matter halo density profile, unlike the NFW model with a cusp [266], is then required to have an extended sufficiently flat shape with a large central nonsingular core [240, 267].

Estimates of the dust mass in the Universe [268] exceed the dust mass observed in galactic disks [23]. This means that most of the dust is located outside galaxies (for example, in circumgalactic coronae) or in the IGM.

In the last five years, some researchers have reported observations of absorption lines from multi-charged ions in galactic coronae inside several virial radii around spiral galaxies located in the local Universe at redshifts $z \leqslant 0.3$. The observations revealed a large number of heavy elements (oxygen, carbon, and nitrogen), sometimes comparable to their mass in interstellar disks. It is logical to assume that in addition to heavy elements in the gaseous medium, dust is present in such halos and accounts for about 30% of the mass (which is close to the galactic dust fraction). However, this assumption can only hold if the dust is not destroyed during the transportation from gaseous disks to the halo. Modern theoretical estimates are mutually inconsistent, being mainly based on observations of absorption lines from heavy-element ions [269, 270] and therefore suffering from the uncertainty in the portion of the area of the galactic sky projection occupied by absorbing or scattering gas condensations, which always decrease the estimates. Thus, a reliable conclusion on the amount of dust in the extended galactic coronae can only be obtained from cold dust observations in the FIR band.

The existence of such extended gas coronae is related to the activity of stellar galactic populations, mainly to SF bursts in galactic nuclei. The 'galactic wind' phenomenon has been known already for more than 20 years as powerful large-scale gas outflows from central parts of galaxies, which are observed in almost all spectral ranges. Initially, this phenomenon was observed in H_α emission and in some heavy-element lines, but in the last few years numerous X-ray observations of the wind have appeared, and quite recently it was observed in molecular lines. The closest of the known gas outflows is generically related to the Galactic nucleus, which demonstrates high SF activity leading to the formation of the so-called Fermi bubble in the center [271].

5.4 Star formation in a low-density environment

Despite long studies of the SF process and significant progress achieved in recent years in explaining it based mainly on IR observations, controversial facts continue to appear. These facts include the discovery of SF under such conditions where it cannot apparently occur. An example is provided by low surface brightness (LSB) galaxies, many of which are localized in galaxy clusters, in Virgo and Fornax in particular [272]. These 'anemic' galaxies are distinguished from other galaxies by their surface brightness being below that of the night sky by at least one stellar magnitude: 23–25 mag per square arcsecond. This is a direct consequence of the extremely low SF efficiency, a small luminosity-to-mass ratio, and the absence of supernovae. The number of LSB galaxies (four per square degree) is significantly smaller (by

three orders of magnitude) than that of ordinary galaxies; however, the possible observational bias should be taken into account.

Another unexpected result in this field is the recent detection of even less bright objects with a surface brightness of 24–26 mag per square arcsecond, which are extremely diffuse anemic galaxies with sizes of about that of the Galaxy, in the central part of the Coma cluster [273, 274].

The physics of LSB galaxies is very interesting from the standpoint of both their origin (during hierarchical clustering) and the SF peculiarities in a very low baryonic density in these galaxies. However, the low surface brightness of these galaxies makes it difficult to study their stellar populations. One of the most extremal LSB galaxies is Malin-1 (Fig. 15), with a surface brightness of $\geqslant 24$ mag per arcsecond and an interstellar HI disk radius and, possibly, a stellar disk of ~ 100 kpc. The dynamic mass of Malin-1 is quite high, of the order of $10^{12}\,M_{\odot}$, which can explain the stability of such galaxies in the dense surroundings of the cluster, but then the lack of SF seems to be even more intriguing.

The weakness of optical glow from stellar populations of LSB galaxies complicates their observational study, which makes IR observations very important. Near-IR observations were carried out by the Spitzer space telescope [275], but no emission was detected from Malin-1. In the galaxy UGC 6614, several spots were detected at 8, 24, and 160 μm; some emissions at 8 and 24 μm were found to be spatially close to weak SF regions observed in the H_{α} line. In addition, the BIMA (Berkeley Illinois Maryland Association) interferometer and the IRAM telescope performed millimeter observations of several LSB galaxies [276]. In two of them, including Malin-1, CO ($1 \to 0$) emission was detected in the disk and central parts, and a flat-spectrum continuum was also observed in the central regions. No traces of dust were found. The absence of an FIR signal is apparently related to the insufficient flux sensitivity of the IRAM telescope (~ 1 mJy). Taking into account that the stellar population in the central regions of Malin-1 is older than at the periphery of the spiral arms [277], it can be assumed that molecular gas and dust are present in the arms and feed a sluggish SF. This can be considered indirect evidence of dust in Malin-1.

In the last few years, other evidence of possible SF in low-density regions has been obtained. Intergalactic SF regions can provide an extremal example. Apparently, this possibility was first pointed out in [278, 279], where weak SF at the periphery of satellites of the M31 galaxy and in the intergalactic space between M81 and NGC 2403 was discovered. Recently, a relatively young (less than 100 mln years) stellar population was discovered in the Magellanic stream [280]. Later, in the same region close to the group of young stars, molecular gas was detected by HCO^{+} line emission and very weak CO emission, although the gas density in this region is apparently extremely low, as suggested by the very low hydrogen column density $N(\mathrm{HI}) < 10^{20}$ cm^{-2} [281]. Similar results were obtained for a nearby HI high-velocity cloud falling onto the Galaxy with a low atomic hydrogen column density $N(\mathrm{HI}) < 5 \times 10^{20}$ cm^{-2} and the volume density $n \sim 0.1$ cm^{-3} [282]. Taking the low surface brightness of such regions into account, it is straightforward to assume that their number is high and that they can represent a separate class of extragalactic objects with anemic SF.

There are at least two reasons why these low-density regions with SF traces are of fundamental interest for the physics of galaxies and cosmology. First, they suggest that the generally accepted Toomre criterion for the SF beginning above some critical surface density is not universal, and the process of star birth is determined by local effects. Second, the recently discovered UFD (ultra faint dwarf) [283] galaxies have extremely low luminosities and baryon densities. Therefore, the extragalactic SF can also be associated, in particular, with such extremely faint dwarf galaxies. Clearly, if UFD galaxies are fragments of the hierarchical galaxy formation, their study becomes necessary.

In the optical range, LSB galaxies can nevertheless have a quite high FIR and millimeter luminosities. Because these galaxies demonstrate both extremely low surface brightness and SFR and have giant sizes and apparently a large fraction of dark matter, their submm observations can bring unexpected results.

Earlier, LSB galaxies were observed in the IR spectrum by the Spitzer space telescope and SCUBA [284]. Of the five galaxies observed, four showed a weak near-IR emission (one and a half to two orders of magnitude lower than in normal galaxies) at 3.6, 4.5, 8, and 24 μm, and two (UGC 6151 and UGC 9024) demonstrated emission at 70 and 160 μm. Unlike

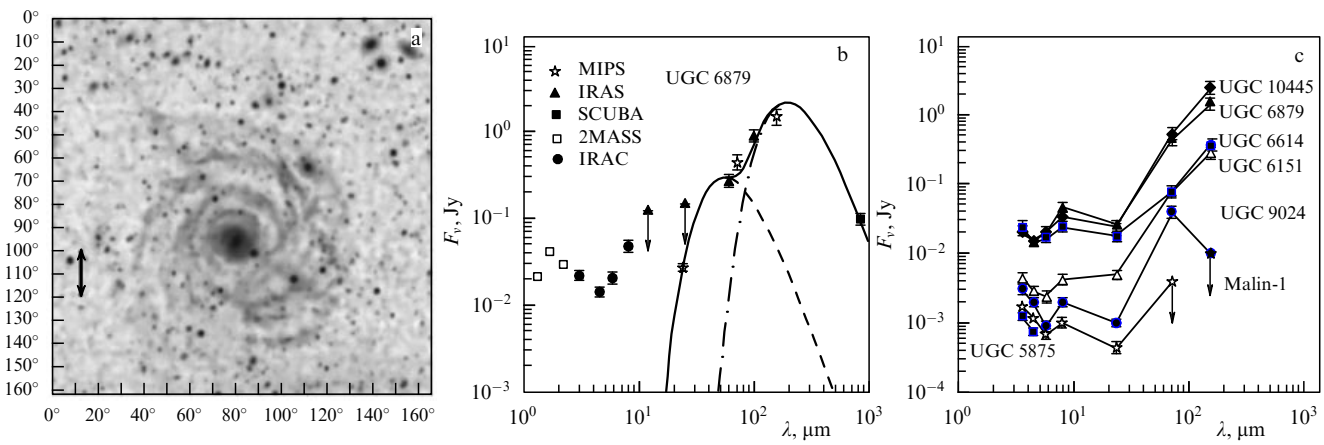

Figure 15. (a) Image of the LSB galaxy Malin-1. The scale interval in the left panel corresponds to twice the galactic size [277]. IR dust emission spectrum (b) in the normal galaxy UGC 6879, where cold dust emission is seen, and (c) in LSB galaxies, which do not show cold dust emission at the 2MASS, SCUBA, and Spitzer sensitivity levels [275].

these galaxies, the normal galaxy UGC 6879 demonstrated emission in the entire IR band, including at 850 μm with a flux corresponding to the dust temperature $T = 15$ K.[34] Moreover, UGC 6879 has a hotter dust component ($T = 50$ K); the total mass of the dust ($\sim 3 \times 10^7\, M_\odot$) is quite high. In view of the mass of atomic hydrogen in this galaxy $M(\mathrm{HI}) \sim 10^9\, M_\odot$, the dust concentration in it is four times as high as in the Milky Way. Apparently, the lack of cold dust emission in other galaxies is related to most of the dust being diffusively distributed over a larger disk and being embedded into a weak radiation field, with emission below the SCUBA sensitivity.

Moreover, recent observations show that the radial distribution of metals (and possibly dust) in LSB galaxies can be inverted, i.e., can have a positive gradient with a larger fraction of metals at the galactic periphery [286]. This assumption can be supported by the observation of cold dust in galaxies UGC 6151 and UGC 9024, predominantly at the periphery. This result is consistent with the assumption that most of the cold dust is concentrated in low-radiation-density regions, and therefore more sensitive observations are required.

In addition, observations of dust in LSB galaxies would be important to explain the dust circulation in the Universe, i.e., the cosmic dust mass balance in its production by stellar sources or in the ISM and destruction by strong shocks from supernovae.

As noted above, all attempts to unify different processes of dust formation and destruction in our Galaxy and other galaxies meet with great difficulties. For example, it is commonly accepted that the dust is produced by early type stars and supernovae and is destroyed by supernova shocks in the ISM. But carefully taking the dust production in galaxies into account has not provided compelling observational support that the total dust destruction rate can be balanced by the production rate in all possible sources. However, direct estimates for the Large and Small Magellanic Clouds, the laboratories for 'measurement' of the dust balance in the ISM based on IR observations, showed only that the dust production mechanisms there are much weaker than required to compensate for rapid dust destruction [287].

Thus, the arguments favoring the dominant dust production by core-collapse supernovae, whose progenitors are massive stars, seem increasingly compelling [288]. However, from the observational standpoint, one supernova can yield no more than $0.01 M_\odot$ of dust, which is clearly insufficient and implies too long a timescale of dust reproduction in the Galaxy, $\tau_{\mathrm{d,g}} \sim 5$ Gyr, which is at least one order of magnitude longer than the characteristic dust destruction time. Currently, there are no viable ways to resolve this issue. The problem, however, is that observations of the dust production rate enable measurements of only sufficiently hot (and hence bright) dust around AGB stars or in expanding supernova remnants, with the cold dust remaining undetected at long distances from the central star. If this is so, then observations of the cold dust around possible sources could be crucial for measuring the dust mass balance.

It is not ruled out, however, that the very nonuniform distribution of the dust production and destruction mechanisms in the interstellar and intergalactic medium can play a very significant role in the dust mass balance. It is known that the condensation of heavy elements on dust grains in dense molecular clouds can significantly increase the dust mass [289]. Under these conditions, the regions where the dust is destroyed by shocks must appear brighter in the near and mid-IR bands, whereas the emission from regions with active growth of dust grains should be shifted mainly to the FIR band. This urges simultaneous joint mid-IR and FIR observations of LSB galaxies, where the dust sources and dust destruction regions are spatially separated and can therefore be easily identified.

[34] The galaxy UGC 6879 was first classified as an LSB galaxy; however, formally this is not the case because of the high surface brightness of the central regions [285]. Nevertheless, UGC 6879 is given in [284] as an example.

6. Dust and gas in galaxy clusters in the intergalactic medium

6.1 Dust and gas in galaxy groups

Extinction measurements in the optical and near- and mid-IR ranges in some galaxies from the Local Group demonstrate certain features that distinguish it from the extinction measured in our Galaxy. These features can be explained by a deficit (or excess) of small dust grains in the galaxies, i.e., by a variation of the dust particle size distribution. The last fact generally complicates dust mass measurements in the Universe. Moreover, the possible measurement of the spatial dust distribution will enable solving several problems of galaxy formation in the standard cosmological ΛCDM (Lambda Cold Dark Matter) model, including the problem of 'missing satellites', the selected orbital plane of the brightest galactic satellites, and the avoidance of large morphological structures by dwarf galaxies.

Dust extinction measurements in galaxy groups from a large sample of SDSS galaxies [290] revealed the presence of a significant amount of dust in both low-mass groups (with a dust mass fraction of about 50% of the galactic value) and massive clusters (with a relative dust mass of about 3% of the galactic value). These observations demonstrate that the dust is destroyed in the hot gas of the clusters. However, both its large amount in big clusters and the similarity of its optical properties to the galactic dust apparently require refining the dynamical dust destruction mechanisms that operate in the course of dust transportation to the galactic periphery. Modern capabilities do not allow drawing any definitive conclusion on the amount of dust in halos of distant galaxies and in galaxy groups. Part of the problem is to separate contributions from the central hot dust and the cold dust at the galactic periphery, including in the halo. Complex studies of FIR emission and extinction from distant quasars could possibly solve this problem, but this has not been done yet [291].

6.2 Dust and gas in galaxy clusters

Observations of extinction from galaxy clusters from the SDSS data revealed the presence of dust in clusters up to distances $\sim 10 R_{200} \sim 10$ Mpc from their centers [292], although nonzero values of the reddening coefficient $E(\mathrm{g-i}) \lesssim 0.003$ extend to much longer distances. (Here, g and i specify the green (4679 Å) and near-IR (7439 Å) photometric bands.) Indeed, field galaxies demonstrate nondecreasing extinction at much longer distances, up to 10 Mpc (which for a typical galaxy is $\sim 100 R_{200}$ in units of the virial radius R_{200}) [270]. Thus, although the hot gas in galaxy clusters rapidly destroys dust, a certain fraction of it never-

theless remains shielded, which limits the dust outflow far away from the clusters. Therefore, the question of where the dust that enters the IGM comes from is of great importance. The answer to this question is essential for understanding the processes of mass exchange between galaxies and the IGM.

When dust and metals are expelled from galaxies, the dust, being connected to the surrounding gas cloud, is destroyed by the hot gas of the cluster after some characteristic time and fills the surrounding volume around the galaxies. Estimates show that depending on the parameters of fragments ejected in the active (or bursting) SF regime, the dust can be carried over distances up to 100 kpc. This means that the dust-containing clouds can be distributed almost homogeneously over the cluster volume. However, because the dust remains to be concentrated in 1–2 pc condensations under such conditions, its localization along the line of sight is highly unlikely, and the dust contribution to extinction is small, as observed in the clusters. On the other hand, if the ejected dusty gas fragments from the galaxies fill all the cluster quite homogeneously, then their thermal emission must be observed from the entire cluster area on the sky. Moreover, as the dust is embedded into cold clouds according to this scenario, its temperature is determined by the diffuse extragalactic UV background only and should not exceed 10 K. By itself, this fact can explain why attempts to discover dust emission in clusters by the Spitzer telescope proved to be unsuccessful.

Observations carried out so far have not yet confirmed the presence of dust in the hot gas of the clusters. For example, a detailed analysis of A_v extinction for a large sample of clusters from SDSS and IRASS [293] showed, on the one hand, the extinction of $\sim 3 \times 10^{-4}$ mag and, on the other hand, an emission at 100 μm with the mean flux $\simeq 0.2$ Jy per cluster. However, the extinction radial profile rather corresponds to the brightness radial profile of galaxies,[35] and hence the total IR emission can be related to the dust emission from spiral galaxies of the clusters, in which case the contribution of the diffuse (extragalactic) dust can be disregarded.

The following fact remains important, however: the mean flux at 100 μm rapidly increases with the redshift, $L \propto (1+z)^{4.7}$ (Fig. 16), suggesting rapidly growing SF, heavy element, and dust production rates. Under these conditions, it is quite natural to expect that at $z \lesssim 1$, dust was swept out from galaxies into the hot gas surroundings, and some small remaining amount of the dust can be found in the cluster gas. Moreover, because galaxies eject dust together with gas (in the form of fragments of dense expanding gas shells), the dust for some time remains partially shielded by the surrounding gas and has a low temperature with the emission peak at a wavelength of more than 100 μm. The result described in [293] was further elaborated by the Planck mission results.

The recently published data of the global galaxy cluster survey by the Planck telescope at $353 \leqslant \nu \leqslant 5000$ GHz [294] revealed a significant amount of dust in a sample of 645 clusters with the average dust temperature $T_d = (19.2 \pm 2.4)$ K (Fig. 17) and the average dust-to-gas mass ratio $\zeta \sim 2 \times 10^{-4}$. Of interest and perhaps of significance is the dust mass fraction decrease $\zeta \sim 10^{-4}$ in low-redshift clusters at $z < 0.25$ compared to $\zeta \sim 4 \times 10^{-4}$ in earlier clusters at $z > 0.25$. However, considering the sampling limitations, it cannot be ruled out that this is due to observational bias.

[35] Although there are more than 2σ deviations in the central parts of the clusters.

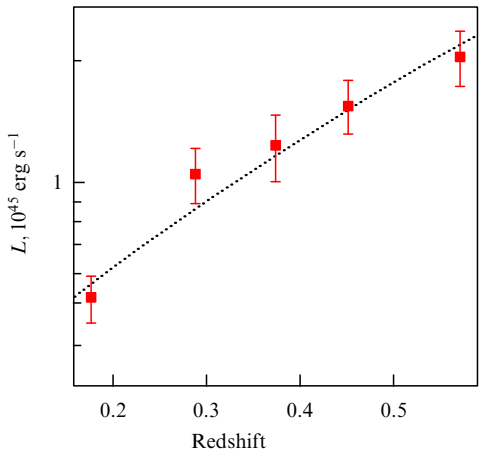

Figure 16. Thermal dust emission at 100 μm averaged over the IRAS galaxy cluster sample [293].

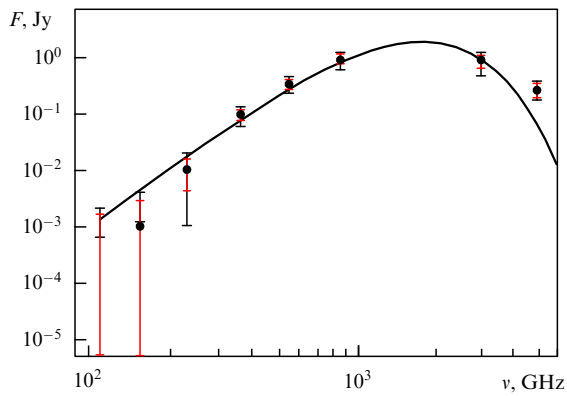

Figure 17. (Color online.) Thermal dust spectrum averaged over a sample of 645 galaxy clusters. Black and orange error bars correspond to different evaluation methods (see [294] for more details).

Of interest here is the following. Due to the low angular resolution of the Planck telescope ($\Delta\theta = 14' - 33'$ in the low-frequency channel 30–70 GHz and $\Delta\theta = 5' - 10'$ in the high-frequency channel 100–857 GHz) in the galaxy cluster survey, it is difficult to separate the dust emission in galaxies from that outside them. For this reason, the nature of dust can only be probed by its mass concentration and, to some extent, by its temperature. The survey data suggest that dust is mostly found outside galaxies. However, we should bear in mind that the fraction of elliptical and spheroidal galaxies in clusters is higher than among the field galaxies. In this case, the dust with the mass concentration $\zeta \sim 10^{-4}$ discovered in clusters could well be related not to the hot cluster gas but to a denser hot gas of the elliptical galaxies of a cluster, which are equally unfavorable for the dust. Here, we should also take into account that a significant number of cold (and possibly large) dust particles may not be detected in these observations, as is possibly suggested by the low-frequency cut-off at $\nu < 200$ GHz found in the average spectrum. In addition, in averaging over a large sample, the cold dust emission can be small compared to the emission from hotter dust in galaxies or outside them.

7. Gas and dust in galactic winds

Interest in galaxies with SF bursts in the central parts has remained high over the last quarter of a century. The galactic

wind is one of the powerful dynamical phenomena related to this activity, which, as is now clear, represents the global evolution factor of the baryonic Universe.

In the last several years, data on molecular lines, including CO, HCN, and HCO^+, from the nuclear regions of galaxies with SF bursts and galactic winds (for example, M82) have been published [295, 296]. The morphology and kinematics of these outflows differ significantly from usual ionized gas flows, and the problem of molecular winds is far from being solved in general. In galactic nuclei, which are the energy sources for galactic winds, different emission components (hot gas emitting in X-rays, atomic and molecular gas, H_α, and the thermal and nonthermal continuum) are found, suggesting a very complicated state of the interstellar gas in this region. Investigation of this gas can be the first step in understanding the physical picture of processes occurring there. From this standpoint, the possibilities offered by Millimetron in continuum observations and gas spectroscopy can be very important.

The nearest object of investigation from this standpoint can be the central region of the Galaxy a few hundred parsecs in size. Most of the molecular gas is concentrated there. A very complicated multiphase gas conglomerate appears in the CO, NH_3, 8.28 μm, 21.3 μm, 24 μm, and 21 cm lines and in the synchrotron emission [297]. The morphology and kinematics of this region suggest a continuous process of mutual transformations of different gas phases, which reflects complicated dynamics. In these conditions, the character of SF occurring there is unclear. Taking the high gas density in this region into account (as suggested by the CO, NH_3 emission lines), it is possible to expect the presence of both hot (observed in the near-IR band) and cold thermal dust emission, emission in fine-structure lines [CI] 370 and 610 μm, [CII] 157.7 μm, [OI] 62, 145, and 63.2 μm, which can be present due to large temperature and density variations in this region, as well as violent dynamics at large time scales.

The near-IR extinction measurements in the direction toward the galactic center (within 4 square degrees) demonstrated that unlike the commonly accepted 'classical' one-parameter extinction law defined by a single constant $R_v = A_v/E(B-V)$, the extinction law in the central galactic region is apparently characterized by two degrees of freedom [298].

A systematic analysis of the extinction law in a broad range from the near-IR to far-UV range was first presented by Fitzpatrick [299] (Fig. 18). The extinction law is determined by dust properties, including the dust grain size distribution, and can vary in space. Figure 19a presents an example of such variations measured by the IUE (International Ultraviolet Explorer) satellite in different directions in the galactic ISM [300]. As shown in [298], in the direction toward the galactic center, band variations of the extinction $A_I/E(V-I)$ and reddening coefficients $E(I-J)/E(V-I)$ and $E(J-K_s)/E(V-I)$ can exceed 20% in the near IR, irrespec-

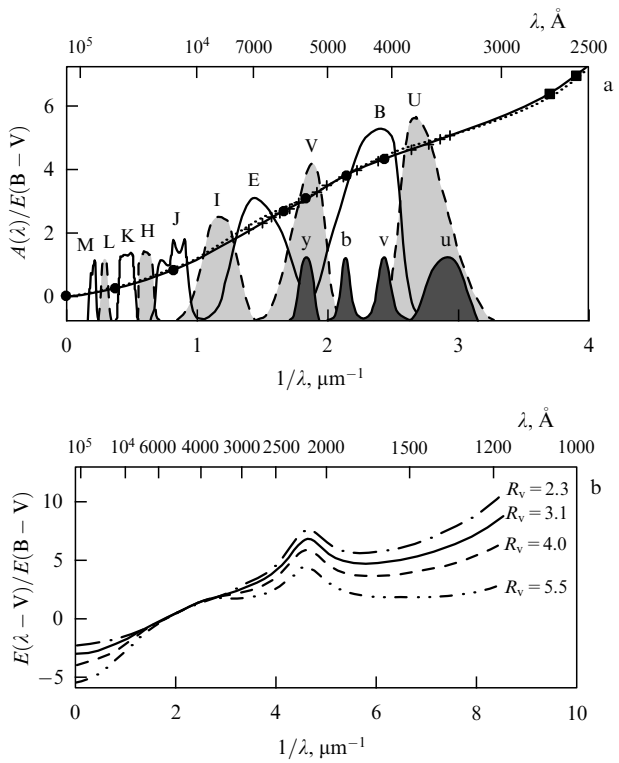

Figure 18. One-parameter extinction law. The thick solid curve corresponds to the 'standard' galactic value $R_v = A_v/E(B-V) = 3.1$. (b) Extinction curves for different values of the parameter R_v. Sensitivity of the curves to R_v in the IR spectrum is seen [299]. Capital letters M, L, K, etc. show photometric bands in the Johnson system; small letters y, b, etc. show the Stromgren photometric bands.

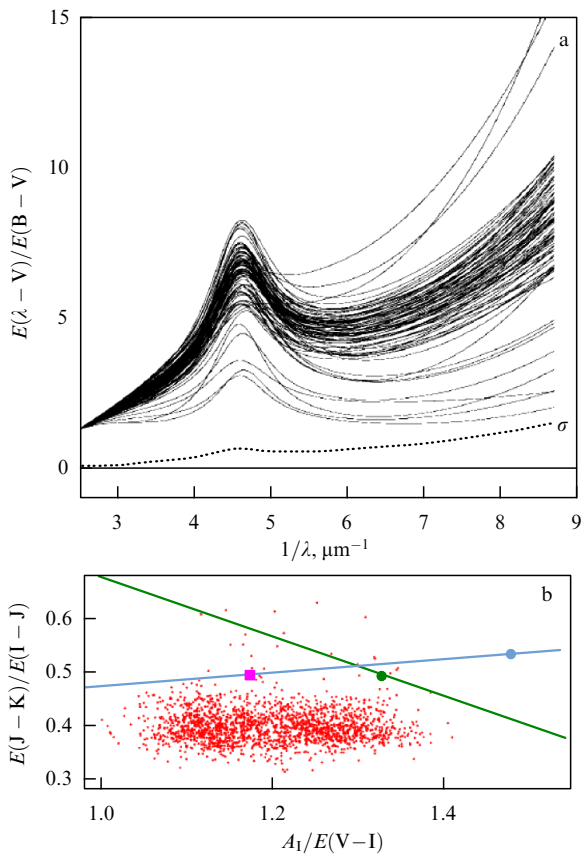

Figure 19. (Color online.) (a) Example of the extinction law variation for 80 directions in the Galaxy by IUE (International Ultraviolet Explorer) observations. The dashed curve in the bottom panel shows the standard deviation $\sigma(R_v)$ normalized to $\sigma(\lambda = 1500\ \text{Å}) = 0.74$ [300]. (b) The $A_I/E(V-I)$—$E(J-K_s)/E(I-J)$ plane from extinction measurements in the IR Planck observatory survey. The 'cloud' of red dots shows data from the Optical Gravitational Lensing Experiment III. The respective green and blue lines approximate the reddening law according to [299] and [300]. The red square corresponds to observations from [300], the respective green and light-blue filled circles show data from [299] and [302].

tive of the value of R_v, and the ratio $\langle A_v/A_{K_s}\rangle = 13.44$ in the optical and the near-IR K_s band ($\lambda = 2.149$ μm) exceeds the 'standard' ISM value by 60%. Moreover, the lack of correlation between variations of $A_I/E(V-I)$ and $E(J-K_s)/E(I-J)$ (see Fig. 19) can suggest that the extinction law is characterized by at least two degrees of freedom.

It remains unclear whether the additional degrees of freedom claimed in [298] that characterize the frequency dependence of the extinction are due to the size of dust grains, their chemical composition, and the properties of gas clouds on the line of sight in different directions. At the same time, the recently reported results of the spectroscopic (with the spectral resolution $R = \lambda/\Delta\lambda = 22500$) survey APOGEE (Apache Point Observatory Galactic Evolution Experiment) of 150,000 stars from the thick galactic disk, in combination with photometry from PanSTARRS1 (Panchromatic Survey Telescope & Rapid Response System (Institute of Astronomy of the University of Hawaii)), 2MASS (Two Micron All-Sky Survey) and WISE (Wide-field Infrared Survey Explorer) surveys, showed that all near-IR and optical extinction variations can be explained by the standard one-parameter dust model with possible substantial variations of the parameter $R_v = A_v/E(B-V)$ [303].

From this standpoint, a detailed study of spatial variations of the thermal dust emission from the four-square-degree region around the galactic center is very interesting for understanding its physical properties. In addition, this task is also important for observational cosmology, in particular because the possible extinction variations can significantly affect the brightness estimates from distant cosmological sources (such as supernovae at $z > 1$) and interpretation of the processes that occur there. In this connection, we note that the authors of [303] note a relation between R_v and the thermal dust spectrum.

8. Dust in early galaxies

The formation of early galaxies is related to early stages of the evolution of the Universe, when its age was not more than 3% of its current age; therefore, the corresponding optical emission is redshifted to the near-IR band, and all near-IR emission from SF regions should be observed in the FIR band. Therefore, to study these galaxies, spectral lines of the main gas 'coolants' (ions [CII] 157.7 μm, [NII] 122 μm, atoms [OI] 62 and 145 μm, molecules CO NH_3, etc.) should be measured. Together with thermal dust radiation measurements, this enables determining the SFR and the general state of the ISM in distant galaxies.

More detailed information can be inferred from observations of rotational transitions of molecular hydrogen in lines 28.22, 17.04, 12.28, 9.67 μm, etc., which fall into the FIR band. These lines cool the very low-metallicity gas that must be present in the first galaxies. Observations of these lines in relatively nearby galaxies (at distances of about 1000 Mpc) with powerful SF by the Spitzer telescope [304] allowed measuring the excitation degree and mass of hydrogen and establishing the role of turbulence and shocks in the gas heating .

High sensitivity is the main requirement in early-galaxy observations. Only recently did the most sensitive ground-based ALMA submm observations detect the [CII] line emission from galaxies at redshifts $z \sim 7$ [305, 306], and the galaxies themselves were discovered by powerful UV emission. Several earlier attempts were unsuccessful [307, 308]. Apparently, distant galaxies can be found in photometric images by their submm 'color', as was demonstrated by the Herschel telescope [309]. For example, using the criterion that the flux at 500 μm is higher than at 350 μm, and the 350 μm flux is higher than the 250 μm flux, 38 high-redshift candidate galaxies were found in the HerMES survey (Herschel Multi-tiered Extragalactic Survey). Subsequent optical observations proved that 80% of these candidates have redshifts $z > 4$.

9. Conclusion

Two circumstances make the FIR and submm studies of cosmic plasma extremely important and interesting:

• the mass and energy exchange in plasma, including between its gas and dust components, appears both in fine-structure spectral lines from plasma particles and in thermal dust emission. Clearly, the exchange processes in the low-temperature cosmic plasma can be accompanied by only long-wavelength electromagnetic radiation. Therefore, the FIR and submm spectral regions enable 'visualization' of the basic energetic physical processes that cannot be probed in other spectral ranges. Because the cosmic plasma is subjected to all possible energy sources in the Universe, the FIR and submillimeter ranges open unique possibilities to probe the nearby Universe;

• the redshift of emission wavelengths in the expanding Universe enables probing violent energy release at the initial stages of stellar nucleosynthesis in the distant Universe using atomic spectral lines in the near- and far-IR ranges and hot ($T_d > 40$ K) dust emission.

The recent results of the Herschel and Planck missions and ALMA observations briefly discussed in this review clearly illustrate these possibilities. Of course, cosmic dust research is important for understanding the fundamental processes determining dust production and destruction, and also because the dust determines the ISM transparency in our Galaxy and thus enables studies of distant objects in the Universe. Fundamental studies of the CMB polarization also require detailed knowledge of the dust properties. However, this topic desires separate consideration.

Acknowledgements
This study was supported by the Russian Foundation for Basic Research (grants 15-02-08293 and 16-02-01043), the Program of Fundamental Research by the Russian Academy of Sciences Presidium P-7 (subprogram Transitional and Explosive Processes in Astrophysics), and a grant from the President of the Russian Federation for the state support of leading scientific schools NSh 6595.3016.2.

References

1. Jansky K G *Proc. Inst. Radio Eng.* **20** 1920 (1932)
2. Jansky K G *Nature* **132** 66 (1933)
3. Shklovskii I S *Problemy Sovremennoi Astrofiziki* (Problems of Modern Astrophysics) (Moscow: Nauka, 1988)
4. Penzias A A, Burrus C A *Annu. Rev. Astron. Astrophys.* **11** 51 (1973)
5. Ginzburg V L *Annu. Rev. Aston. Astrophys.* **28** 1 (1990)
6. Reich W, Wielebinski R *Astron. Nachrich.* **323** 530 (2002)
7. Silk J *Infinite Cosmos. Questions from the Frontiers of Cosmology* (Oxford: Oxford Univ. Press, 2008)
8. Lukash V N, Mikheeva E V *Fizicheskaya Kosmologiya* (Physical Cosmology) (Moscow: Fizmatlit, 2010); Lukash V N, Mikheeva E V *Fizicheskaya Kosmologiya* (Physical Cosmology) (Moscow: Fizmatlit, 2012)

9. Phillips T F et al., in *Millimetre and Submillimetre Astronomy. Lectures Presented at a Summer School, Stirling, Scotland, June 21–27, 1987* (Astrophysics and Space Science Library, Vol. 147, Eds R D Wolstencroft, W B Burton) (Dordrecht: Kluwer Acad. Publ., 1988) p. 1
10. Salomonovich A E *Sov. Phys. Usp.* **12** 731 (1970); *Usp. Fiz. Nauk* **99** 417 (1969)
11. Kislyakov A G *Sov. Phys. Usp.* **13** 495 (1971); *Usp. Fiz. Nauk* **101** 607 (1970)
12. Torgashin M Yu et al. *IEEE Trans. Appl. Supercond.* **17** 379 (2007)
13. Koshelets V P et al. *J. Phys. Conf. Ser.* **486** 012026 (2014)
14. Karasik B S, McKitterick C B, Prober D E *J. Low Temp. Phys.* **176** 249 (2014)
15. Nomoto K, Kobayashi C, Tominaga N *Annu. Rev. Astron. Astrophys.* **51** 457 (2013)
16. Karlsson T, Bromm V, Bland-Hawthorn J *Rev. Mod. Phys.* **85** 809 (2013)
17. Pagel B E J *Nucleosynthesis and Chemical Evolution of Galaxies* (Cambridge: Cambridge Univ. Press, 2009)
18. Krügel E *The Physics of Interstellar Dust* (Bristol: Institute of Physics Publ., 2003)
19. Songaila A *Astrophys. J.* **561** L153 (2001)
20. Simcoe R A et al. *Astrophys. J.* **637** 648 (2006)
21. Schaye J, Carswell R F, Kim T-S *Mon. Not. R. Astron. Soc.* **379** 1169 (2007)
22. Voshchinnikov N V, Henning Th *Astron. Astrophys.* **517** A45 (2010)
23. Ménard B, Fukugita M *Astrophys. J.* **754** 116 (2012)
24. Richards P L *J. Appl. Phys.* **76** 1 (1994)
25. Hoffmann W F et al. *Astron. J.* **72** 804 (1967)
26. Hoffmann W F et al. *Science* **157** 187 (1967)
27. Shivanandan K, Houck J R, Harwit M O *Phys. Rev. Lett.* **21** 1460 (1968)
28. Doroshkevich A G, Novikov I D *Sov. Phys. Dokl.* **9** 111 (1964); *Dokl. Akad. Nauk SSSR* **154** 745 (1964)
29. Gaitskell J N, Gear A E *Icarus* **5** 237 (1966)
30. Fedoseev L I, Lubyako L V, Kukin L M *Sov. Astron.* **11** 953 (1968); *Astron. Zh.* **44** 1191 (1967)
31. Afonchenkov N G et al. *Sov. Astron.* **20** 95 (1976); *Astron. Zh.* **53** 178 (1976)
32. Cheung A C et al. *Phys. Rev. Lett.* **21** 1701 (1968)
33. Kellermann K I, Pauliny-Toth I I K *Astrophys. J.* **152** 639 (1968)
34. Vasil'chenko N V et al. *Sov. Astron.* **11** 720 (1968); *Astron. Zh.* **44** 897 (1967)
35. Gebbie H A et al. *Astrophys. J.* **154** 405 (1968)
36. Doroshkevich A G, Zel'dovich Ya B, Syunyaev R A *Sov. Astron.* **22** 523 (1978); *Astron. Zh.* **55** 913 (1978)
37. Partridge R B *Rep. Prog. Phys.* **51** 647 (1988)
38. Boggess N W et al. *Astrophys. J.* **397** 420 (1992)
39. Bennett C L et al. *Astrophys. J.* **396** L7 (1992)
40. Smoot G F et al. *Astrophys. J.* **396** L1 (1992)
41. Strukov I A et al. *Sov. Astron. Lett.* **18** 153 (1992); *Pis'ma Astron. Zh.* **18** 387 (1992)
42. Mather J C et al. *Adv. Space Res.* **11** 181 (1991)
43. Silverberg R F et al., COBE Preprint 93-10E (1993)
44. Hauser M G, in *Extragalactic Background Radiationa. A Meeting in honor of Riccardo Giacconi. Proc. of the Extragalactic Background Radiation Meeting, Baltimore, 1993 May 18–20* (Space Telescope Science Inst. Symp. Ser., Vol. 7, Eds D Calzetti, M Livio, P Madau) (Cambridge: Cambridge Univ. Press, 1995) p. 135
45. Hauser M G, in *The Extragalactic Infrared Background and Its Cosmological Implications. IAU Symp. 204. Proc. of the 24th General Assembly of the IAU, Manchester, United Kingdom, 15–18 August 2000* (Eds M Harwit, M G Hauser) (San Francisco, CA: Astronomical Society of the Pacific, 2001) p. 101
46. Hauser M G et al. *Astrophys. J.* **508** 25 (1998)
47. Fall S M, Charlot S, Pei Y C *Astrophys. J.* **464** L43 (1996)
48. Fixsen D J et al. *Astrophys. J.* **490** 482 (1997)
49. Spitzer L (Jr.) *Astron. Quart.* **7** 131 (1990)
50. Werner M W et al. *Astrophys. J. Suppl.* **154** 1 (2004)
51. Fazio G G et al. *Astrophys. J. Suppl.* **154** 10 (2004)
52. Kennicutt R C (Jr.) et al. *Publ. Astron. Soc. Pacific* **115** 928 (2003)
53. Sholomitskii G B et al., in *Nauchnoe Kosmicheskoe Priborostroenie. Materialy Seminara, 27 Sentyabrya–1 Oktyabrya, 1982, Odessa* (Scientific Space Instrumentation Design. Proc. of the Seminar September 27–October 1, 1982, Odessa) Issue 1 (Exec. Ed. V M Balebanov) (Moscow: Metallurgiya, 1983) p. 10
54. Sholomitskii G B et al. *Sov. Astron.* **30** 514 (1986); *Astron. Zh.* **63** 867 (1986)
55. Pilbratt G L *Proc. SPIE* **7010** 701002 (2008)
56. Vaccari M, arXiv:1605.01215
57. Madau P, Dickinson M *Annu. Rev. Astron. Astrophys.* **52** 415 (2014)
58. Heckman T M, Best P N *Annu. Rev. Astron. Astrophys.* **52** 589 (2014)
59. Grossi M et al. *Astron. Astrophys.* **518** L52 (2010)
60. di Serego Alighieri S et al. *Astron. Astrophys.* **552** A8 (2013)
61. Coppin K E K et al. *Mon. Not. R. Astron. Soc.* **416** 680 (2011)
62. Ade P A R et al. (Planck Collab.) *Astron. Astrophys.* **594** A13 (2016)
63. Verkhodanov O V *Phys. Usp.* **59** 3 (2016); *Usp. Fiz. Nauk* **186** 3 (2016)
64. Ade P A R et al. (Planck Collab.) *Astron. Astrophys.* **581** A14 (2015)
65. Adam R et al. (Planck Collab.) *Astron. Astrophys.* **586** A135 (2016)
66. Naylor D A et al. *Mon. Not. R. Astron. Soc.* **315** 622 (2000)
67. Holland W S et al. *Proc. SPIE* **3357** 305 (1998); astro-ph/9809121
68. Seaquist E et al. *Mon. Not. R. Astron. Soc.* **349** 1428 (2004)
69. Vlahakis C, Dunne L, Eales S *Mon. Not. R. Astron. Soc.* **364** 1253 (2005)
70. Sanders D B *Adv. Space Res.* **34** 535 (2004)
71. Thomas H C et al. *Mon. Not. R. Astron. Soc.* **351** 362 (2004)
72. Ward-Thompson D et al. *Astrophys. J.* **537** L135 (2000)
73. Crutcher R M et al. *Astrophys. J.* **600** 279 (2004)
74. Ward-Thompson D et al., in *Star Formation at High Angular Resolution. Proc. of the 221st Symp. of the Intern. Astronomical Union, Sydney, Australia, 22–25 July 2003* (Eds M G Burton, R Jayawardhana, T L Bourke) (San Francisco, CA: Astronomical Society of the Pacific, 2004) p. 43
75. Matthews B C, in *Astronomical Polarimetry: Current Status and Future Directions, Proc. of a Meeting, Waikoloa, Hawaii, USA, 15–19 March 2004* (Astronomical Society of the Pacific Conf., Vol. 343, Eds A Adamson et al.) (San Francisco, CA: Astronomical Society of the Pacific, 2005) p. 99
76. Matthews B C et al. *Astrophys. J. Suppl.* **182** 143 (2009)
77. Franco G A P, Alves S O *Astrophys. J.* **807** 5 (2015)
78. Ade P A R et al. (Planck Collab.) *Astron. Astrophys.* **586** A136 (2016)
79. Holland W S et al. *Mon. Not. R. Astron. Soc.* **430** 2513 (2013)
80. Bustos R et al. *Publ. Astron. Soc. Pacific* **126** 1126 (2014)
81. Wootten A, Thompson A R *Proc. IEEE* **97** 1463 (2009)
82. Herrera C N et al. *Astron. Astrophys.* **538** L9 (2012)
83. Ziurys L M, in *AAS Meeting* (228) 203.02 (2016)
84. Simpson J M et al. *Astrophys. J.* **807** 128 (2015)
85. Chen C-C et al. *Astrophys. J.* **820** 82 (2016)
86. Imanishi M, Nakanishi K, Izumi T *Astrophys. J.* **825** 44 (2016)
87. Strandet M L et al. *Astrophys. J.* **822** 80 (2016)
88. Casey C M, Narayanan D, Cooray A *Phys. Rep.* **541** 45 (2014)
89. Dunlop J S et al. *Mon. Not. R. Astron. Soc.* **466** 861 (2017); arXiv:1606.00227
90. Sibthorpe B et al., in *Conditions and Impact of Star Formation. From Lab to Space. In memory of Charles H. Towes. The 6th Zermatt ISM-Symp., Zermatt, Switzerland, September 7–11, 2015* (EAS Publ. Ser., Vol. 75–76, Eds R Simon, R Schaaf, J Stutzki) (Les Ulis: EDP Sciences, 2016) p. 411
91. Kardashev N S et al. *Phys. Usp.* **57** 1199 (2014); *Usp. Fiz. Nauk* **184** 1319 (2014)
92. Wild W et al. *Exp. Astron.* **23** 221 (2009)
93. Smirnov A V et al. *Proc. SPIE* **8442** 84424C (2012)
94. Bradford C M et al., arXiv:1505.05551
95. Kravtsov A V *Astrophys. J.* **764** L31 (2013)
96. Aalto S, in *Revolution in Astronomy with ALMA. The Third Year. Proc. of a Conf., Tokyo Intern. Forum, Tokyo, Japan 8–11 December 2014* (ASP Conf. Ser., Vol. 499, Eds D Iono et al.) (San Francisco, CA: Astronomical Society of the Pacific, 2015) p. 85
97. Salak D, Nakai N, Miyamoto Y, in *Revolution in Astronomy with ALMA. The Third Year. Proc. of a Conf., Tokyo Intern. Forum, Tokyo, Japan 8–11 December 2014* (ASP Conf. Ser., Vol. 499, Eds D Iono et al.) (San Francisco, CA: Astronomical Society of the Pacific, 2015) p. 155

98. Kennicutt R C (Jr.), Evans N J *Annu. Rev. Astron. Astrophys.* **50** 531 (2012)
99. Vasiliev E O, Shchekinov Yu A *Astron. Rep.* **60** 924 (2016); *Astron. Zh.* **93** 892 (2016)
100. Lada C J, in *Star Forming Regions. Proc. of the 115th Symp. of the International Astronomical Union, Tokyo, Japan, November 11 – 15, 1985* (Eds M Peimbert, J Jugaku) (Dordrecht: D. Reidel Publ. Co., 1987) p. 1
101. Lada C, in *The Origin of Stars and Planetary Systems* (NATO Science Series, Ser. C, Vol. 540, Eds C J Lada, N D Kylafis) (Dordrecht: Kluwer Acad. Publ., 1999) p. 143
102. Van Doshoeck E F, Hogerheijde M R, in *The Origin of Stars and Planetary Systems* (NATO Science Series, Ser. C, Vol. 540, Eds C J Lada, N D Kylafis) (Dordrecht: Kluwer Acad. Publ., 1999) p. 97
103. Seifried D et al. *Mon. Not. R. Astron. Soc.* **459** 1892 (2016)
104. Dunham M M et al. *Astrophys. J.* **823** 160 (2016); arXiv:1604.04027
105. Takakuwa S et al. *IAU General Assembly Meeting* (29) 2230558 (2015)
106. Men'shchikov A et al. *Astron. Astrophys.* **518** L103 (2010)
107. André Ph et al. *Astron. Astrophys.* **518** L102 (2010)
108. Könyves V et al. *Astron. Astrophys.* **518** L106 (2010)
109. Arzoumanian D et al. *Astron. Astrophys.* **529** L6 (2011)
110. Ibañez S M H, Sigalotti L Di G *Astrophys. Space Sci.* **95** 145 (1983)
111. Inutsuka S-I, Miyama S M *Astrophys. J.* **388** 392 (1992)
112. Kawachi T, Hanawa T *Publ. Astron. Soc. Jpn.* **50** 577 (1998)
113. Hill T et al. *Astron. Astrophys.* **533** A94 (2011)
114. Roy A et al. *Astron. Astrophys.* **562** A138 (2014)
115. Tremblin P et al. *Astron. Astrophys.* **564** A106 (2014)
116. Dibai E A, Kaplan S A *Sov. Astron.* **8** 520 (1965); *Astron. Zh.* **41** 652 (1964)
117. Elmegreen B G, Lada C J *Astrophys. J.* **214** 725 (1977)
118. Gerola H, Seiden P E *Astrophys. J.* **223** 129 (1978)
119. Efremov Yu N *Sov. Astron. Lett.* **5** 12 (1979); *Pis'ma Astron. Zh.* **5** 21 (1979)
120. Sandford M T (II), Whitaker R W, Klein R I *Astrophys. J.* **260** 183 (1982)
121. LaRosa T N *Astrophys. J.* **274** 815 (1983)
122. Cammerer M, Shchekinov Yu *Astron. Astrophys.* **283** 845 (1994)
123. Zel'dovich Ya B, Mamaev A V, Shandarin S F *Sov. Phys. Usp.* **26** 77 (1983); *Usp. Fiz. Nauk* **139** 153 (1983)
124. Elmegreen B G, Scalo J *Annu. Rev. Astron. Astrophys.* **42** 211 (2004)
125. Young J S, Scoville N Z *Annu. Rev. Astron. Astrophys.* **29** 581 (1991)
126. Blitz L, Shu F H *Astrophys. J.* **238** 148 (1980)
127. Cohen R S et al. *Astrophys. J. Lett.* **239** L53 (1980)
128. Goldsmith P F, Li D, Krčo M *Astrophys. J.* **654** 273 (2007)
129. Scoville N Z, Hersh K *Astrophys. J.* **229** 578 (1979)
130. Pringle J E, Allen R J, Lubow S H *Mon. Not. R. Astron. Soc.* **327** 663 (2001)
131. Koda J, Scoville N, Heyer M *Astrophys. J.* **823** 76 (2016)
132. Dame T M, Hartmann D, Thaddeus P *Astrophys. J.* **547** 792 (2001)
133. Heyer M H et al. *Astrophys. J.* **602** 723 (2004)
134. Fukui Y et al. *Astrophys. J.* **705** 144 (2009)
135. Rand R J, Kulkarni S R *Astrophys. J.* **349** L43 (1990)
136. Koda J et al. *Astrophys. J. Suppl.* **193** 19 (2011)
137. Pety J et al. *Astrophys. J.* **779** 43 (2013)
138. Roman-Duval J et al. *Astrophys. J.* **699** 1153 (2009)
139. Kalberla P M W, Dedes L *Astron. Astrophys.* **487** 951 (2008)
140. Nakanishi H, Sofue Y *Publ. Astron. Soc. Jpn.* **68** 5 (2016)
141. Kawamura A et al. *Astrophys. J. Suppl.* **184** 1 (2009)
142. Sofue Y, Nakanishi H *Publ. Astron. Soc. Jpn.* **68** 63 (2016)
143. Hartmann D, Burton W B *Atlas of Galactic Neutral Hydrogen* (Cambridge: Cambridge Univ. Press, 1997)
144. Kerr F J et al. *Astron. Astrophys. Suppl.* **66** 373 (1986)
145. Kalberla P M W et al. *Astron. Astrophys.* **440** 775 (2005)
146. Sofue Y, Nakanishi H *Publ. Astron. Soc. Jpn.* **68** 63 (2016)
147. van Doshoeck E F, in *Millimetre and Submillimetre Astronomy. Lectures, Summer School, Stirling, Scotland, June 21 – 27, 1987* (Astrophysics and Space Science Library, Vol. 147, Eds R D Wolstencroft, W B Burton) (Dordrecht: Kluwer Acad. Publ., 1988) p. 117
148. Shchekinov Yu A *Astrophysics* **47** 205 (2004); *Astrofizika* **47** 241 (2004)
149. Wolfire M G, Hollenbach D, McKee C F *Astrophys. J.* **716** 1191 (2010)
150. Vlahakis C et al. *Mon. Not. R. Astron. Soc.* **433** 1837 (2013)
151. Tosaki T et al. *Publ. Astron. Soc. Jpn.* **63** 1171 (2011)
152. Ade P A R et al. (Planck Collab.) *Astron. Astrophys.* **536** A17 (2011)
153. Abergel A et al. (Planck Collab.) *Astron. Astrophys.* **536** A21 (2011)
154. Hollenbach D J, Tielens A G G M *Annu. Rev. Astron. Astrophys.* **35** 179 (1997)
155. Burton M G et al. *Astrophys. J.* **811** 13 (2015)
156. Langer W D et al. *Astron. Astrophys.* **561** A122 (2014)
157. Hollenbach D J, Tielens A G G M *Rev. Mod. Phys.* **71** 173 (1999)
158. Bolatto A D, Wolfire M, Leroy A K *Annu. Rev. Astron. Astrophys.* **51** 207 (2013)
159. de Vries H W, Heithausen, Thaddeus P *Astrophys. J.* **319** 723 (1987)
160. Reach W T, Koo B-C, Heiles C *Astrophys. J.* **429** 672 (1994)
161. Ade P A R et al. (Planck Collab.) *Astron. Astrophys.* **536** A19 (2011)
162. Glassgold A E, Huggins P J, Langer W D *Astrophys. J.* **290** 615 (1985)
163. Maloney P, Black J H *Astrophys. J.* **325** 389 (1988)
164. Heyer M H, Tereby S *Astrophys. J.* **502** 265 (1998)
165. Arabadjis J S, Bregman J N *Astrophys. J.* **510** 806 (1999)
166. Grenier I A, Casandjian J-M, Terrier R *Science* **307** 1292 (2005)
167. Wolfire M G, Hollenbach D, McKee C F *Astrophys. J.* **716** 1191 (2010)
168. Poglitsch A et al. *Astrophys. J.* **454** 293 (1995)
169. Madden S C et al. *Astrophys. J.* **483** 200 (1997)
170. Leroy A K et al. *Astron. J.* **137** 4670 (2009)
171. Fukui Y et al. *Astrophys. J.* **798** 6 (2015)
172. Lee M-Y et al. *Astrophys. J.* **809** 56 (2015)
173. Hollenbach D, McKee C F *Astrophys. J. Suppl.* **41** 555 (1979)
174. Hollenbach D, McKee C F *Astrophys. J.* **342** 306 (1989)
175. Jenkins E B, Tripp T M *Astrophys. J. Suppl.* **137** 297 (2001)
176. Vasiliev E O, Shchekinov Yu A *Astron. Rep.* **61** 342 (2017); *Astron. Zh.* **94** 333 (2017)
177. Wolfire M G et al. *Astrophys. J.* **587** 278 (2003)
178. Spaans M, Norman C A *Astrophys. J.* **483** 87 (1997)
179. Vasiliev E O *Mon. Not. R. Astron. Soc.* **431** 638 (2013)
180. Madden S C et al. *Publ. Astron. Soc. Pacific* **125** 600 (2013)
181. De Looze I et al. *Astron. Astrophys.* **568** A62 (2014)
182. Cormier D et al. *Astron. Astrophys.* **578** A53 (2015)
183. Vallini L et al. *Astrophys. J.* **813** 36 (2015)
184. Maiolino R et al. *Astron. Astrophys.* **440** L51 (2005)
185. Stacey G J et al. *Astrophys. J.* **724** 957 (2010)
186. Cox P et al. *Astrophys. J.* **740** 63 (2011)
187. De Breuck C et al. *Astron. Astrophys.* **565** A59 (2014)
188. Maiolino R et al. *Mon. Not. R. Astron. Soc.* **452** 54 (2015)
189. Inoue A K et al. *Science* **352** 1559 (2016)
190. Shibuya T et al. *Astrophys. J.* **752** 114 (2012)
191. Hashimoto T et al. *Astrophys. J.* **812** 157 (2015)
192. Kakiichi K et al. *Mon. Not. R. Astron. Soc.* **463** 4019 (2016); arXiv:1510.05647
193. Jimmy et al. *Astrophys. J.* **825** 34 (2016)
194. Aravena M et al. *Astrophys. J.* **833** 71 (2016); arXiv:1607.06772
195. Pentericci L et al. *Astrophys. J.* **504** 139 (1998)
196. Pentericci L et al. *Astron. Astrophys.* **396** 109 (2002)
197. Kurk J D et al. *Astron. Astrophys.* **428** 793 (2004)
198. Dannerbauer H et al. *Astron. Astrophys.* **570** A55 (2014)
199. Pentericci L et al. *Astron. Astrophys.* **361** L25 (2000)
200. Ogle P et al. *Astrophys. J.* **751** 13 (2012)
201. Nesvadba N P H et al. *Astrophys. J.* **650** 693 (2006)
202. Vasiliev E O *Mon. Not. R. Astron. Soc.* **431** 638 (2013)
203. Shapiro P R, Moore R T *Astrophys. J.* **207** 460 (1976)
204. Suchkov A A, Shchekinov Yu A *Sov. Astron. Lett.* **10** 13 (1984); *Pis'ma Astron. Zh.* **10** 35 (1984)
205. Vasiliev E O, Ryabova M V, Shchekinov Yu A *Mon. Not. R. Astron. Soc.* **446** 3078 (2015)
206. Oppenheimer B D et al. *Mon. Not. R. Astron. Soc.* **460** 2157 (2016)
207. Draine B T, in *Cosmic Dust: Near and Far. Proc. of a Conf., 8 – 12 September 2008, Heidelberg, Germany* (ASP Conf. Ser., Vol. 414, Eds T Henning, E Grün, J Steinacker) (San Francisco: Astromomical Society of the Pacific, 2009) p. 453
208. Jones A P, Nuth J A (III) *Astron. Astrophys.* **530** A44 (2011)
209. Whittet D C B *Dust in the Galactic Environment* (Bristol: A. Hilger, 1992)

210. Bode M F, in *Dust in the Universe. Proc. of the Conf., Manchester, England, Dec. 14–18, 1987* (Eds M E Bailey, D A Williams) (Cambridge: Cambridge Univ. Press, 1988) p. 73
211. Priddey R S et al. *Mon. Not. R. Astron. Soc.* **344** L74 (2003)
212. Todini P, Ferrara A *Mon. Not. R. Astron. Soc.* **325** 726 (2001)
213. Maiolino R et al. *Nature* **431** 533 (2004)
214. Gall C, Hjorth J, Andersen A C *Astron. Astrophys. Rev.* **19** 43 (2011)
215. Matsuura M et al. *Science* **333** 1258 (2011)
216. Bouchet P et al. *Astrophys. J.* **611** 394 (2004)
217. Dwek E, Galliano F, Jones A P *Astrophys. J.* **662** 927 (2007)
218. Indebetouw R et al. *Astrophys. J. Lett.* **782** L2 (2014)
219. Grün E et al. *Nature* **362** 428 (1993)
220. Landgraf M et al. *Science* **286** 2319 (1999)
221. Frisch P C et al. *Astrophys. J.* **525** 492 (1999)
222. Mathis J S, Rumpl W, Nordsieck K H *Astrophys. J.* **217** 425 (1977)
223. Meisel D D, Janches D, Mathews J D *Astrophys. J.* **567** 323 (2002)
224. Meisel D D, Janches D, Mathews J D *Astrophys. J.* **579** 895 (2002)
225. Baggaley W J et al. *Q. J. R. Astron. Soc.* **35** 293 (1994)
226. Taylor A D, Baggaley W J, Steel D I *Nature* **380** 323 (1996)
227. Landgraf M et al. *J. Geophys. Res.* **105** 10343 (2000)
228. Wang S, Li A, Jiang B W *Astrophys. J.* **811** 38 (2015)
229. Afanasiev V L, Kalenichenko V V, Karachentsev I D *Astrophys. Bull.* **62** 301 (2007); *Astrofiz. Byull.* **62** 319 (2007)
230. Krüger H, Grün E *Space Sci. Rev.* **143** 347 (2009)
231. Krüger H et al. *Planet. Space Sci.* **58** 951 (2010)
232. Westphal A J et al. *Meteor. Planet. Sci.* **49** 1720 (2014)
233. Scicluna P et al. *Astron. Astrophys.* **584** L10 (2015)
234. Wong K T et al. *Astron. Astrophys.* **590** A127 (2016); arXiv:1603.03371
235. Kamiński T et al. *Astron. Astrophys.* **592** A42 (2016)
236. Gupta A et al. *Astrophys. J. Lett.* **756** L8 (2012)
237. Nicastro F et al. *Mon. Not. R. Astron. Soc.* **457** 676 (2016)
238. Fang T et al. *Astrophys. J.* **762** 20 (2013)
239. Salem M et al. *Astrophys. J.* **815** 77 (2015)
240. Fang T et al. *Astrophys. J. Suppl.* **217** 21 (2015)
241. Leroy A K et al. *Astrophys. J.* **737** 12 (2011)
242. Rémy-Ruyer A et al. *Astron. Astrophys.* **563** A31 (2014)
243. Shi Y et al. *Nature* **514** 335 (2014)
244. Polikarpova O L, Shchekinov Yu A *Astron. Rep.* **61** 89 (2017); *Astron. Zh.* **94** 99 (2017)
245. Al Najm M N, Polikarpova O L, Shchekinov Yu A *Astron. Rep.* **60** 389 (2016); *Astron. Zh.* **93** 355 (2016)
246. Howk J C, Savage B D *Astron. J.* **114** 2463 (1997)
247. Howk J C, Savage B D *Astron. J.* **117** 2077 (1999)
248. Hughes T M et al. *Astron. Astrophys.* **565** A4 (2014)
249. Bocchio M et al. *Astron. Astrophys.* **586** 8B (2015)
250. Khoperskov S A, Shchekinov Yu A, arXiv:1403.7075
251. Irwin J A et al. *Mon. Not. R. Astron. Soc.* **433** 2958 (2013)
252. Holwerda B W et al. *Astron. Astrophys.* **444** 101 (2005)
253. Holwerda B W *Astron. Nachr.* **334** 268 (2013)
254. Fritz J et al. *Astron. Astrophys.* **546** A34 (2012)
255. Smith M W L et al. *Astrophys. J.* **756** 40 (2012)
256. Mattsson L et al. *Mon. Not. R. Astron. Soc.* **444** 797 (2014)
257. Holwerda B W et al. *Astron. J.* **137** 3000 (2009)
258. Wang J et al. *Mon. Not. R. Astron. Soc.* **441** 2159 (2014)
259. Martinsson T P K et al. *Astron. Astrophys.* **585** A99 (2016)
260. Fall S M, Pei Y C *Astrophys. J.* **402** 479 (1993)
261. Pei Y C, Fall S M, Hauser M G *Astrophys. J.* **522** 604 (1999)
262. Hauser M G et al. *Astrophys. J.* **508** 25 (1998)
263. Fixsen D J et al. *Astrophys. J.* **508** 123 (1998)
264. Driver S P et al. *Mon. Not. R. Astron. Soc.* **379** 1022 (2007)
265. Kollmeier J A et al. *Astrophys. J. Lett.* **789** L32 (2014)
266. Navarro J F, Frenk C S, White S D M *Astrophys. J.* **462** 563 (1996)
267. Feldmann R, Hooper D, Gnedin N Y *Astrophys. J.* **763** 21 (2013)
268. Fukugita M, arXiv:1103.4191
269. Peeples M S et al. *Astrophys. J.* **786** 54 (2014)
270. Peek J E G, Ménard B, Corrales L *Astrophys. J.* **813** 7 (2015)
271. Su M, Slatyer T R, Finkbeiner D P *Astrophys. J.* **724** 1044 (2010)
272. Impey C, Bothun G *Annu. Rev. Astron. Astrophys.* **35** 267 (1997)
273. van Dokkum P G et al. *Astrophys. J. Lett.* **804** L26 (2015)
274. Koda J et al. *Astrophys. J. Lett.* **807** L2 (2015)
275. Rahman N et al. *Astrophys. J.* **663** 908 (2007)
276. Das M et al. *Astrophys. J.* **651** 853 (2006)
277. Galaz G et al. *Astrophys. J. Lett.* **815** L29 (2015)
278. Kaisin S S, Karachentsev I D *Astrophysics* **49** 287 (2006); *Astrofizika* **49** 337 (2006)
279. Karachentsev I et al. *Mon. Not. R. Astron. Soc.* **415** L31 (2011)
280. Casetti-Dinescu D I et al. *Astrophys. J. Lett.* **784** L37 (2014)
281. Murray C E et al. *Astrophys. J.* **808** 41 (2015)
282. Stark D V, Baker A D, Kannappan S J *Mon. Not. R. Astron. Soc.* **446** 1855 (2015)
283. Giallongo E et al. *Astrophys. J.* **813** 68 (2015)
284. Hintz J L et al. *Astrophys. J.* **663** 895 (2007)
285. Impey C D et al. *Astrophys. J. Suppl.* **105** 209 (1996)
286. Young J E, Kuzio de Naray R, Wang S X *Mon. Not. R. Astron. Soc.* **452** 2973 (2015)
287. Matsuura M *Proc. Int. Astron. Union* **8** (S292) 267 (2012)
288. Lazzati D, Heger A *Astrophys. J.* **817** 134 (2016)
289. Linsky J L et al. *Astrophys. J.* **647** 1106 (2006)
290. McGee S L, Balogh M L *Mon. Not. R. Astron. Soc.* **405** 2069 (2010)
291. Kashiwagi T, Suto Y *Mon. Not. R. Astron. Soc.* **451** 4162 (2015)
292. Chelouche D, Koester B P, Bowen D V *Astrophys. J.* **671** L97 (2007)
293. Gutiérrez C M, López-Corredoira M *Astron. Astrophys.* **571** A66 (2014)
294. Adam R et al. (Planck Collab.) *Astron. Astrophys.* **596** A104 (2016)
295. Walter F, Weiss A, Scoville N *Astrophys. J.* **580** L21 (2002)
296. Salas P et al. *Astrophys. J.* **797** 134 (2014)
297. Diederik Kruijssen J M et al. *Mon. Not. R. Astron. Soc.* **440** 3370 (2014)
298. Nataf D M et al. *Mon. Not. R. Astron. Soc.* **456** 2692 (2016)
299. Fitzpatrick E L *Publ. Astron. Soc. Pacific* **111** 63 (1999)
300. Fitzpatrick E L, Massa D *Astrophys. J. Suppl.* **72** 163 (1990)
301. Nataf D M et al. *Mon. Not. R. Astron. Soc.* **456** 2692 (2016)
302. Cardelli J A, Clayton G C, Mathis J S *Astrophys. J.* **345** 245 (1989)
303. Schlafly E F et al. *Astrophys. J.* **821** 78 (2016); arXiv:1602.03928
304. Higdon S J U et al. *Astrophys. J.* **648** 323 (2006)
305. Capak P L et al. *Nature* **522** 455 (2015)
306. Maiolino R et al. *Mon. Not. R. Astron. Soc.* **452** 54 (2015)
307. Ota K et al. *Astrophys. J.* **792** 34 (2014)
308. Ouchi M et al. *Astrophys. J.* **778** 102 (2013)
309. Darren Dowell C et al. *Astrophys. J.* **780** 75 (2014)